DFT Study of the Interaction between Single-walled Carbon Nanotubes and Organic Conjugated Oligomers

by

©Suad Aljohani

A thesis submitted to the School of Graduate Studies in partial fulfillment of the requirements for the degree of Master of Science

M.Sc.

Department of Physics and Physical Oceanography
Memorial University of Newfoundland

Memorial University of Newfoundland

May 2015

ST. JOHN'S NEWFOUNDLAND

Abstract

Using dispersion corrected density functional theory (DFT) methods, we study the interaction between oligo(phyenylene ethynylene)s (OPEs) having different end groups: aldehyde (ALD) and dithiafulvene (DTF) (abbreviated as OPE-ALD and OPE-DTF respectively) with single-wall carbon nanotube (SWCNT). We investigate the structure and electronic properties of isolated OPEs and OPE/SWCNT molecular combinations. This research is important for developing of more effective linear conjugated oligomer-based dispersants for SWCNTs. In particular, we focus on understanding of the role of the end groups in the dispersion of nanotubes. We consider a number of dispersion corrected DFT methods: B97D, wB97XD, and CAM-B3LYP and employ the 6-31G* basis set in all of our calculations. We obtain geometries, dipole moments, binding energies, and intermolecular distances for the oligomer and nanotube combinations. The comparison of results obtained using different DFT approximations is also made. Our results show that OPE-DTF interact more strongly with the nanotube than OPE-ALD.

Abbreviations

- **CNTs** Carbon Nanotubes
- **SWCNTs** Single-wall Carbon Nanotubes
- **OPEs** Oligo(Phyenylene Ethynylene)s
- **ALD** Aldehyde
- **DTF** Dithiafulvene
- **MO** Molecular Orbital
- **HF** Hartree-Fock
- **DFT** Density Functional Theory
- **LDA** Local Density Approximation
- **LSDA** Local Spin Density Approximation
- **R** Bond Lengths
- **A** Bond Angles
- **D** Dihedral Angles
- **ACEnet** Atlantic Computational Excellenece Network

- **Westgrid** Western Canadian Research Grid
- **RMS** Root Mean Square
- **SCF** Self Consistent Field
- **HOMO** Highest Occupied Molecular Orbital
- **LUMO** Lowest Unoccupied Molecular Orbital
- **nqs** no-quota scratch

Acknowledgements

I would never have been able to finish my dissertation without protection and ability from Allah to do this work.

First and foremost, I would like to express my deepest gratitude to my supervisor, Dr. J. B. Lagowski, for being extremely helpful by giving greate advice and her honest encouragement and consultation, which guided me through my graduate and future studies.

I would like to convey my thanks to Mr. Fred Perry for his technical help. I also appreciate ACE-net and Westgrid program and services, used for carrying out our computational work.

I am also deeply thankful to my beloved Mom, Fatimah, who has always encouraged me and prayed for me throughout my studies.

I would like to give a million thanks to my husband, Ayad Aljohani, for his wonderful support. It is my pleasure to give special thanks to Dr. Abdullah Alodhayb. I appreciate all the information he has provided, which helped me complete my studies here.

Last but not least, I would like to thank my brothers and sisters. They have always supported me and encouraged me with their best wishes.

Table of Contents

List of Tables

List of Figures

Chapter 1

Introduction

1.1 Carbon nanotubes (CNTs)

Allotropes are different forms of the same compound that have different chemical structures. Some common examples of allotropes are phosphorus ("white" or "yellow", "red", and "black/ purple"), oxygen (O_2 and O_3) and others. The allotropes of carbon include: diamond (carbon atoms that are bonded together in a tetrahedral lattice arrangement), graphite (carbon atoms that are bonded together in sheets of a hexagonal lattice), graphene (single sheet of graphite), fullerenes (carbon atoms that are bonded together in spherical, or ellipsoidal formations), and carbon nanotubes (CNTs) [1].

Carbon atoms have the ability to form different configurations (corresponding to different electronic states), and hence, to create various polymorphs [2]. The four (two s and two p) valence electrons experience a weaker attraction force than the two inner (s) electrons, causing the valence electrons to mix and reduce their energy by creating a hybrid orbital called sp hybridization. The two most common types of hybridization of carbons are those of the sp^2 and sp^3 hybrid orbitals. CNTs are

composed of sp^2 carbons. These sp^2 hybrid orbitals lie in plane forming ("double") bonds that are stronger than the ("single") bonds due to sp^3 hybrid orbitals, say in diamond, and give the nanotubes their unique strength [3].

Prior to the discovery of CNTs, in 1985 a group of researchers led by Richard Smalley made an interesting discovery of another carbon-based material [4]. Using the technique of laser evaporation of graphite, they produced a stable carbon compound that had the shape of a soccer ball which they called buckminsterfullerene (C_{60}) or just fullerene for short. The buckminsterfullerene molecule is a net of 12 pentagons and 20 hexagons folded into a sphere (also called buckyball). Today we define fullerenes as spherically shaped molecules of various sizes (not just C_{60}) composed entirely of carbons [5]. Other fullerene shaped like "buds" are called carbon buckytubes. Typically, a carbon buckytube has a similar structure to a fullerene, but instead of forming a sphere, the atoms form a cylindrical tube that may be capped off at each end by a half of a fullerene molecule [6] (sometime these elongated capped buckytubes are referred to as nanotubes).

The term of "carbon nanotubes" was "invented" by Sumio Iijima in 1991 [7] (however, they were observed prior to his invention). CNTs are cylindrical carbon molecules which have the appearance of rolled graphene. Nanotubes are open ended whereas fullerenes are closed structures. They are characterized by high aspect ratios. Typically, CNTs are a few nanometers in diameters and have a very broad range of electronic, thermal, and structural properties. In recent years, significant progress in the research and applications of CNTs has been achieved. They have been used in organic solar cells [8], biosensors [9], and conductive textiles [10]. In the year of 2000, Luzzi and Smith reported the first production method for carbon peapods [11] (which are

defined as fullerenes trapped inside a carbon nanotube). Since their discovery, CNTs have become enormously popular and, because of their unusual properties, they have started an explosive growth of research and development in the field of nanotechnology and nanomaterials.

CNTs can be classified into two major groups: single-walled carbon nanotubes (SWCNTs) that contain one graphene sheet that is rolled up to form a cylinder, and multi-walled carbon nanotubes (MWCNTs), that can be thought of as several sheets of graphene stacked on top of each other [12,13]. In this research, we focus on SWCNTs as illustrated in Fig. 1.1. SWCNTs are very useful in the fundamental investigations of the structure/property relationships of CNTs since they do not include the interactions between concentric tubes in MWCNTs which tend to further complicate the study of their properties.

The structures of SWCNTs can be described by their chirality or helicity, which is defined by the following equation:

$$C_h = na_1 + ma_2 \tag{1.1}$$

where the C_h is chiral vector, (n, m) are the numbers of steps along the ziz-zag bonds of the hexagonal lattice, and a_1 and a_2 are unit vectors (for example see diagram below). The zigzag nanotubes are semiconductors. For symmetry reasons the chirality vector classifies completely all the carbon nanotubes. θ is the chiral angle between C_h and a_1 and it is given by

$$\tan\theta = \sqrt{3m}/(2n+m). \tag{1.2}$$

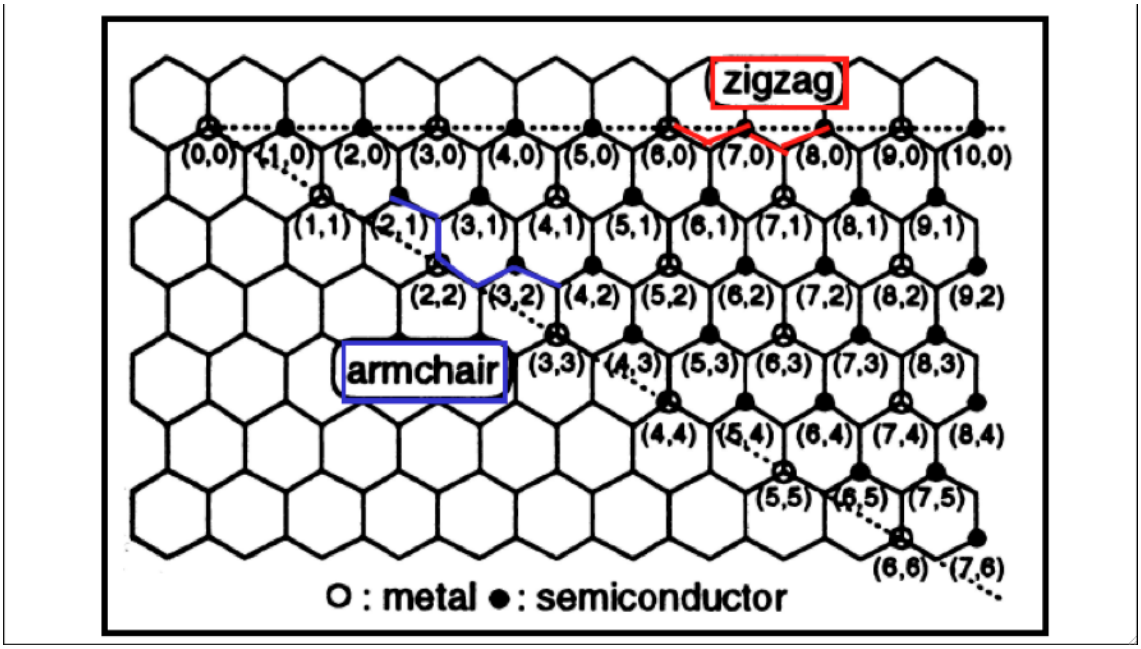

When m=0 and θ=0°, the tube formed is a zigzag tube with C_h=na_1. The preparation of SWCNTs with specific diameters and lengths is very challenging [14].

Some groups have been engaged in synthesizing structurally uniform SWCNTs. For example, in 2013, Itami and co-workers reported the total synthesis of SWCNT by using nanorings such as cyclic polypheneylenes as templates [15]. As stated above, SWCNTs have been proposed as promising materials for a variety of applications, including molecular electronics and polymer reinforcement[16]. However, pristine SWCNTs have many drawbacks in terms of processing and device fabrication. To address some of the difficulties of pristine CNTs, researchers have developed a number of methods that improve the functionality of CNTs. These can be classified into two categories: covalent and noncovalent methods [17].

Covalent functionalization involves the surface modification of carbon nanotubes.

It can be associated with a change of hybridization from sp^2 to sp^3. These functionalization methods are available both in solution and in the gas phase. On the other hand, the noncovalent functionalization typically preserves the sp^2 hybridization of the carbon atoms. CNTs are functionalized noncovalently by aromatic compounds, surfactants, oligomers and polymers. Noncovalent functionalization presents a particularly useful approach because it not only, provides a direct solution to the problems of insolubility and poor processability of as-produced SWNTs, but it also provides easy ways for sorting specific types of SWCNTs out of as-produced SWCNT mixtures. In general, functionalization methods tend to improve the dispersion of CNTs. As stated above, one possible way of dispersal CNTs is to use organic conjugated oligomers such as oligo(phenylene ethynylene) (OPE) [18].

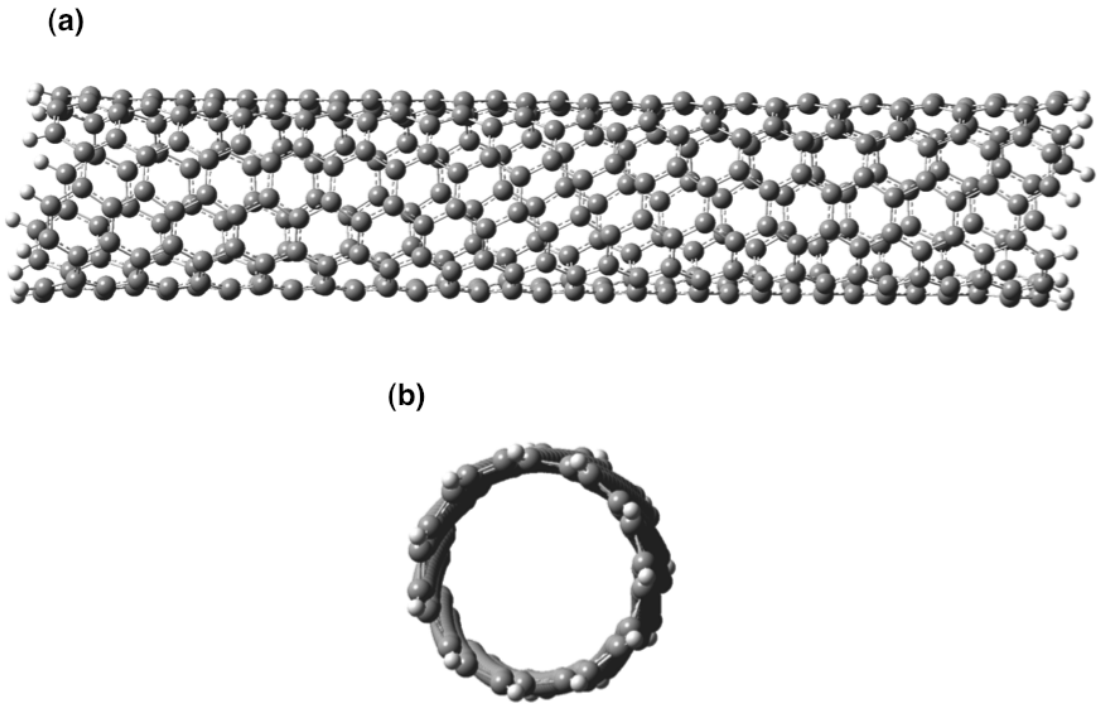

Figure 1.1: Single-walled carbon nanotube (SWCNT) with (6,5): (a) side view and (b) top view.

1.2 Organic Conjugated Oligomers

Organic conjugated oligomers and polymers have attracted considerable interest in recent years due to their optical and electronic properties that have led to their applications in photovoltaic cells, light-emitting diodes (LED), and electrochromic devices [19].

Conjugated polymers are π-conjugated organic materials exhibiting high electrical conductivity when doped, as well as other optoelectronic properties. They are characterized by flexibility, a wide spectral range, and are easily patterned. These characteristics make them competitive in comparison with their inorganic counterparts [20]. Electrical conductivity of conjugated polymers was first demonstrated in polyacetylene (PA) whose conductivity was increased after several orders of magnitude after oxidation with iodine [21], reaching a value of 10^{-5} S. These types of polymers are, today, called conducting polymers. This unique conducting property of organic conjugated polymers opened a door to a new area in materials science.

In the 1990's, it was discovered that organic conjugated polymers, in addition to having conducting properties, can also display electroluminescence [22]. This optical property has become one of the most important landmarks in the history of polymer science. Improved performance of these materials is continually being sought. This effort requires better knowledge of their optoelectronic properties such as band gaps, band widths and energy levels and of their transport properties such as charge mobility and energy transfer [23]. Improved processability and lowered operating voltages

are also being sought [24]. π-Conjugated polymers also show promising application potential [25]. Today, they have been extensively investigated and very successfully applied in many devices such as light emitting diodes, solar cells, field effect transistors and others [26]. Smaller conjugated oligomers also show interesting properties. The well defined monodispersed π-conjugated oligomers have been shown to be good alternatives to their relatively large polymers. Progress has been made on the study of well-defined conjugated oligomers, and there have been many research articles and reviews devoted to related topics [27]. The word "oligomer" is generally used to refer to the compound that carries relatively fewer repeating units than a polymer structure, or in a simple way, oligomer can considered as the intermediate structure between a small molecule and a polymer. Oligomers are easy to prepare and their purification requires less effort. All oligomer molecules have an identical number of repeat units in the backbone which is the reason for their monodispersity [28].

Recently, conjugated oligomers have attracted considerable attention due to their potential applications in the area of nanoelectronics [29], where they are used to produce semiconducting molecular wires or rods. These oligomers can be generalized into X-, Y-, Z-, and H-shaped assemblages that are referred to as X-mers, Y-mers, Z-mers, and H-mers [30]. As an example, in 2008, Zhao and co-workers prepared a series of H-shaped π-conjugated co-oligomers based on linear OPEs and oligo(phenylene vinylene)s (OPVs). They studied the molecular properties of these H-shape oligomers and linear shaped oligomers [31] (examples of which are given in Scheme. 1.1).

The focus of this work is the class of fully conjugated molecules such as OPEs with different end-groups: aldehyde (ALD) and dithiafulvenyl (DTF) (see Scheme 1.1). Significant experimental and computational efforts have been devoted to studying

the electronic properties of conjugated oligomers [32]. These properties can lead to unexpected results in CNT-oligomer or CNT-polymer composites. For example, CNT-polymer composite displays higher electrical conductivity than CNT alone [33]. The CNTs possess one of the highest thermal conductivities known [34] which helps their use in composites. However, their high aspect ratio and flexibility [35] along with the strong van der Waals forces between them cause CNTs to be severely entangled in close packing upon synthesis [36], which in turn degrades their processability and performance. Significant research efforts have been devoted to ameliorate this through the dispersion of CNTs in a polymer or oligomer matrices.

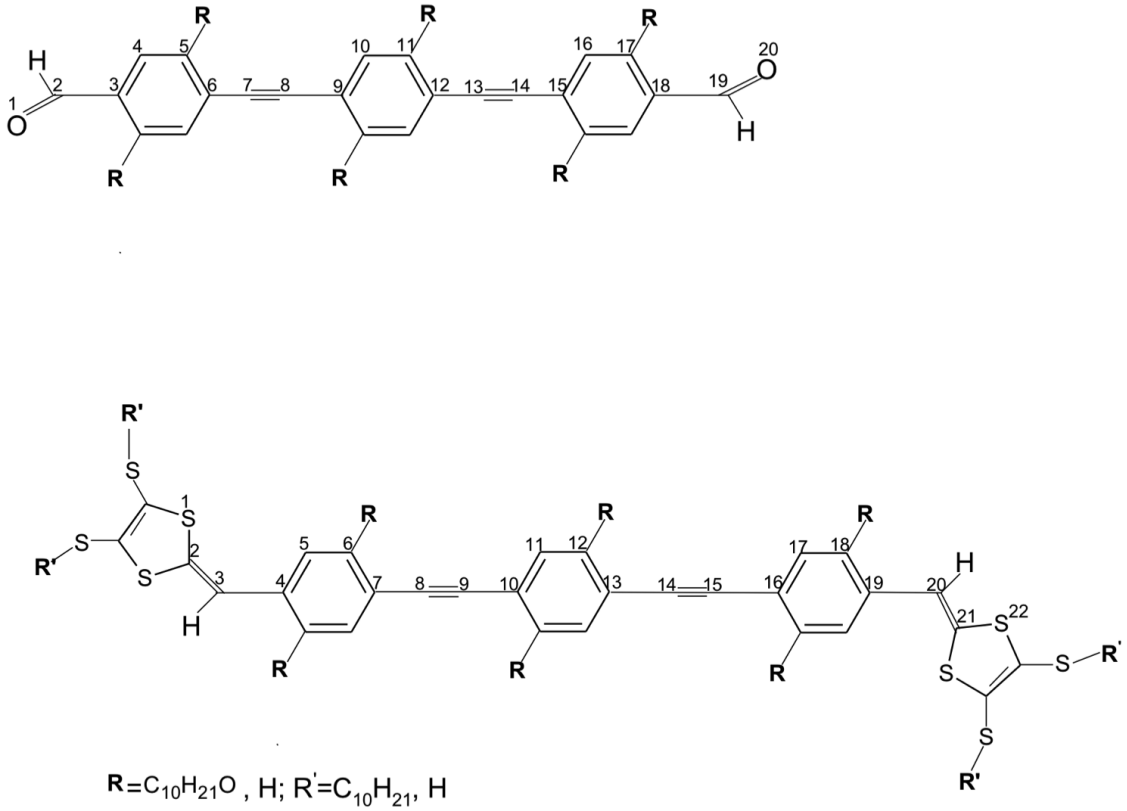

Scheme 1.1: Chemical structures of ALD- and DTF-ended OPEs.

1.3 Dispersion of carbon nanotubes

Dispersion is a process in which particles are dispersed in a continuous phase of a different composition (for example see reference [37]). In recent years, there is a great interest in polymer composites containing carbon nanotubes because they display a novel combination of electrical, optical and mechanical properties [36]. In this work we are primarily interested in the understanding dispersion of CNTs with conjugated oligomers to prevent their entanglement [37].

The dispersion of CNTs is affected by at least two competitive interactions: van der Waals forces among nanotubes, and the interactions between CNTs and dispersive medium. There are several different methods for dispersing CNTs [38]. They can be broadly classified as mechanical and chemical ones. Mechanical dispersion in conjunction with the surface active agents reduces the van der Waals forces between CNTs. Oligomers can interact with CNTs by noncovalent interactions to result in their dispersion in solvents [39]. A recent study has shown that for the dispersion of SWCNT in a solvent, dispersing agents (dispersants) are required to have sufficient binding forces toward SWCNTs so as to break apart their heavily entangled bundles. They discovered that relatively short phyenylene ethynylene and phyenylene vinylene oligomers when endcapped with dithiafulvenyl (DTF) groups, exhibited strong supramolecular interactions with SWCNTs [40-41].

1.4 Current Research

The motivation of this thesis is to understand the (noncovalent) dispersion of single-walled carbon nanotubes (SWCNTs) with the dithiafulvene (DTF)-ended and aldehyde (ALD)-ended organic oligomers such as oligo(phenylene ethynylene)s. The main

objective of this work is to study the interaction of these oligomers with SWCNTs. We have employed dispersion corrected density functional theory (DFT) for all calculations. To study there interactions, we use the following approximation: B97D, CAM-B3LYP, and wB97XD. In these DFT methods the dispersion correction accounts for the weak van der Waals type of intermolecular interactions.

The outline of thesis is: Chapter 2 summarizes briefly the density functional theory (DFT), starting with molecular orbital theory and Hartree-Fock (HF) methods. The basic concepts of dispersion corrected, long-range corrected, and long-range corrected with dispersion corrections DFT are reviewed. Chapter 3 gives a summary of the computational details. Chapter 4 discusses the results of molecular structures of the OPEs with different end groups such as ALD and DTF and then describes the effect of side chain lengths on the oligomer structures in vacum. Chapter 5 discusses the results obtained from computations involving the OPE-DTF oligomers with SWCNT, and OPE-ALD oligomers with SWCNT. The effect of dispersion on oligomers in the presence of SWCNTs will be analyzed. Chapter 6 summarizes the conclusions of this thesis.

Chapter 2

Theoretical Approach

In this chapter, we summarize the theoretical approaches used in this thesis. First, we briefly review molecular orbital (MO) theory in order to introduce the basic quantum mechanical concepts. Then, density functional theory (DFT) will be discussed. DFT is a very successful approach used to calculate, amongst other theories, the (ground state) properties of $2N$-electrons systems from first principles.

2.1 Molecular Orbital Theory

MO theory is primarily used to study the electronic structure and properties of molecular systems. MO theory was developed to solve the non-relativistic Schrodinger equation for a system of $2N$-electrons in the presence of M nuclei [42]. The non-relativistic Schrodinger equation is given by

$$\hat{H}\psi = E\psi \tag{2.1}$$

or

$$\hat{H}\psi(r, R) = E\psi(r, R) \tag{2.2}$$

where $\hat{H}$ is the molecular Hamiltonian operator, ψ is the total wave function, r and R stand for are the electronic and nuclear coordinates respectively, and E is the total energy of the system [43]. The non-relativistic Hamiltonian for atoms ($2N$ electrons) is given by

$$\hat{H} = -\frac{1}{2}\left(\frac{h^2}{4\pi^2 m_e}\right)\sum_{j=1}^{2N}\nabla_j^2 - \left(\frac{e^2}{4\pi\epsilon_0}\right)\sum_{j=1}^{2N}\frac{Z}{\vec{r}_j} + \left(\frac{e^2}{4\pi\epsilon_0}\right)\sum_{i=1}^{2N}\sum_{j>i}^{2N}\frac{1}{\mid \vec{r}_i - \vec{r}_j \mid} \quad (2.3)$$

where ϵ_0 is the permittivity of free space, h is the Planck's constant, e is the electron's charge, m_e denotes electron's mass and Z is the atomic number [44]. For molecules ($2N$ electrons, M nuclei), $\hat{H}$ is given by

$$\hat{H} = \hat{H}_e + \hat{H}_N = \hat{T}_e + \hat{V}_{N-e} + \hat{V}_{e-e} + \hat{T}_N + \hat{V}_{NN} \quad (2.4)$$

or

$$\begin{aligned}\hat{H} = \Bigg[& -\frac{1}{2}\left(\frac{h^2}{4\pi^2 m_e}\right)\sum_{j=1}^{2N}\nabla_j^2 - \left(\frac{e^2}{4\pi\epsilon_0}\right)\sum_{j=1}^{2N}\sum_{A=1}^{M}\frac{Z_A}{\mid \vec{r}_j - \vec{r}_A \mid} + \left(\frac{e^2}{4\pi\epsilon_0}\right)\sum_{i=1}^{2N}\sum_{j>i}^{2N}\frac{1}{\mid \vec{r}_i - \vec{r}_j \mid} \\ & -\frac{1}{2}\left(\frac{h^2}{4\pi^2}\right)\sum_{A=1}^{M}\frac{1}{M_A}\nabla_A^2 + \left(\frac{e^2}{4\pi\epsilon_0}\right)\sum_{A=1}^{M}\sum_{B>A}^{M}\frac{Z_A Z_B}{\mid \vec{R}_A - \vec{R}_B \mid}\Bigg] \end{aligned} \quad (2.5)$$

where the first and fourth terms are the kinetic energy operators due to electrons and nuclei respectively, and the other three terms are the potential energy operators due to the nucleus-electron attraction, the electron-electron repulsion and the nucleus-nucleus repulsion respectively [45]. In addition to the constants as defined above, we note that M_A stands for mass of the nuclei, and $\mid \vec{R}_A - \vec{R}_B \mid$ denotes the relative nuclear distance between the A^{th} and B^{th} nucleus, $\mid \vec{r}_i - \vec{r}_j \mid$ and $\mid \vec{r}_i - \vec{R}_A \mid$ are the relative distances between between i^{th} and j^{th} electron, and i^{th} electron and A^{th} nucleus respectively. We choose units such that, $h/2\pi = \hbar = 1(a.u.)$, $\frac{e^2}{4\pi\epsilon_0} = 1\ (a.u.)$

and $\mu = \frac{m_e m_N}{m_e + m_N} \approx m_e = 1$ $(a.u.)$. Then the simplified Hamiltonian in Eq.(2.5) can be written as

$$\begin{aligned} \hat{H} &= \left[-\frac{1}{2}\sum_{j=1}^{2N}\nabla_j^2 - \sum_{j=1}^{2N}\sum_{A=1}^{M}\frac{Z_A}{\mid \vec{r}_j - \vec{r}_A \mid} + \sum_{i}^{2N}\sum_{j>i}^{2N}\frac{1}{\mid \vec{r}_i - \vec{r}_j \mid}\right] \\ &+ \left[-\frac{1}{2}\sum_{A=1}^{M}\frac{1}{M'_A}\nabla_A^2 + \sum_{A=1}^{M}\sum_{B>A}\frac{Z_A Z_B}{\mid \vec{R}_A - \vec{R}_B \mid}\right] \end{aligned} \tag{2.6}$$

where $M'_A = \frac{M_A}{m_e}$.

Born-Oppenheimer (BO) approximation is the first of several approximations used to obtain the solution of the Schrodinger equation for the motion of electrons. In the BO approximation, due to the larger mass of a nucleus compared to an electron's, we can consider the electrons to be moving in the field of fixed nuclei [46]. This means that, in Eq.(2.6) ∇_A^2 term can be neglected (rotation and vibration of nuclei can be treated separately) and V_{NN} to be taken as a constant

$$V_{NN} = \sum_{A}^{M}\sum_{B>A}\frac{Z_A Z_B}{\mid \vec{R}_A - \vec{R}_B \mid} = \text{constant.} \tag{2.7}$$

Therefore, the total energy of the system with fixed nuclei can be written as

$$E_T = E_{elec}(R) + V_{NN} = E(R). \tag{2.8}$$

This is a good approximation with few exceptions [47]. In BO approximation, we have,

$$\hat{H}\Psi(r,R) = E_T\Psi(r,R) \tag{2.9}$$

where

$$\hat{H} = \hat{H}_e + \hat{V}_{NN}(R). \tag{2.10}$$

It is usual to use the method of separation of variables to solve the above Schrodinger equation (Eq. (2.6)), that is,

$$\Psi(r, R) = \psi_R^{elec}(r)\psi^{nucl}(R) \tag{2.11}$$

where $\psi_R^{elec}(r)$ is an electronic wavefunction with fixed nuclei located at R which stands for their nuclear coordinates, and $\psi^{nucl}(R)$ is the nuclear wavefunction determined in some average electron cloud potential field [48].

Then, Eq. (2.9) can be written as

$$(\hat{H}_e + \hat{V}_{NN})\psi_R^{elec}(r)\psi^{nucl}(R) \quad = \quad E_T\psi_R^{elec}(r)\psi^{nucl}(R), \tag{2.12}$$

where $\hat{H}_e$ is referred to as the electronic Hamiltonian. Therefore, in BO approximation (for fixed R), we can divide by $\psi^{nucl}(R)$ and obtain

$$[\hat{H}_e + V_{NN}(R)]\psi_R^{elec} = E(R)\psi_R^{elec}(r) \tag{2.13}$$

where $E_T = E(R)$ (see Eq. (2.8)). Or since V_{NN} gives rise to a constant in BO approximation, we can write the simplified electronic Schrodinger equation as given by

$$\hat{H}_e\psi_R^{elec} = E_{elec}(R)\psi_R^{elec}(r). \tag{2.14}$$

It is noted that if we want to study the motion of nuclei [49], we can re-introduce nuclear-kinetic energy ($\hat{T}_N$) term into the Schodinger equation (Eq. (2.13))

$$[\hat{T}_N + \hat{H}_e + \hat{V}_{NN}(R)]\psi_R^{elec}(r)\psi^{nucl}(R) = E_T\psi_R^{elec}(r)\psi^{nucl}(R). \tag{2.15}$$

And assuming that

$$\hat{T}_N \psi_R^{elec}(r)\psi^{nucl}(R) \cong \psi_R^{elec}(r)\hat{T}_N\psi^{nucl}(R) \tag{2.16}$$

we can rewrite Eq. (2.15) as

$$\psi_R^{elec}(r)[\hat{T}_N + E(R)]\psi^{nucl}(R) = E_{total}\psi_R^{elec}(r)\psi^{nucl}(R). \tag{2.17}$$

Then, cancelling $\psi_R^{elec}(r)$ on both side leads to the nuclear Schrodinger equation,

$$[\hat{T}_N + E(R)]\psi^{nucl}(R) = E_{total}\psi^{nucl}(R) \tag{2.18}$$

where $E(R)$ is the potential energy for the motion of the nuclei and E_{total} is the total energy of the system that includes nuclear (including kinetic energy of nuclei) and electronic contributions.

In this thesis, our focus is on solving the electronic Schrodinger equation Eq. (2.14) with $\hat{H}$ given as

$$\hat{H} \equiv \hat{H}_e = -\frac{1}{2}\sum_{j=1}^{2N}\nabla_j^2 - \sum_{j=1}^{2N}\sum_{A=1}^{M}\frac{Z_A}{\mid \vec{r}_j - \vec{r}_A \mid} + \sum_{i}^{2N}\sum_{j>i}^{2N}\frac{1}{\mid \vec{r}_i - \vec{r}_j \mid}. \tag{2.19}$$

Because electrons are indistinguishable, the $2N$ electron wavefunction, $\psi_R^{elec}(r_1, r_2, ..., r_{2N})$ must be antisymmetric with the interchange of electrons' space coordinates, that is , $\psi_R^{elec}(r_1, ..., r_i, ..., r_j, ..., r_N) \rightarrow -\psi_R^{elec}(r_1, ..., r_j, ..., r_i, ..., r_N)$ (in other words, $\psi_R^{elec}(r_1, r_2, ..., r_{2N})$ must satisfy the Pauli exclusion principle). Therefore, for the $2N$-electrons with N occupied single electron MOs (also called spin-orbitals), $\psi_R^{elec}(r_1, r_2, ..., r_{2N})(= \psi_R^{elec}(1, 2...., 2N))$ can be written in a form of a Slater determinant as follows

$$\psi_R^{elec}(1,2,....,2N) = \frac{1}{\sqrt{(2N)!}} \begin{vmatrix} \psi_1\alpha(1)\ \psi_1\beta(1) & ..... & \psi_N\alpha(1)\ \psi_N\beta(1) \\ \psi_1\alpha(2)\ \psi_1\beta(2) & ..... & \psi_N\alpha(2)\ \psi_N\beta(2) \\ \\ \psi_1\alpha(2N)\ \psi_1\beta(2N) & ..... & \psi_N\alpha(2N)\ \psi_N\beta(2N) \end{vmatrix}$$
$$\equiv |\psi_1\bar{\psi}_1....\psi_N\bar{\psi}_N\rangle. \tag{2.20}$$

where ψ_i is the orbital part of MO, i.e. $\psi_i(\vec{r}_j)$ where i stand for single-electron quantum numbers and α or β is the spin part of the MO. For the $2N$ electrons-single determinant, the electronic energy is obtained as the expectation value of the Hamiltonian [50],

$$E_{elec} = \langle\psi_R^{elec}(1,2,.....,2N)|H_e|\psi_R^{elec}(1,2,.....,2N)\rangle \tag{2.21}$$

where ψ_R^{elec} is normalized and given as in Eq. (2.20). In an expanded form (where we integrated over spin) the total electronic energy is given by,

$$E_{elec} = 2\sum_{j=1}^{N} H_{jj}^{\psi} + \sum_{i}^{N}\sum_{j}^{N}(2J_{ij}^{\psi} - K_{ij}^{\psi}) \tag{2.22}$$

where the one-electron integrals are given by
$H_{ij}^{\psi} = \langle\psi_i(\vec{r}_1) \mid -\frac{1}{2}\nabla_1^2 - \sum_A^M \frac{Z_A}{\vec{r}_{1A}} \mid \psi_j(\vec{r}_1)\rangle = \langle\psi_i(\vec{r}_1) \mid \hbar(\vec{r}_1) \mid \psi_j(\vec{r}_1)\rangle,$
the Coulomb intergrals are given by
$J_{ij}^{\psi} = \langle\psi_i(\vec{r}_1)\psi_j(\vec{r}_2) \mid \frac{1}{\vec{r}_{ij}} \mid \psi_i(\vec{r}_1)\psi_j(\vec{r}_2)\rangle$
and the exchange integrals are given by
$K_{ij}^{\psi} = \langle\psi_i(\vec{r}_1)\psi_j(\vec{r}_2) \mid \frac{1}{\vec{r}_{ij}} \mid \psi_j(\vec{r}_1)\psi_i(\vec{r}_2)\rangle.$

Eq.(2.22) can be solved for the lowest (ground) state energy of the molecular

system using the variational principle [51]

$$\frac{\partial E}{\partial \psi_i} = \frac{\partial \langle \psi \mid H_e \mid \psi \rangle}{\partial \psi_i} = 0. \tag{2.23}$$

This leads to the single-electron Hartree-Fock equations,

$$\hat{f}\psi_i = \epsilon_i \psi_i \; i = 1, 2, ..., N \tag{2.24}$$

where $\hat{f}$ is Hartree-Fock operator and is defined as,

$$\hat{f} = \hat{h} + \sum_{j}^{N} (2\hat{J}_j - \hat{K}_j). \tag{2.25}$$

In Eq. (2.25) $\hat{h}(\vec{r}_1)$ is the single electron energy operator given by

$$\hat{h}(\vec{r}_1) = -\frac{1}{2}\nabla_1^2 - \sum_{A}^{M} \frac{Z_A}{\vec{r}_{1A}}, \tag{2.26}$$

the Coulomb operator is given by

$$\hat{J}_i(\vec{r}_1)\psi_j(\vec{r}_1) = \langle \psi_i(\vec{r}_2) \mid \frac{1}{\vec{r}_{12}} \mid \psi_i(\vec{r}_2) \rangle \psi_j(\vec{r}_1), \tag{2.27}$$

and the exchange operator is given by,

$$\hat{K}_i(\vec{r}_1)\psi_j(\vec{r}_1) = \langle \psi_i(\vec{r}_2) \mid \frac{1}{\vec{r}_{12}} \mid \psi_j(\vec{r}_2) \rangle \psi_i(\vec{r}_1). \tag{2.28}$$

We expand the single electron MOs in terms of basis functions φ_μ,

$$\psi_i = \sum_{\mu=1}^{K} \varphi_\mu C_{\mu i} \tag{2.29}$$

where $C_{\mu i}$ are the molecular orbital expansion coefficients. Therefore, the total electronic wave function can now be written in the matrix form as

$$(\psi_1\psi_2....\psi_K) \;=\; (\varphi_1\varphi_2.....\varphi_K) \begin{bmatrix} C_{11} & C_{12} & \cdots & C_{1K} \\ C_{21} & C_{22} & \cdots & C_{2K} \\ \vdots & \vdots & \ddots & \vdots \\ C_{K1} & C_{K2} & \cdots & C_{KK} \end{bmatrix}. \tag{2.30}$$

Substituting Eq. (2.29) into the Hartree-Fock equations (Eq. (2.24)), we obtain

$$\hat{f}\sum_{\mu}^{K}\varphi_\mu C_{\mu i} = \epsilon_i \sum_{\mu}^{K}\varphi_\mu C_{\mu i}. \tag{2.31}$$

Then, multiplying both side by φ_μ and integrating gives the so called Roothaan's equations which can be written in a matrix form as follows:

$$F^{\chi}C = \varepsilon S^{\chi} C_\epsilon \tag{2.32}$$

where ϵ is a diagonal (eigenvalue) matrix, S^{χ} is the overlap matrix, F^{χ} is Fock matrix, and C is MO coefficient (eigenvector) matrix [52].

Hartree-Fock is not an exact theory since the total electronic wave function is approximated by Slater determinant as given in Eq. (2.20). Hence, HF is an approximation to the solution of $2N$-electron Schrodinger equation. The result of this wave function approximation is that HF theory can only account in part for electron-electron interactions. HF approximation neglects the correlation energy. Correlation energy is defined as the difference between the exact total energy and the total HF

energy of the given molecular system. Correlation energy can be included with the use of density functional theory. The main variable in DFT is the electron density $\rho = \Psi * \Psi$ rather than the electronic wave function Ψ. DFT is discussed below [53, 54, 55].

2.2 Density Functional Theory (Ground State)

Density functional theory is an alternative to ab initio (orbital based) methods for solving the (electronic) Schrodinger equation Eq. (2.1) with the Hamiltonian as given by Eq. (2.19) (in this work we consider the non-relativistic and time-independent solution to Eq. (2.1)). When it was first formulated DFT was thought of as a theory of an atomic or molecular electronic ground state of a system consisting of N-electrons moving in the presence of the nuclear (often called the external) potential. For this (historical) reason we switch to N-electrons (that is the total number of electrons is taken as N instead of $2N$-electrons) in this section [56]. In contrast to the ab initio theories, in the DFT, the energy is taken as a functional of the electron density, $\rho(\vec{r})$, [57]

$$E = E[\rho]. \tag{2.33}$$

Historically, Thomas and Fermi [58] were the first (around 1930) to introduce the total energy of the system as a functional of density. That is, for a uniform electron gas in a solid, they obtained the expression of the total kinetic energy as a functional

of local electron density ρ as given by [59]

$$T_s[\rho] = \frac{3}{10}(3\pi^2)^{2/3}\int d^3\vec{r}\rho^{5/3}(\vec{r}), \tag{2.34}$$

and approximated the exact exchange energy for the interacting N-particle system by

$$E_x[\rho] = -\frac{3}{4}(\frac{3}{\pi})^{1/3}\int \rho^{4/3}(\vec{r})d^3r. \tag{2.35}$$

Thomas and Fermi used the density based energy functionals to calculate ground state energy of metals. However, given the fact that most systems of interest do not have uniform density, Thomas-Fermi theory was of limited applicability. It was not until the 1960's when a more useful density based theory was proposed by Hohenberg and Kohn [60, 61] for the N-electron systems.

2.2.1 Hohenberg-Kohn Theorems

In 1964, Pierre Hohenberg and Walter Kohn formulated the foundations of the DFT [60, 61],which are based on two fundamental theorems. The first Hohenberg-Kohn theorem is an existence theorem that states that ground state electron density ρ of a system uniquely determines (to within a constant) the external potential $v(\vec{r})$ and the Hamiltonian of the N system. Since the N-electron Hamiltonian determines the ground state and all the other properties of the system, the above theorem says that the electron density determines all the ground state properties of the system. Therefore, the total energy of the system can be written as a density functional as

$$E[\rho] = \int \rho(\vec{r})v(\vec{r})d^3r + F[\rho] \tag{2.36}$$

with

$$F[\rho] = T[\rho] + V_{ee}[\rho] \tag{2.37}$$

where $F[\rho]$ is the universal functional of the electron density, ρ, that includes the kinetic energy functional of N electrons ($T[\rho]$) and the potential energy functional due to the electron-electron interactions ($V_{ee}[\rho]$). The form of this functional ($F[\rho]$) is not known. The expression $\int \rho(\vec{r})v(\vec{r})d^3r$ is the potential energy functional due to electron-nucleus interactions [62].

The second Hohenberg-Kohn theorem uses the energy variational principle to state that a given trial electron density ρ gives higher energy than the true ground state energy that is for

$$\rho(\vec{r}) \geq 0 \tag{2.38}$$

with the constraint that

$$\int \rho(\vec{r})d^3r = N \tag{2.39}$$

$$E_o \leq E_v[\rho] \tag{2.40}$$

where the $E(\rho)$ is the energy of the system in the external potential v and E_0 is the exact ground state energy [63]. Given the above constraint, the following variational equation,

$$\frac{\delta E[\rho]}{\delta \rho(\vec{r})} - \mu = 0 \tag{2.41}$$

where μ is the Lagrange multiplier and it is identified to be the chemical potential of the system [64], which must be solved in order determine the ground state density and all the other properties (including the total energy) of an N-electron system.

The above discussion reviews the foundation of the DFT but the suggested solution (i.e. the variational method) is not a very practical one, since as indicated above, the functional form of the universal energy functional $F[\rho]$ is not known. An alternative method was suggested by Kohn and Sham [65]. Their method is discussed below.

2.2.2 The Kohn-Sham Equations

In 1965, Kohn-Sham proposed a practical way of solving the above variational equation [65] (see Eq. (2.41)). In their method they introduce a fictitious system of N-non-interacting electrons with the external poterntial $v_s(\vec{r})$ that produces the (actual) $\rho(\vec{r})$ as described above. In this approach, the ground state kinetic energy (T_s) is expressed as [66],

$$T_s[\rho] \;=\; \sum_i^N \langle\psi_i|-\frac{1}{2}\nabla^2|\psi_i\rangle \tag{2.42}$$

where the ψ_i's are the single particle orbitals for non-interacting N-electron system (oftern referred to as the s-system) and the electrons density is given by

$$\rho(\vec{r}) \;=\; \sum_i |\psi_i(\vec{r})|^2. \tag{2.43}$$

The ground state energy for the interacting N-electron system then becomes,

$$E \;=\; T_s + \int d^3r\, v(\vec{r})\,\rho(\vec{r}) + J[\rho] + E_{xc}[\rho] \tag{2.44}$$

where $J[\rho]$ is the functional that contains the contribution due to Coulomb electron-electron interactions and E_{xc} is the exchange-correlation functional given by,

$$E_{xc}[\rho] \;=\; T[\rho] - T_s[\rho] + V_{ee}[\rho] - J[\rho] \tag{2.45}$$

where $T[\rho]$ is the kinetic energy determined from the orbitals ψ_i ($T_s = -1/2 \sum_i^{occ} \langle \psi_i \mid \nabla^2 \mid \psi_i \rangle$) that are the solutions to Eq. (2.46).

The variational method is again applied to Eq.(2.44) and the resultant equations are the so called Kohn-Sham equations [67]. That is, the electrons satisfy the one-particle Schrodinger equations given as

$$[-\frac{1}{2}\nabla^2 + v_{eff}(\vec{r})]\psi_i \;=\; \varepsilon_i \psi_i, \qquad i = 1, ...N \tag{2.46}$$

which are similar to the usual single particle Schodinger equations, except that the effective potential $v_{eff}(\vec{r})$ is given by

$$v_s = v_{eff}(\vec{r}) = V_c + v_{xc}(\vec{r}) = v(\vec{r}) + \int \frac{\rho(\vec{r}\,')}{\mid \vec{r} - \vec{r}\,' \mid} d\vec{r}\,' + \frac{\delta E_{xc}}{\delta \rho(\vec{r})}. \tag{2.47}$$

The expression for $v_{eff}(\vec{r})$ includes an additional exchange-correlation potential v_{xc} (the V_c is the usual term that includes the potential due to nuclei ($v(\vec{r})$) and the Coulomb potential due to ρ). v_{xc} is the functional derivative of the exchange-correlation energy functional with respect to the density,

$$v_{xc}(\vec{r}) \;=\; \frac{\delta E_{xc}[\rho]}{\delta \rho}. \tag{2.48}$$

As stated above, this set of nonlinear equation is called Kohn-Sham equations. These equations have a similar structure to the HF equations but with the non-local (HF) exchange potential replaced by the local exchange-correlation potential v_{xc} and orbitals are now single electron. It should be noted that E_{xc} contains an element of the kinetic energy and is not just the sum of the exchange and correlation energy as they are understood in HF and correlated wavefunction theories [68]. Today Kohn-Sham formulation of the DFT has become one of the the most popular electronic structure theories that is employed to obtain the ground state properties (including the energy) of a given N-electron system [69].

2.2.3 Exchange-Correlation Functionals

The exact form of the exchange-correlation energy functional is not known. Approximations for E_{xc} must be used in computations. The simplest E_{xc} functional is the local density approximation (LDA) [70]. The basis of all approximate exchange-correlation functionals is the LDA, which has the following form

$$E_{xc}^{LDA}[\rho] = \int \rho(\vec{r})\varepsilon_{xc}(\rho(\vec{r}))d^3r. \tag{2.49}$$

Here, $\varepsilon_{xc}(\rho(\vec{r}))$ is the exchange-correlation energy of a homogeneous electron gas with density $\rho(\vec{r})$. If the spin up and spin down electron densities are not equal (i.e. $\rho_\uparrow \neq \rho_\downarrow$) then local LDA is generalized to include spin dependance and LDA becomes LSDA where S stands for spin. The exchange-correlation energy functional is typically

splitted into exchange and correlation energy contributions,

$$E_{xc}[\rho] \quad = \quad E_x[\rho] + E_c[\rho]. \tag{2.50}$$

Many approximations have been proposed for $E_{xc}[\rho]$ [71]. In this work, we used one of the most popular hybrid functionals, which includes a mixture of Hartree-Fock exchange with DFT exchange-correlation, it is called the B3LYP method and is defined by

$$E_{xc}^{B3LYP} = (1-a)E_x^{LSDA} + aE_x^{exact} + b\Delta E_x^{B88} + (1-c)E_c^{LSDA} + cE_c^{LYP} \tag{2.51}$$

where, the a, b and c parameters are determined by fitting to experimental data and depend on the chosen forms for E_x^{GGA} and E_c^{GGA}, with values $a \sim 0.2$, $b \sim 0.7$ and $c \sim 0.8$ [72]. Also, the E_x^{LSDA} is the LSDA non-gradient corrected exchange functionals, E_x^{exact} is the exact HF exchange energy, E_x^{B88} is the Becke88 exchange functional (it was proposed by A. D. Becke as a correction to the LSDA exchange energy), E_c^{LSDA} is the LSDA for local correlation (due to VWN is the Vosko, Wilk and Nusair functional introduced in 1980) [73]) , and E_c^{LYP} is the LYP correlation functional (due to Lee, Yang and Parr) [74].

2.3 Dispersion Corrected DFT

In other molecular cases, we used the empirically dispersion corrected DFT approach B97D [75, 76] (B97D was obtained from the nonhybrid generalized gradient B97). The B97D was proposed and developed by Grimme. In the B97D functional, power expansion series coefficients of the original functional (B97) description were opti-

mized by Grimme to restrict the density functional description to the shorter electron correlation ranges, while the medium to long-range descriptions were handled by the semiempirical correction term [77].

DFT/B97D approach has been proven accurate for descripetions of non-covalent interactions between organic molecules [77]. These inter-molecular interactions are type of forces acting between atoms and molecules due to the instantaneous dipole-induced dipole forces, also referred to as van der Waals or dispersion. From semiempirical treatment of non-bonded interactions we can obtain the dispersion correction, and the total energy is given by

$$E_{total} = E_{DFT} + E_{disp} \tag{2.52}$$

$$E_{disp} \propto CR^{-6} \tag{2.53}$$

where E_{DFT} is the usual self-consistent Kohn-Sham energy as obtained from the chosen DFT approximation and E_{disp} is an empirical dispersion correction (see section 1.4 for the definition of dispersion).

2.4 Long-Range Corrected DFT

As we explained above the hybrid functional B3LYP is very successful in obtaining electronic properties of molecular systems. However, it is unsuccessful in a number of important applications [78] such as determining the polarizability of long chains. For this reason, Yanai combines the features of hybrid exchange-correlation functional such as B3LYP with the long range corrected functionals, and proposed a new

Coulomb attenuated hybrid exchange-correlation functional (CAM-B3LYP) [78].

Yanai has replaced the Becke parameter α by two parameters α and β for mixing Becke's 1988 exchange and HF exchange, with μ describing the conversion from one to the other. According to his prescription he divides the one over the interelectronic distance $\frac{1}{r_{12}}$ as follows

$$\frac{1}{r_{12}} = \frac{1-[\alpha+\beta(erf(\mu r_{12}))]}{r_{12}} + \frac{\alpha+\beta(erf(\mu r_{12}))}{r_{12}} \tag{2.54}$$

where the first part corresponds to the short range and the second part to the long range and $0 \leq \alpha+\beta \leq 1$, $0 \leq \alpha \leq 1$, $0 \leq \beta \leq 1$ and erf is an error function. In CAM-B3LYP approximation the E_{xc} is given by

$$E_x^{B3} = (1-\alpha)E_x^{Slater} + \alpha E_x^{HF} + c^{B88}\Delta E_x^{B88} \tag{2.55}$$

where $\alpha = 0.19$, $\alpha+\beta = 0.65$ and $\mu = 0.33$ [79]. The CAM-B3LYP method improves long range interaction and gives better description of molecules with long bonds and reaction barriers.

2.5 Long-Range Corrected DFT with Dispersion Corrections

A new functional (wB97XD) results from the re-optimizing of a recently proposed long-range corrected (LC) hybrid density functional, with empirical dispersion corrections [79]. Chai [80, 81] introduced an empirical dispersion correction to the wB97X, to provide the missing pieces of the long-range vdW interactions and following Grimme's

work [82, 83], he denoted the new functional as wB97XD. The following equation represents the total energy,

$$E_{DFT-D} = E_{KS-DFT} + E_{disp} \tag{2.56}$$

where wB97X approximation is used for E_{KS-DFT} and the dispersion correction is given by

$$E_{disp} = -\sum_{i=1}^{N_{at}-1} \sum_{j=i+1}^{N_{at}} \frac{C_6^{ij}}{R_{ij}^6} f_{damp}(R_{ij}). \tag{2.57}$$

C_6^{ij} is the dispersion coefficient for atom pair ij, N_{at} is the number of atoms in the system, and R_{ij} is an interatomic distance. The parameters in the wB97X-D are determined self-consistently by a least squares fitting procedure, and the optimized value of w= 0.2 Bohr^{-1}.

The performance of w-D type of functionals was tested by comparing with the results obtained with three well-established DFT-D functionals (B97D, B3LYP-D, and BLYP-D) and with LC hybrid functionals (wB97X and wB97) for atomization energies, equilibrium geometries, reaction energies, non-covalent interaction energies, and a charge transfer excited states [84]. The optimized functional such as wB97XD is shown to be significantly superior for non-bonded interactions and very similar in performance for bonded interactions.

Chapter 3

Computational Details

The electronic structure calculations, to compute the energies, and geometry optimizations of the molecules in vacuo, were performed with the Gaussian 09 [85] package available on the computer cluster (Placentia) at the Atlantic Computational Excellence Network (ACEnet) and the computer cluster (Grex) in the Western Canadian Research Grid (Westgrid) facilities. The CPU (Central Processing Unit) in our group at ACE-net uses four processors and the requirement of the RAM (Random Access Memory) is of the order of 5 GB per job for each CPU. Also, the ACEnet machines have extra space for parallel jobs with large scratch files on queue called "no-quota scratch" (nqs). Jobs submitted to Westgrid take about a month for each calculation to be completed on 6 CPUs and the requirement of the memory is of the order of 6 GB for each job.

All calculations were performed using density functional theory (DFT). We used four DFT approximations, B3LYP, B97D, CAM-B3LYP, and wB97XD, which were discussed in Chapter 2. First we used the popular hybrid functional B3LYP to obtain the optimized structure of isolated oligomers. Then we continued our calculations us-

ing the dispersion corrected DFT's (B97D, wB97XD) because of the demonstrated importance of the non-covalent dispersion forces when treating interactions of oligomers with nanotubes. Long range corrected DFT/CAM-B3LYP was also used for comparison purposes.

6-31G(d) basis set (called the polarized split-valence double zeta basis set) was used in all our calculations. It comprises a linear combination of six Gaussian primitives for the inner-shell functions, and combinations 3 and 1 represent the valence orbitals, 2s, 2s′, 2p(3), and 2p′(3). Number 3 in the basis set indicates the number of Gaussian primitives used to construct the 2s and 2p(3) basis functions. Number 1 gives the number of Gaussian primitives used to construct the 2s′ and 2p′(3) basis functions. d means d-type polarization functions (function of higher angular momentum than the occupied atomic orbitals) and is added to each non-hydrogen atom in the molecule. The criteria of the self consistent force (SCF) convergence are as follows: the maximum component of the force is below the cutoff value 0.00045 N; the root mean square of the force (RMS) is below 0.0003 N; the calculated displacement for the next step should be below the cutoff value 0.0018 Å; and the root mean square of the displacement for the next step is below 0.0012 Å [86]. These criteria for convergence were set by Gaussian [85] and are considered sufficient for obtaining energy minima.

VMD, a molecular visualization program for displaying, animating and analyzing large molecular systems using 3-D graphics and built-in scripting was used to generate the input file for SWCNTs with (6,5) [87]. In addition, we used ACD/ChemSketch (Freeware) to sketch the OPE-ALD and OPE-DTF conjugated oligomers schemes [88].

All single molecular system (isolated oligomer and nanotubes) calculations were

fully geometry optimized. For the combinations of nanotube and oligomer, we used "opt=modredundant". This allowed us to explicitly freeze (F) the variables in the nanotube atoms during the optimization while keeping the oligomers geometry parameters active.

GaussView 5.0.8 was used as a visualization tool for generating the input files, displaying the output file geometries and analyzing Gaussian data files [89]. GaussView can be used to determine the bond lengths (R), bond angles (A), dihedral angles (D) (as labelled in Scheme 1.1), and other properties such as dipole moment. The dipole moment (which is defined as the sum of the products of the charge and the distance between the two charges) provides information about the charge polarization in the polymer since dipole moment becomes nonvanishing when there is a separation of charge. They can occur between two ions in an ionic bond or between atoms in a covalent bond; they arise from differences in electronegativity. If the difference in electronegativity is large, then the dipole moment is also large. The distance between the charge separation is also a deciding factor in the size of the dipole moment. The polarity of the molecule can be estimated from its dipole moment. We determined the effect of the dispersion on the dipole moment of the isolated oligomer by calculating dipole moment difference.

$$\Delta\mu = \sqrt{(\mu_x - \mu'_x)^2 + (\mu_y - \mu'_y)^2 + \mu_z - \mu'_z)^2} \tag{3.1}$$

where, for example, μ_x, μ_y, and μ_z are the dipole moment components of the oligomer in gas phase, and μ'_x, μ'_y, and μ'_z are the dipole moment components of the oligomer interacting with nanotube. They were obtained by subtracting nanotubes dipole moment components from the respective dipole moment components of the oligomer

nanotube combination. We also computed the difference between the total magnitudes of their dipole moments, $\Delta\mu_{Total}$, defined as:

$$\Delta\mu_{Total} = |\vec{\mu}_{Total}| - |\vec{\mu}'_{Total}|. \tag{3.2}$$

In addition, for the gas phase oligomers, we obtained the highest occupied (HOMO) and the lowest unoccupied (LUMO) molecular orbital eigenvalues and their differences ($\Delta\varepsilon_{H-L}$=ε_{LUMO}-ε_{HOMO}).

Wolfram Mathematica version 9.0 [90] was used to calculate the average intermolecular distance between OPE and SWCNT. Using two sets of data that represent the x, y, and z coordinates of SWCNT and OPE, we determined the location of the centre coordinates of SWCNT and OPE and obtained the total distance (d_{total}) by subtracting them (see Fig. 3.1). Next, we determine the radius of SWCNT (see Fig. 3.2). Finally, we subtracted the radius of SWCNT from the total distance and obtained intermolecular distance (Δd) as follow

$$\Delta d = d_{total} - r. \tag{3.3}$$

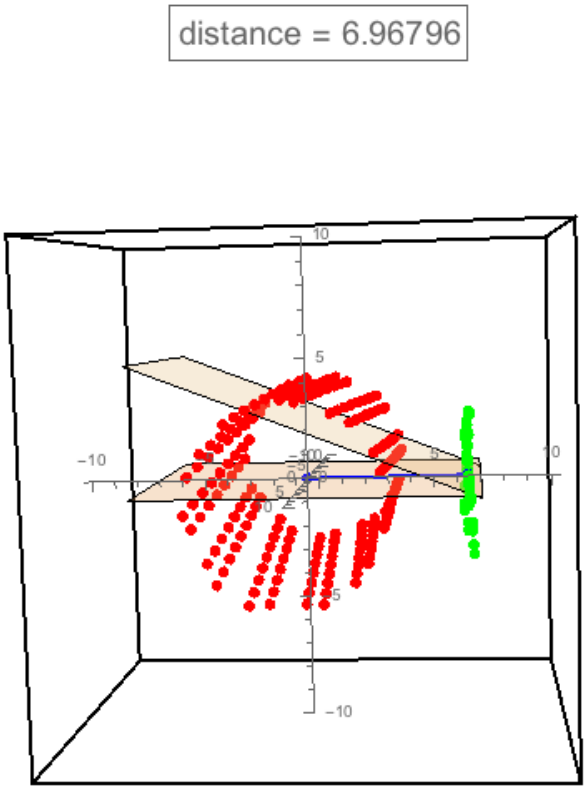

Figure 3.1: Typical example of the distance between the centre of SWCNT (red) and the centre of the oligomer (green) using Mathematica.

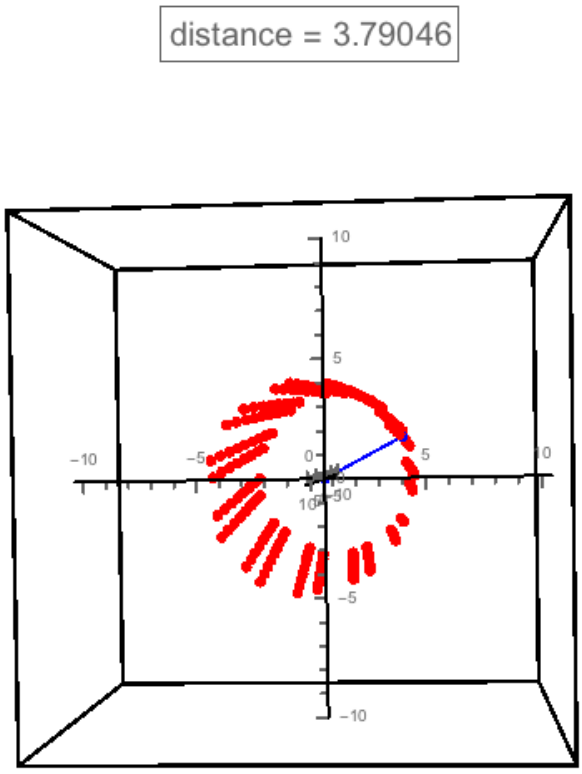

Figure 3.2: Typical example of the radius of SWCNT using Mathematica.

Chapter 4

Structure and Electronic Properties of Isolated Oligo(phenylene ethynylene)s

In this chapter, we apply DFT methods to obtain the geometrical and electronic structure of the oligo(phenylene ethynylene) (OPE), with different end groups, aldehyde (ALD) and dithiafulvene (DTF), in the gas phase. In particular, B3LYP, B97D, wB97XD, and CAM-B3LYP-DFT approximations (with 6-31G(d) basis set) are used to investigate the structure and electronic properties of OPE-ALD and OPE-DTF in the gas phase. We also include the results of MM calculations (using UFF). Since the electronic properties are closely related to the geometries of the systems, we first discuss the geometrical parameters, such as bond lengths (R), bond angles (A), and dihedral angles (D), of OPE-ALD and OPE-DTF.

4.1 Comparison of DFT Methods

4.1.1 Geometry of OPEs

OPE molecules belong to a class of fully conjugated molecules. The benzenes and alkynes in the OPE molecule contain delocalized states in the form of π-bonds, which are beneficial for electron transport. This particular type of molecules has recently attracted much attention because of the high electron conductivity of the phenylene ethynylene backbone [91]. We have optimized ALD/DTF-end-capped OPE conjugated oligomers in a linear-shaped molecular structure (Figs. 4.1 and 4.5 without side chains, and in Figs. 4.3 and 4.7 with side chains). In the initial structure of the DFT computation, all bonds are set to be equal along the backbone. The geometry optimization (which minimizes the energy) modifies the molecular bonds in such a way that the output structure has alternating shorter and longer bonds along the backbone. The chemical structure and labelling of atoms of OPEs are depicted in Scheme 4.1. In this section, we compare the optimized structure of OPE obtained using B3LYP with those obtained using other DFT approximations and MM (UFF). The complete details regarding the structure are given in the Appendix.

Fig. 4.1 shows the typical optimized geometric structure of OPE-ALD. As expected, the phenylene ethynylene unit (-C_6H_4-C≡C-C_6H_4-C≡C-C_6H_4-) forms a nearly straight line. Fig. 4.2 shows the differences between the B3LYP bond lengths, bond angles and dihedral angles and other DFT methods and MM (UFF) for OPE-ALD (without side chains). In Fig 4.2, chart (a) the differences in bond lengths are shown. As we can see, all DFT methods are very similar (differences are less than 0.01 Å) except for UFF which shows larger differences. Fig 4.2 chart (a) also shows that B97D gives bond lengths that are longer than those for B3LYP while wB97XD and

CAM-B3LYP give bond lengths that are shorter than those for B3LYP. This pattern of large differences for the MM (UFF) and the small differences for the DFT methods can also be seen in bond angle chart (b). In fact, it is not shown in the Fig. 4.2 (b) but for MM (UFF), the bond angles differences for (6-7-8), (7-8-9), (12-13-14), and(13-14-15) bond angles, are of the order of 55° (for bond angles (1-2-3), (5-6-7), (8-9-10), (11-12-13), (14-15-16), and (18-19-20), the differences are of the order of 3°). Bond angles differ by less than 0.5° in most cases for DFT methods. Fig. 4.2. (c) shows the difference in dihedral angles (torsional angle). We see that the dihedral angles differences are largest for the four central dihedral angles (6-7-8-9), (7-8-9-10), (11-12-13-14), and (12-13-14-15). The differences are less than 20° in these four cases. It should be noted that the OPE-ALD structure as obtained using MM (UFF) is not linear, instead it has the trans geometry (also has wrong middle C-C bonds which are double instead of triple, see Fig. A.1 in the Appendix).

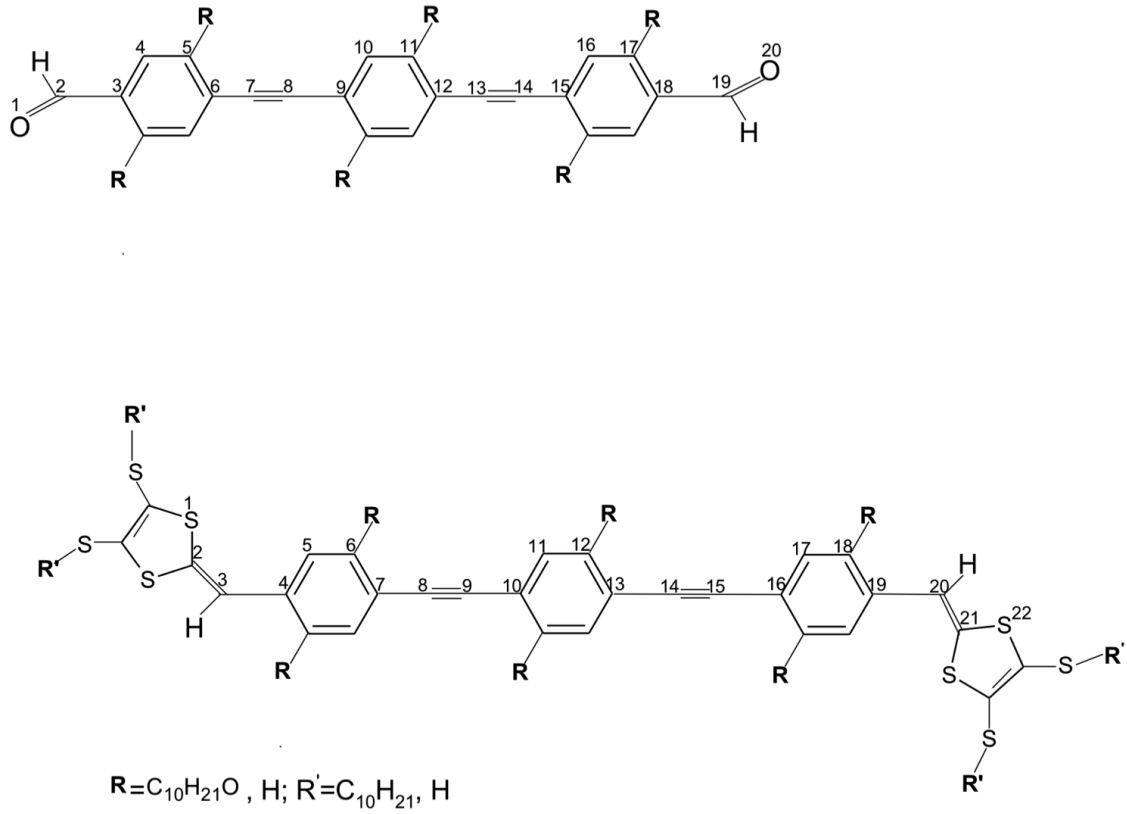

Scheme 4.1: Chemical structures of ALD- and DTF-ended OPEs with the atoms labelled.

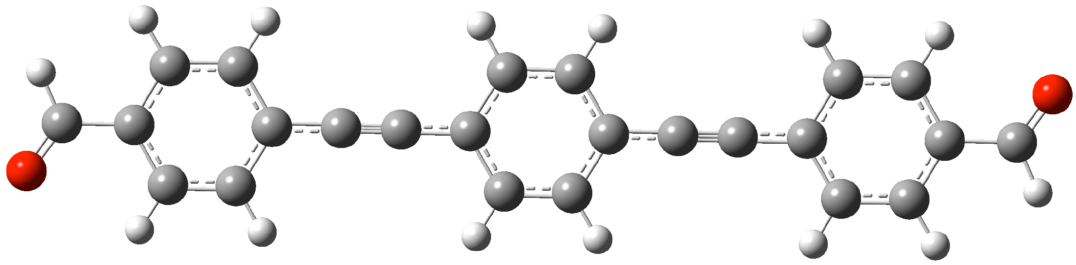

Figure 4.1: Representative optimized structure of OPE-ALD (without side chains) in gas phase obtained using DFT/B97D (similar results were obtained with B3LYP, wB97XD, and CAM-B3LYP with 6-31G* basis set).

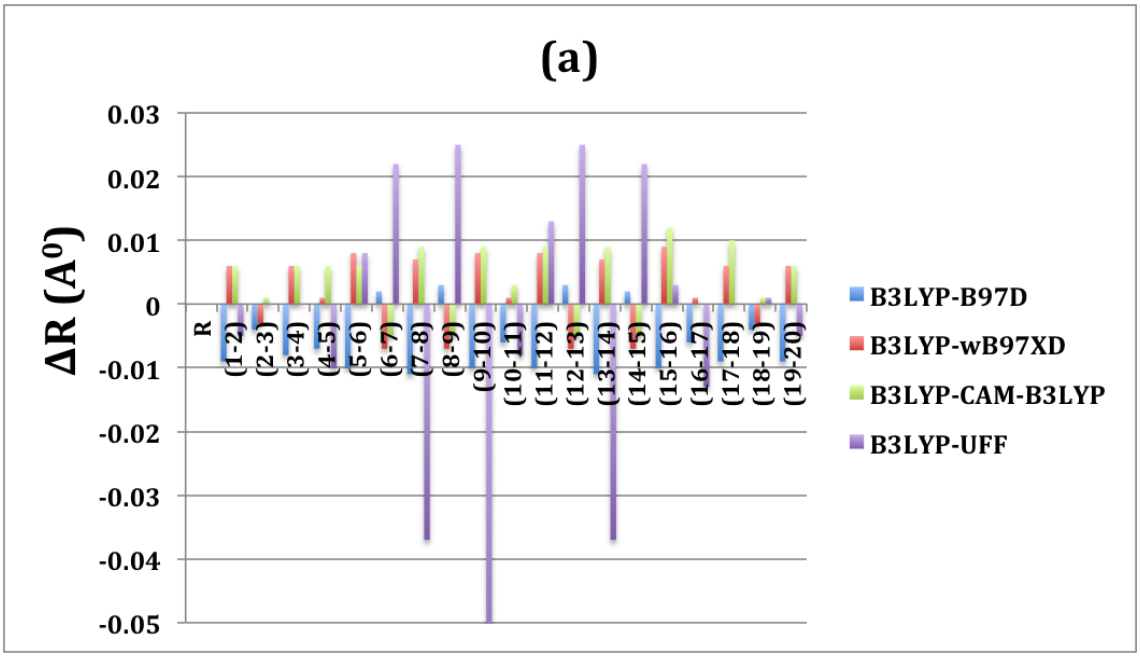
(a)
ΔR (A⁰)
0.03
0.02
0.01
0
-0.01
-0.02
-0.03
-0.04
-0.05
R
(1-2)
(2-3)
(3-4)
(4-5)
(5-6)
(6-7)
(7-8)
(8-9)
(9-10)
(10-11)
(11-12)
(12-13)
(13-14)
(14-15)
(15-16)
(16-17)
(17-18)
(18-19)
(19-20)
B3LYP-B97D
B3LYP-wB97XD
B3LYP-CAM-B3LYP
B3LYP-UFF

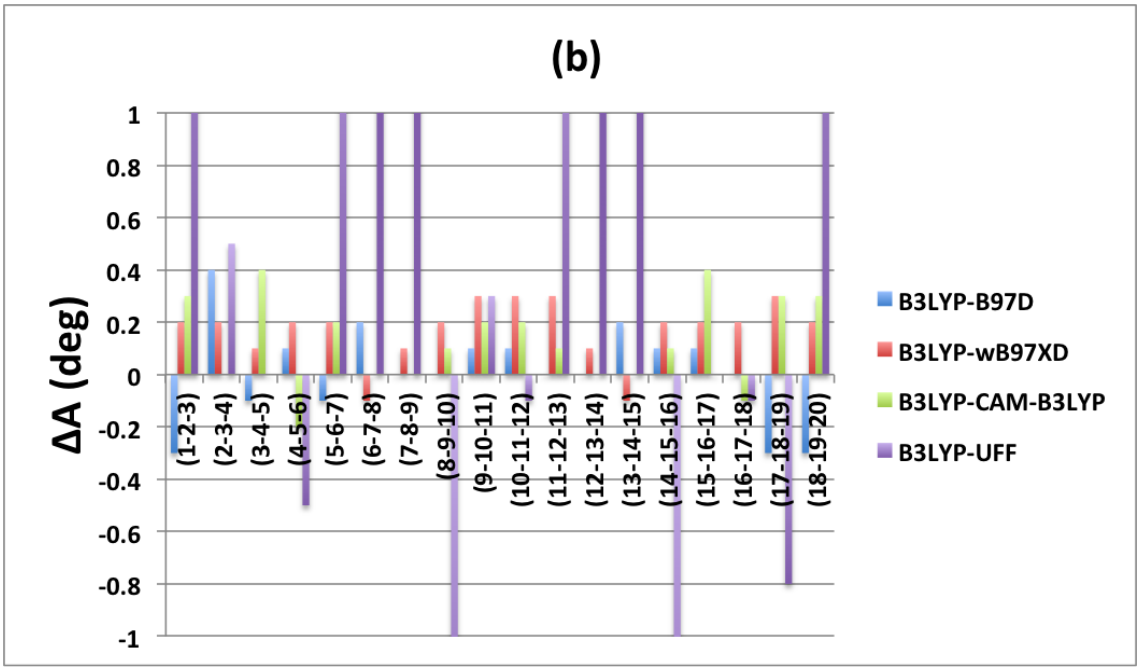
(b)
ΔA (deg)
1
0.8
0.6
0.4
0.2
0
-0.2
-0.4
-0.6
-0.8
-1
(1-2-3)
(2-3-4)
(3-4-5)
(4-5-6)
(5-6-7)
(6-7-8)
(7-8-9)
(8-9-10)
(9-10-11)
(10-11-12)
(11-12-13)
(12-13-14)
(13-14-15)
(14-15-16)
(15-16-17)
(16-17-18)
(17-18-19)
(18-19-20)
B3LYP-B97D
B3LYP-wB97XD
B3LYP-CAM-B3LYP
B3LYP-UFF

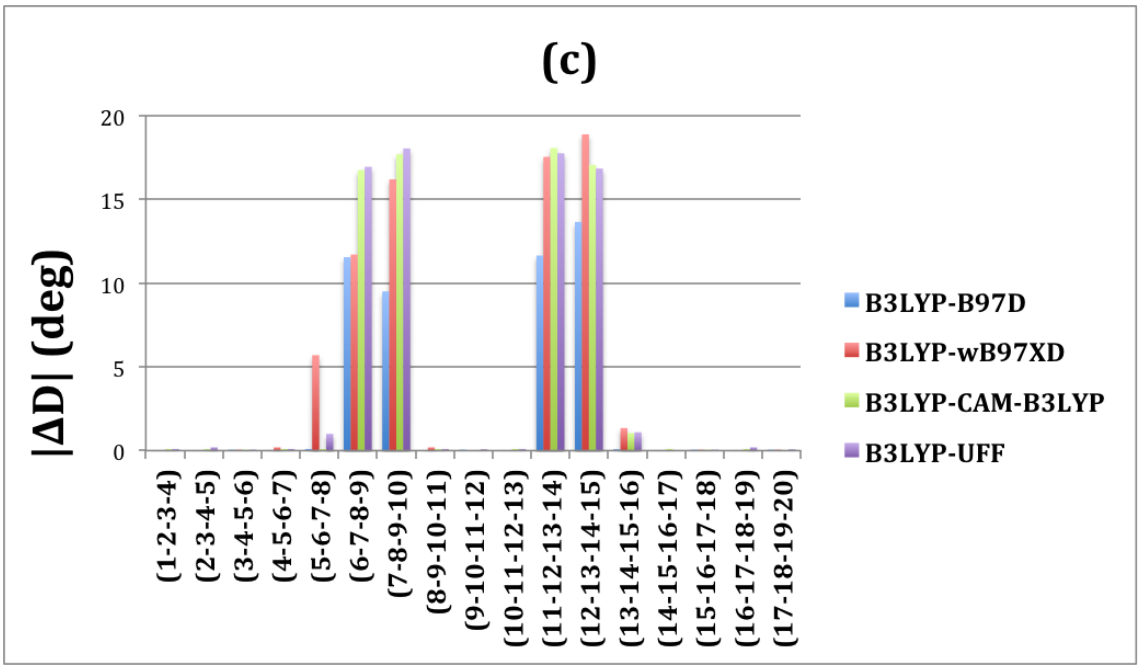

Figure 4.2: Comparison of B3LYP structure with other DFT approximations and molecular mechanics (UFF) results for OPE-ALD (without side chains). The labelling of atoms is shown in Scheme. 4.1. This figure shows differences between (a) bond lengths, (b) bond angles, and (c) dihedral angles as obtained with a given DFT or UFF approximation relative to B3LYP corresponding results.

Fig. 4.3 shows the typical (DTF) optimized structure of OPE-ALD with side chains. Fig. 4.4, chart (a) shows that MM (UFF) gives the largest deviations from B3LYP bond lengths (could be as large as 0.04 Å). B97D, wB97XD and CAM-B3LYP show similar differences of the order of 0.01 Å. As before B97D gives bond lengths that are longer and wB97XD and CAM-B3LYP give bond lengths that are shorter than those for B3LYP. B97D has the smallest difference. In Fig. 4.4 (b), we can see that MM (UFF) also has the largest differences. As for OPE-ALD without side chains, the four angles (6-7-8), (7-8-9), (12-13-14), and (13-14-15) display differences of the order of 55° which is consistent with the trans structures of OPE-ALD obtained using MM (UFF). For the DFT methods, B97D gives the largest differences (of the order of 1.5° for ((6-7-8) and (13-14-15) bond angles). In Fig. 4.4, chart (c), the result show that the structures of OPE-ALD obtained using wB97XD becomes more nonplanar than those obtained using the other DFT methods.

Fig. 4.5 shows the typical optimized geometric structure of OPE-DTF without side chains. For bond lengths and bond angles (see Figs. 4.6 (a) and (b)), we observe similar trends in their differences to what we obtained for OPE-ALD (see discussion above). For the dihedral angles (Fig 4.6 (c)), the biggest differences again have been observed in the ethynylene part of OPE-DTF (similar to OPE-ALD).

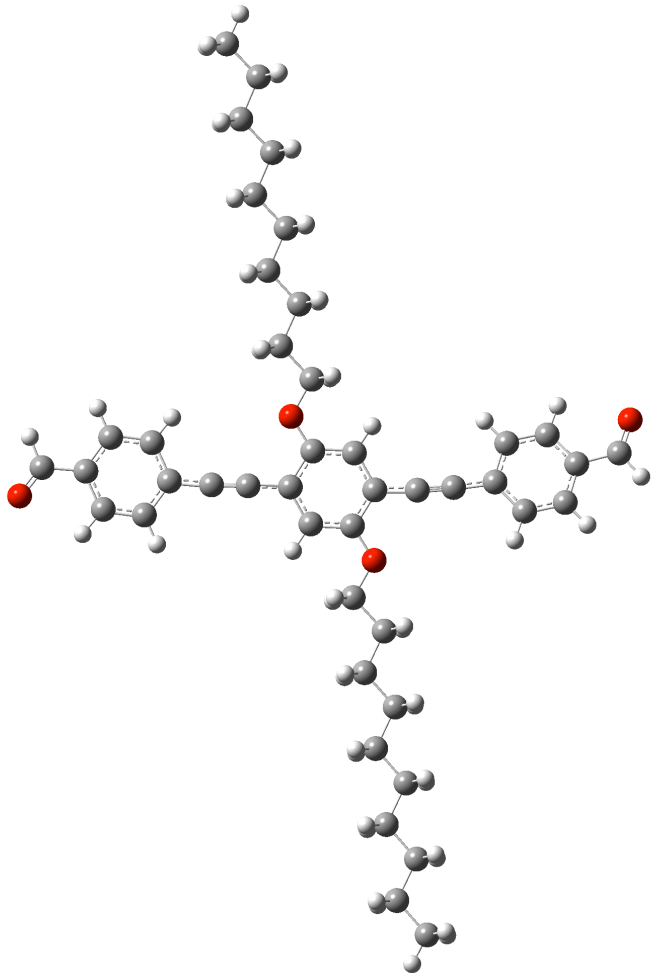

Figure 4.3: Representative optimized structure of OPE-ALD (with side chains) in gas phase obtained using DFT/B97D (similar results were obtained with B3LYP, wB97XD and CAM-B3LYP with 6-31G* basis set).

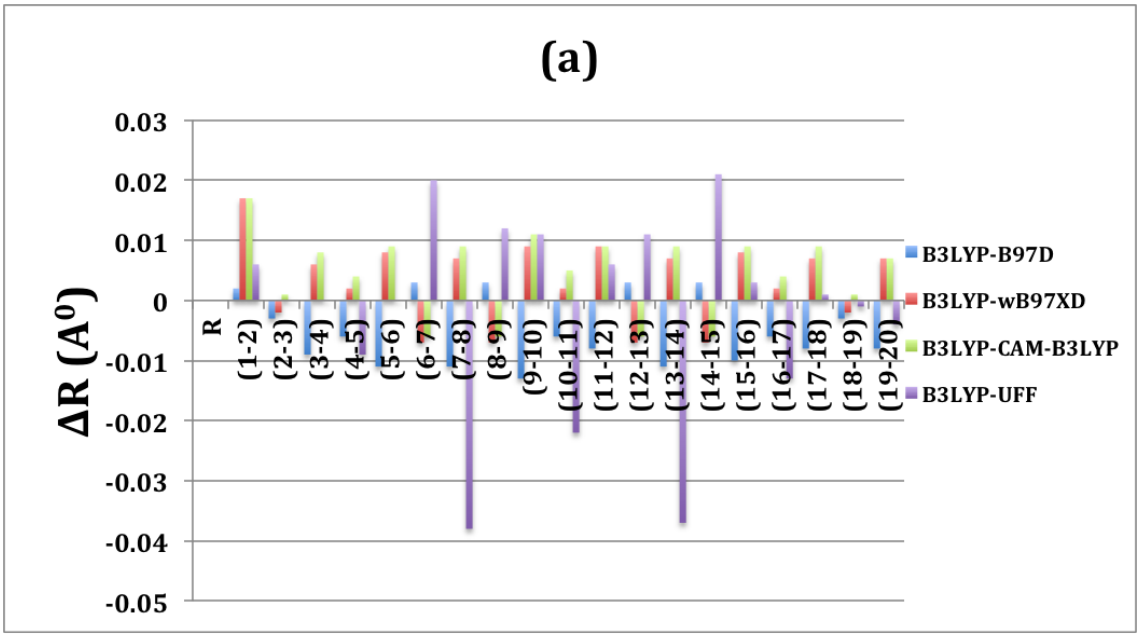
(a)
0.03
0.02
0.01
0
-0.01
-0.02
-0.03
-0.04
-0.05
ΔR (A⁰)
R
(1-2)
(2-3)
(3-4)
(4-5)
(5-6)
(6-7)
(7-8)
(8-9)
(9-10)
(10-11)
(11-12)
(12-13)
(13-14)
(14-15)
(15-16)
(16-17)
(17-18)
(18-19)
(19-20)
B3LYP-B97D
B3LYP-wB97XD
B3LYP-CAM-B3LYP
B3LYP-UFF

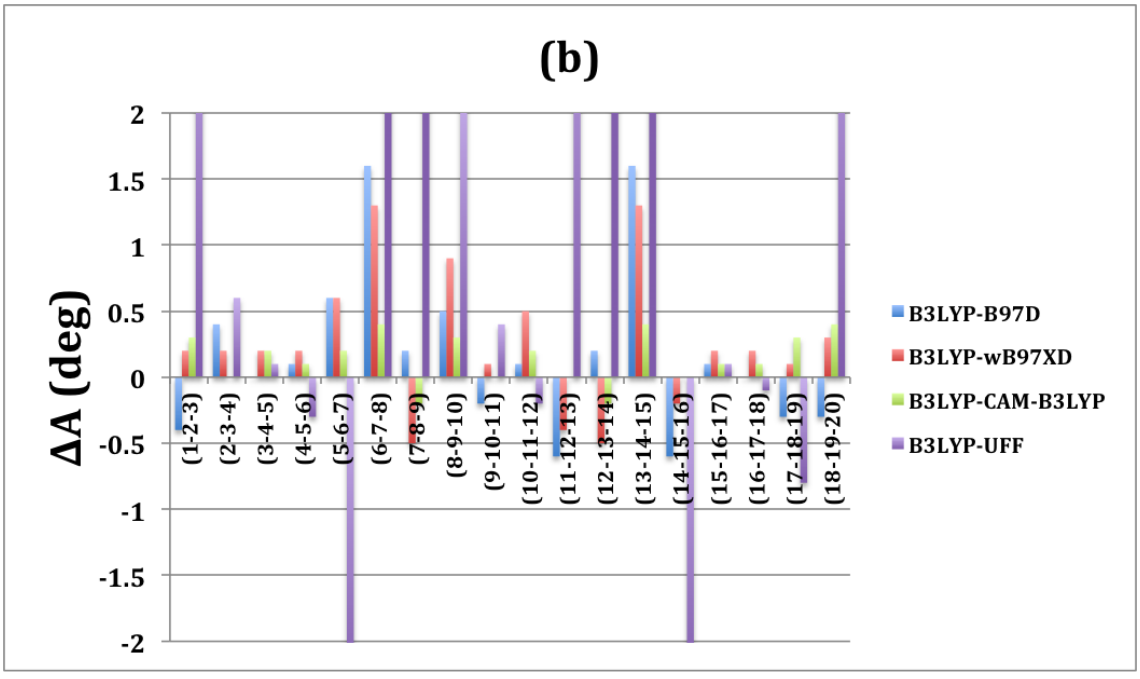
(b)
2
1.5
1
0.5
0
-0.5
-1
-1.5
-2
ΔA (deg)
(1-2-3)
(2-3-4)
(3-4-5)
(4-5-6)
(5-6-7)
(6-7-8)
(7-8-9)
(8-9-10)
(9-10-11)
(10-11-12)
(11-12-13)
(12-13-14)
(13-14-15)
(14-15-16)
(15-16-17)
(16-17-18)
(17-18-19)
(18-19-20)
B3LYP-B97D
B3LYP-wB97XD
B3LYP-CAM-B3LYP
B3LYP-UFF

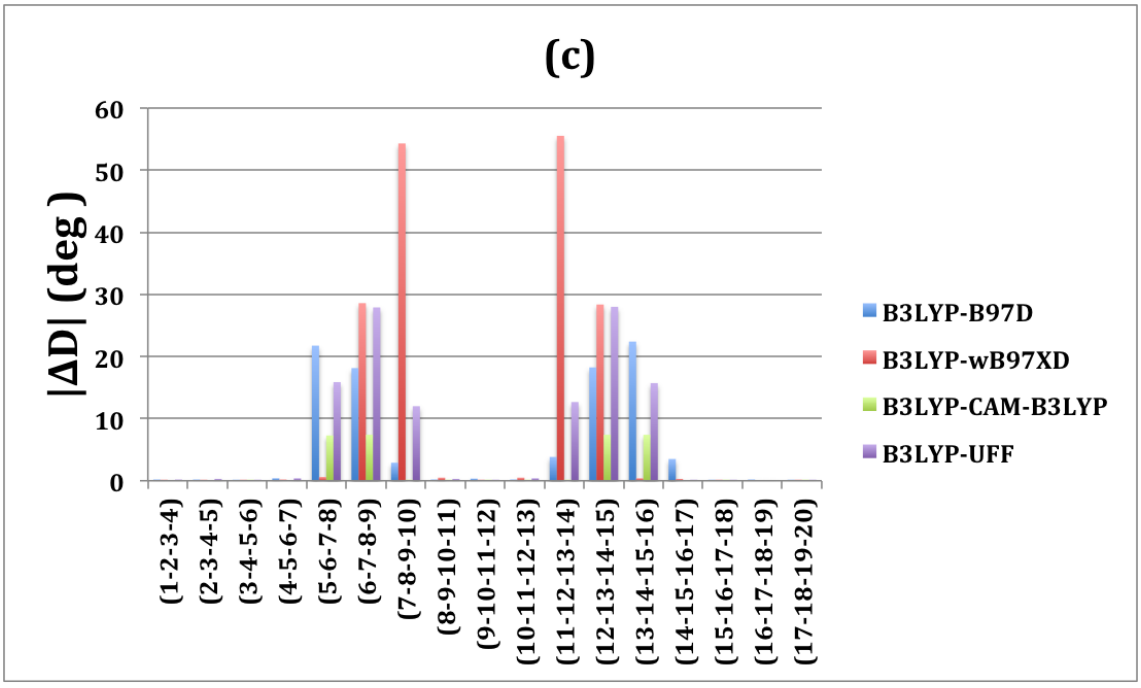

Figure 4.4: Comparison of B3LYP structure with other DFT approximations and molecular mechanics (UFF) results for OPE-ALD (with side chains). The labelling of atoms is shown in Scheme. 4.1. This figure shows difference between (a) bond lengths, (b) bond angles and (c) dihedral angles as obtained with a given DFT or UFF approximation relative to B3LYP corresponding results.

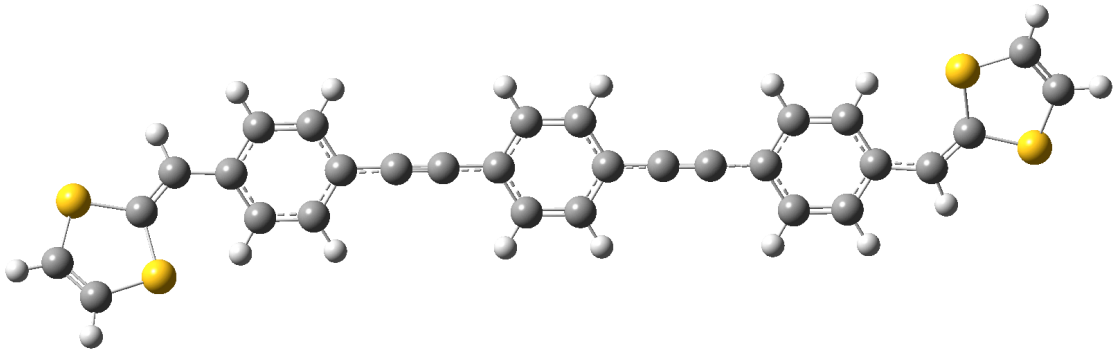

Figure 4.5: Representative optimized structure of OPE-DTF (without side chains) in gas phase obtained using DFT/B97D (similar results were obtained with B3LYP, wB97XD, and CAM-B3LYP with 6-31G* basis set).

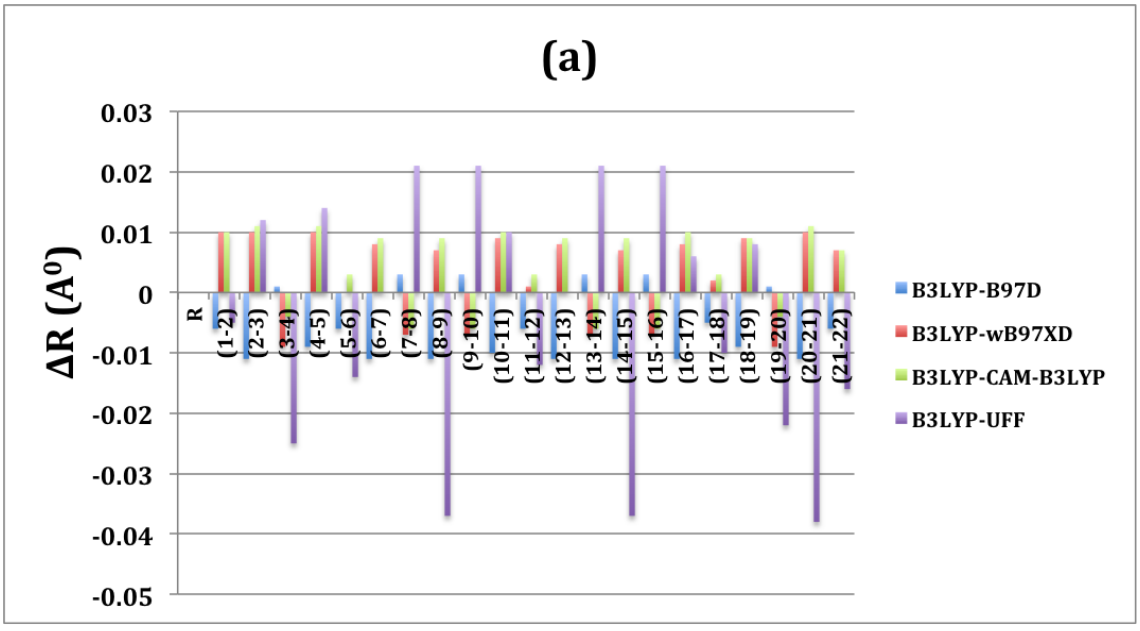

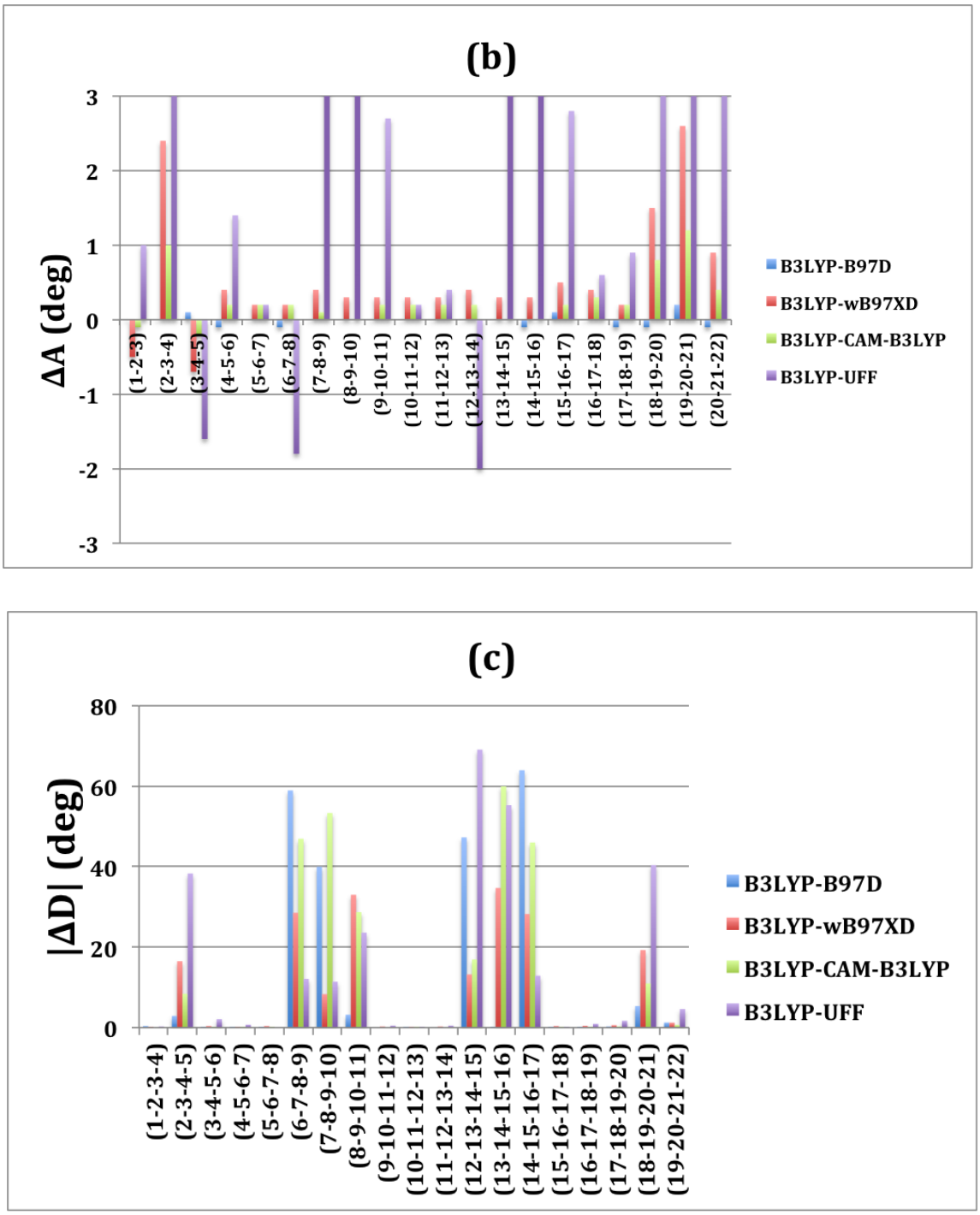

Figure 4.6: Comparison of B3LYP structure with other DFT approximations and molecular mechanics (UFF) results for OPE-DTF (without side chains). The labelling of atoms is shown in Scheme 4.1. This figure shows difference between (a) bond lengths, (b) bond angles and (c) dihedral angles as obtained with a given DFT or UFF approximation relative to B3LYP corresponding results.

The typical optimized structure of OPE-DTF (with side chains) in the gas phase is shown in Fig. 4.7. Similar comments, regarding bond lengths, bond angles, and dihedral angles, can made for OPE-DTF with side chains as for the previous OPEs discussed above (see Fig. 4.8).

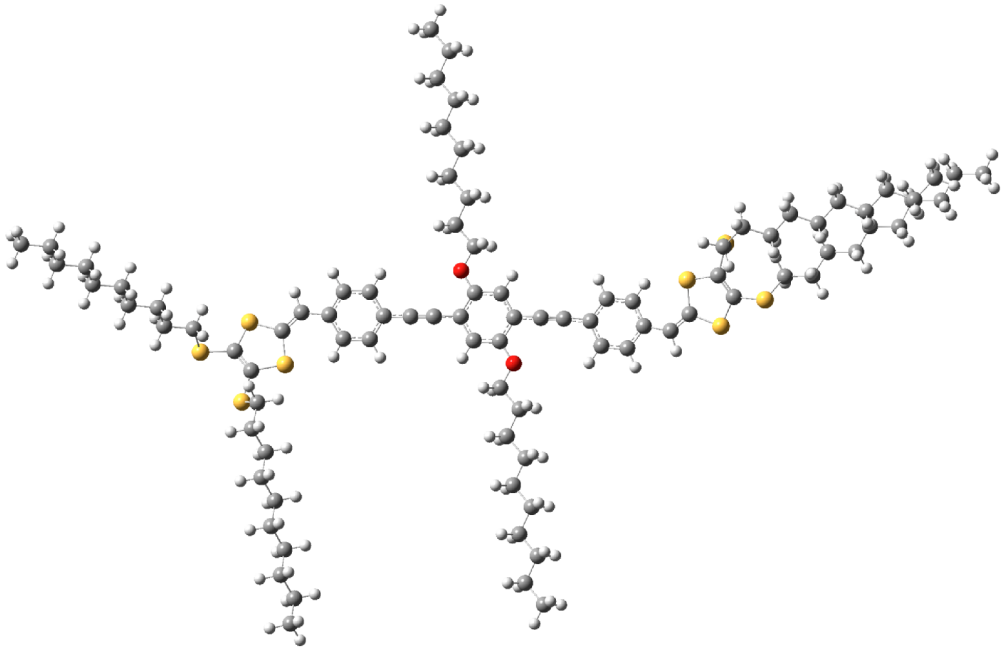

Figure 4.7: Representative optimized structure of OPE-DTF (with side chains) in gas phase obtained using DFT/B97D (similar results were obtained with B3LYP, wB97XD, and CAM-B3LYP with 6-31G* basis set).

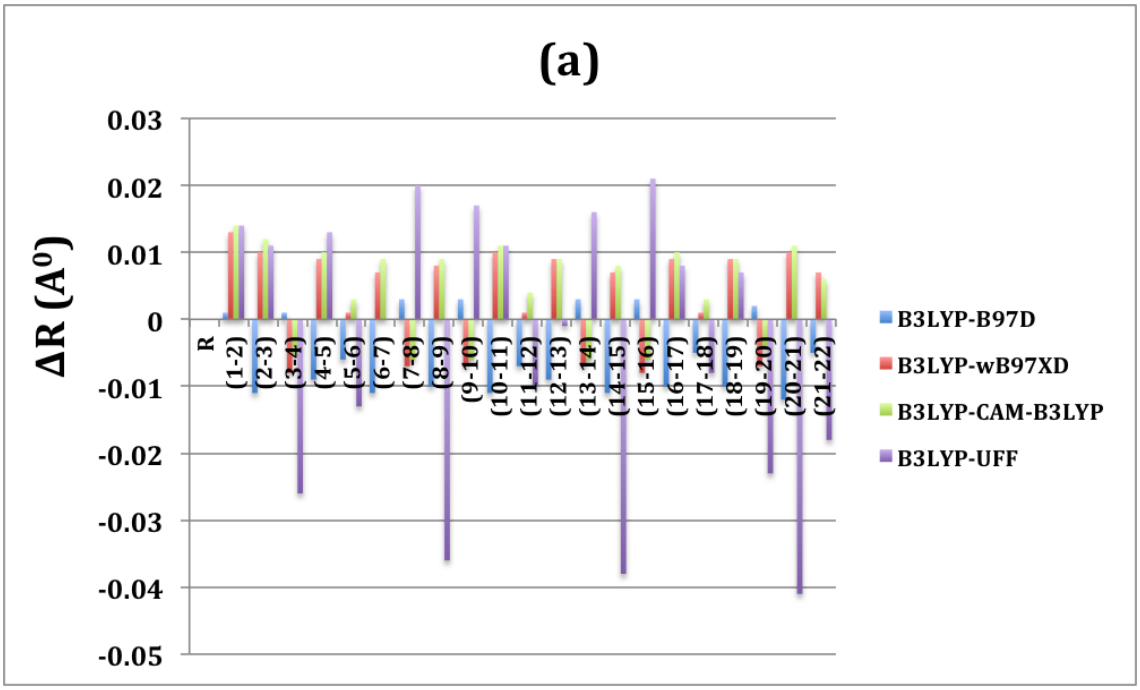
(a)
ΔR (A⁰)
0.03
0.02
0.01
0
-0.01
-0.02
-0.03
-0.04
-0.05
R
(1-2)
(2-3)
(3-4)
(4-5)
(5-6)
(6-7)
(7-8)
(8-9)
(9-10)
(10-11)
(11-12)
(12-13)
(13-14)
(14-15)
(15-16)
(16-17)
(17-18)
(18-19)
(19-20)
(20-21)
(21-22)
B3LYP-B97D
B3LYP-wB97XD
B3LYP-CAM-B3LYP
B3LYP-UFF

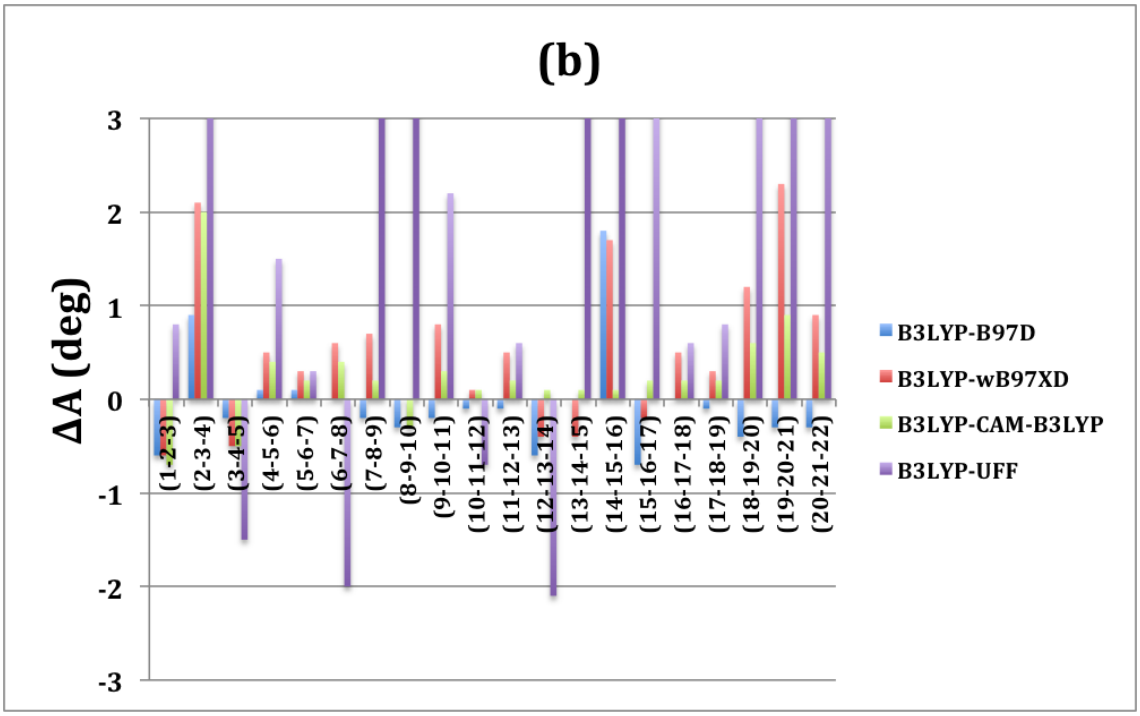
(b)
ΔA (deg)
3
2
1
0
-1
-2
-3
(1-2-3)
(2-3-4)
(3-4-5)
(4-5-6)
(5-6-7)
(6-7-8)
(7-8-9)
(8-9-10)
(9-10-11)
(10-11-12)
(11-12-13)
(12-13-14)
(13-14-15)
(14-15-16)
(15-16-17)
(16-17-18)
(17-18-19)
(18-19-20)
(19-20-21)
(20-21-22)
B3LYP-B97D
B3LYP-wB97XD
B3LYP-CAM-B3LYP
B3LYP-UFF

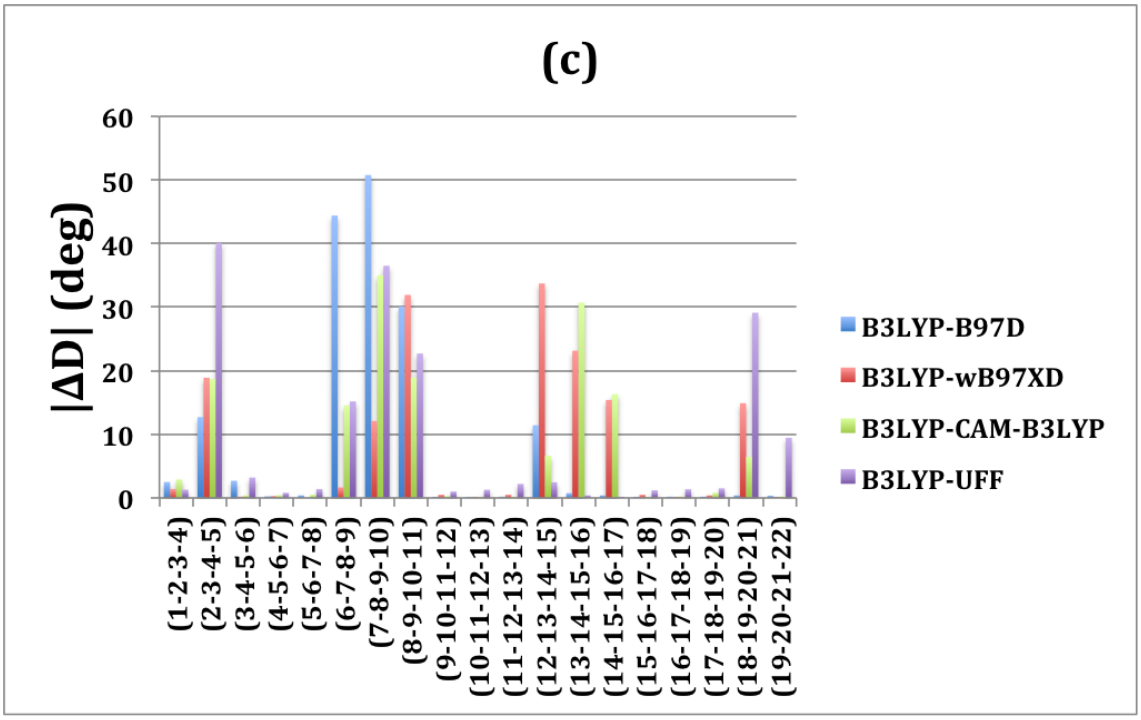

Figure 4.8: Comparison of B3LYP structure with other DFT approximations and molecular mechanics (UFF) results for OPE-DTF (with side chains). The labelling of atoms is shown in Scheme 4.1. This figure shows difference between (a) bond lengths, (b) bond angles and (c) dihedral angles as obtained with a given DFT or UFF approximation relative to B3LYP corresponding results.

4.1.2 Eigenvalues and Dipole Moments

The magnitude and direction of dipole moment give the information about the charge polarizations in the oligomer. The dipole moment is defined as the sum of the products of the charge and the distance between the two charges. Typical example of the x, y, and z axes used in the determination of the dipole moment direction is shown in Fig. 4.9 for a given oligomer without side chains. The three components of dipole moments are aligned along the backbone (x), perpendicular (y) and out of the oligomer plane (z) directions. Tables 4.1 shows that, in the case of OPE-ALD (without side chains), the magnitude and components of dipole moments are almost equal to zero for all DFT methods. The magnitude and components of dipole moments for OPE-ALD with side chains (see Table 4.2) are also nearly equal to zero but their components are determined relative to coordinate system as shown in Fig. 4.10.

Table 4.3 shows that in the case of OPE-DTF without side chains the dipole moments are all close to 1 Debye and the largest components points out of the oligomer plane. For OPE-DTF with side chains the results for dipole moment as given in Table 4.4 show that the dipole moments increase to approximately 5 Debye in all DFT cases and the largest components still point out of the oligomer plane (the components are determined relative to coordinate system as shown in Fig. 4.11).

We present the results of the HOMO (ε_{HOMO}) and LUMO (ε_{LUMO}) eigenvalues and their differences (HOMO-LUMO gaps $\Delta\varepsilon_{H-L}$) calculated using four different DFT methods: B3LYP, B97D, wB97XD, and CAM-B3LYP in Tables 4.1 - 4.4. DFT/B3LYP is known is give relatively accurate values for $\Delta\varepsilon_{H-L}$ for molecular systems [92]. Relative to the B3LYP HOMO-LUMO gaps, the B97D values are smaller by approximately 1 eV in all cases OPE-ALD and OPE-DTF with and without side

chains (see Tables 4.1-4.4). wB97XD and CAM-B3LYP give values that are considerably larger than B3LYP (wB97XD is larger approximately by 3.5 eV and CAM-B3LYP is larger approximately by 2.5 eV, see Tables 4.1-4.4). The reason why wB97XD and CAM-B3LYP give such large $\Delta\varepsilon_{H-L}$'s is because in these DTF approximations the HOMO is lowered (by less than 2 eV) and the LUMO is raised (by more than 1 eV) relative to B3LYP values.

Table 4.1: The dipole moment components (μ_x, μ_y, μ_z), total magnitude (μ) (in Debye), and HOMO and LUMO eigenvalues and their difference ($\Delta\varepsilon_{H-L} = \varepsilon_{LUMO}$-$\varepsilon_{HOMO}$) (all in eV) for OPE-ALD (without side chains) determined using B97D, wB97XD, CAM-B3LYP, and B3LYP with 6-31G* basis set.

	B97D	**wB97XD**	**CAM-B3LYP**	**B3LYP**
μ **(μ_x, μ_y, μ_z)**	**0.00** **(0.00, 0.00, 0.00)**	**0.00** **(0.00, -0.00, 0.00)**	**0.00** **(0.00, 0.00, 0.00)**	**0.00** **(0.00, 0.00, 0.00)**
ε_{HOMO}	**-5.26**	**-7.72**	**-7.14**	**-5.92**
ε_{LUMO}	**-3.15**	**-0.84**	**-1.35**	**-2.58**
$\Delta\varepsilon_{H-L}$	**2.10**	**6.87**	**5.78**	**3.33**

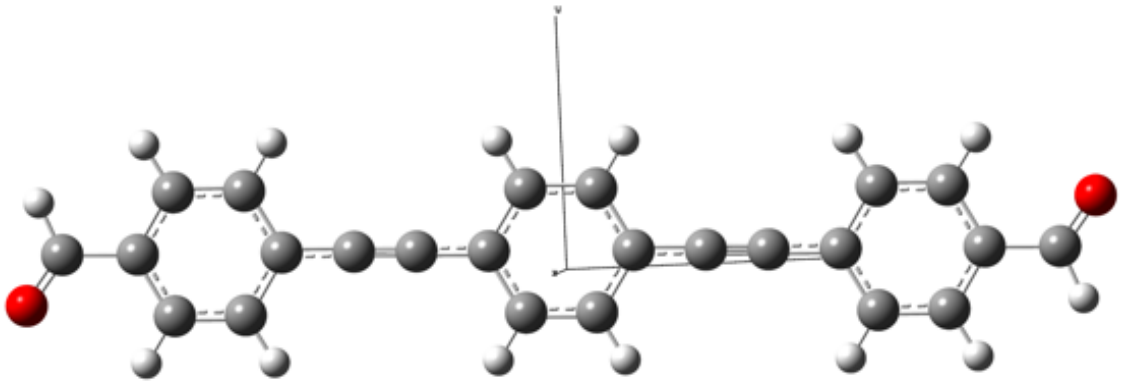

Figure 4.9: Typical example of the x, y, and z axes used in the determination of the dipole moment direction in Table 4.1.

Table 4.2: The dipole moment components (μ_x, μ_y, μ_z), total magnitude (μ) (in Debye), and HOMO and LUMO eigenvalues and their difference ($\Delta\varepsilon_{H-L} = \varepsilon_{LUMO}$-$\varepsilon_{HOMO}$) (all in eV) for OPE-ALD (with side chains) determined using B97D, wB97XD, CAM-B3LYP, and B3LYP with 6-31G* basis set.

	B97D	**wB97XD**	**CAM-B3LYP**	**B3LYP**
μ (μx, μy, μz)	**0.00 (0.00, 0.00, 0.00)**	**0.00 (-0.00, -0.00, 0.00)**	**0.00 (0.00,0.00,0.00)**	**0.00 (0.00, 0.00,-0.00)**
εHOMO	**-4.72**	**-7.19**	**-6.63**	**-5.42**
εLUMO	**-2.96**	**-0.70**	**-1.22**	**-2.42**
ΔεH-L	**1.76**	**6.48**	**5.40**	**2.99**

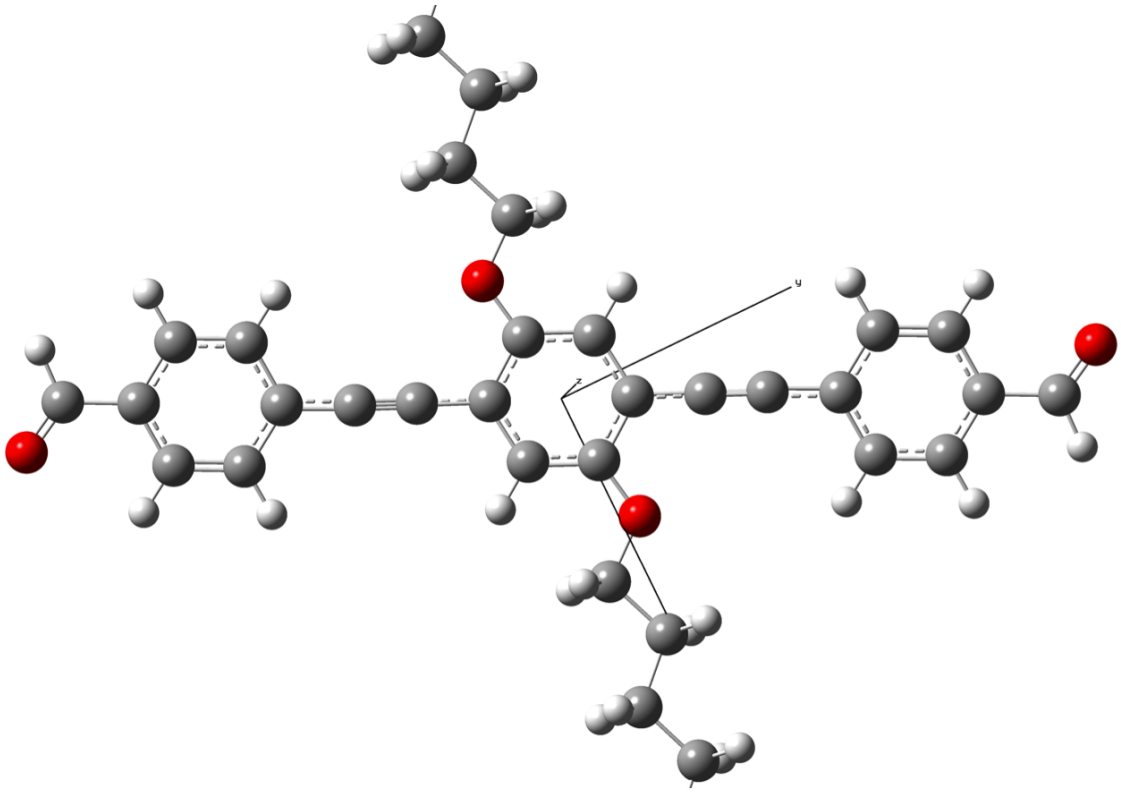

Figure 4.10: Typical example of the x, y, and z axes used in the determination of the dipole moment direction of OPE-ALD (with side chains) in Table 4.2.

Table 4.3: The dipole moment components (μ_x, μ_y, μ_z), total magnitude (μ) (in Debye), and HOMO and LUMO eigenvalues and their difference ($\Delta\varepsilon_{H-L}$ = ε_{LUMO}-ε_{HOMO}) (all in eV) for OPE-DTF (without side chain) determined using B97D,wB97XD, CAM-B3LYP, and B3LYP with 6-31G* basis set.

	B97D	**wB97XD**	**CAM-B3LYP**	**B3LYP**
μ **(μ_x, μ_y, μ_z)**	**0.77** **(-0.00, 0.00, 0.77)**	**1.31** **(0.00, 0.00, 1.31)**	**0.89** **(0.00, 0.00, 0.89)**	**0.49** **(0.02, -0.00, 0.49)**
ε_{HOMO}	**-4.10**	**-6.66**	**-6.06**	**-4.78**
ε_{LUMO}	**-2.29**	**-0.18**	**-0.69**	**-1.81**
$\Delta\varepsilon_{H-L}$	**1.80**	**6.47**	**5.36**	**2.96**

Table 4.4: The dipole moment components (μ_x, μ_y, μ_z), total magnitude (μ) (in Debye), and HOMO and LUMO eigenvalues and their difference ($\Delta\varepsilon_{H-L} = \varepsilon_{LUMO}$-$\varepsilon_{HOMO}$) (all in eV) for OPE-DTF (with side chains) determined using B97D,wB97XD, CAM-B3LYP, and B3LYP with 6-31G* basis set.

	B97D	wB97XD	CAM-B3LYP	B3LYP
μ (μ_x, μ_y, μ_z)	2.43 (1.72, 0.94, 1.43)	4.79 (0.65, -1.39, 4.53)	1.76 (0.00, 0.00, 1.76)	3.82 (-1.79, -1.34, 3.09)
ε_{HOMO}	-3.88	-6.46	-5.91	-4.6
ε_{LUMO}	-2.15	-0.07	-0.62	-1.70
$\Delta\varepsilon_{H-L}$	1.73	6.39	5.29	2.90

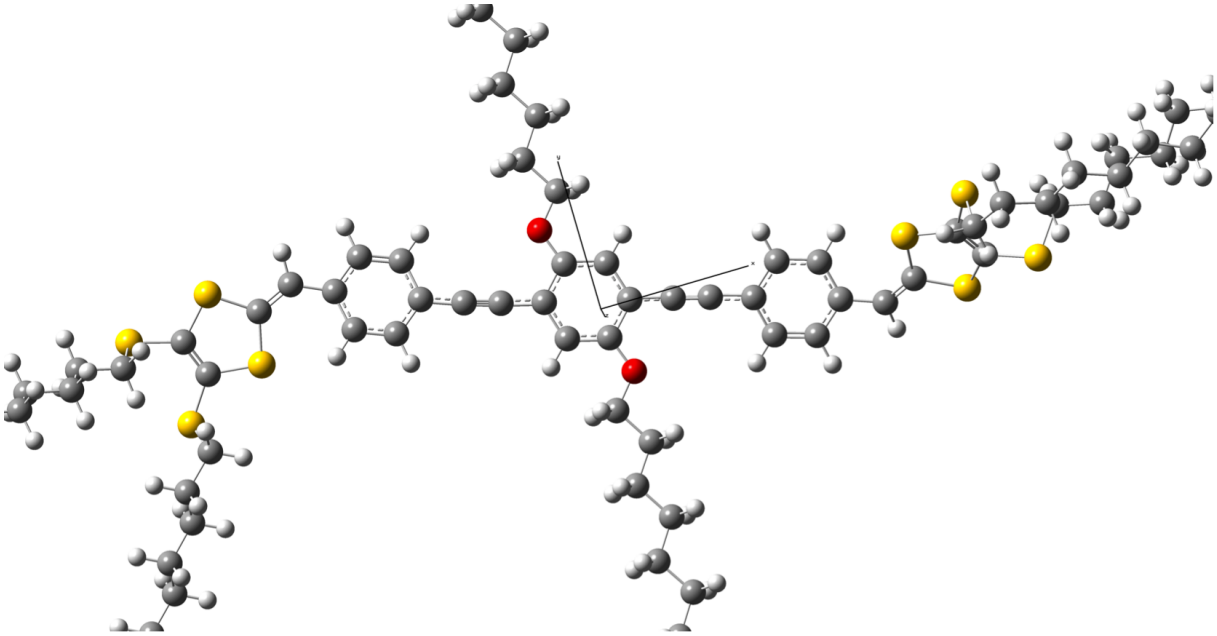

Figure 4.11: Typical example of the x, y, and z axes used in the determination of the dipole moment direction of OPE-DTF (with side chains) in Table 4.4.

4.2 The Effect of End Groups

4.2.1 Geometry of OPEs

In this section, we investigate the effect of the end-group on the backbone structure of OPE, using again B3LYP, B97D, wB97XD, and CAM-B3LYP DFT methods. We compared the backbone structure (which starts with atom 2 and ends with atom 19 for OPE-ALD and starts with atom 3 and ends with atom 20 for OPE-DTF in Scheme 4.1) of OPE-ALD with OPE-DTF. Figs. 4.12 and 4.13 show the differences between their bond lengths, bond angles, and dihedral angles.

In Fig. 4.12 (a) we present the comparison of bond lengths of OPE-ALD with those of OPE-DTF without side chains. Only the end bonds, (2-3) and (3-4) in OPE-ALD and (3-4) and (5-6) in OPE-DTF, show differences of the order of 0.02 Å for all DFT methods. Similarly for bond angles, the biggest difference are observed at the ends of the oligomer backbones (the differences are in the range 2-5°). In contrast, for the dihedral angles, the biggest differences are observed for the central angles ((5-6-7-8), (6-7-8-9), (7-8-9-10) and (11-12-13-14), (12-13-14-15), (13-14-15-16)) located between the phenyl rings. This leads to OPE-DTF becoming somewhat twisted relative to OPE-ALD planar structure (see Fig. 4.14). Fig. 4.13 shows similar trends for bond length, bond angle, and dihedral angle differences between OPE-ALD and OPE-DTF with side chains.

In summary, the end groups have, as expected, affected the end bonds and angles in the oligomer backbones. However, in some cases, the end groups can also have an effect on the central parts of the backbone. In particular, DTF causes the backbone to become nonplanar.

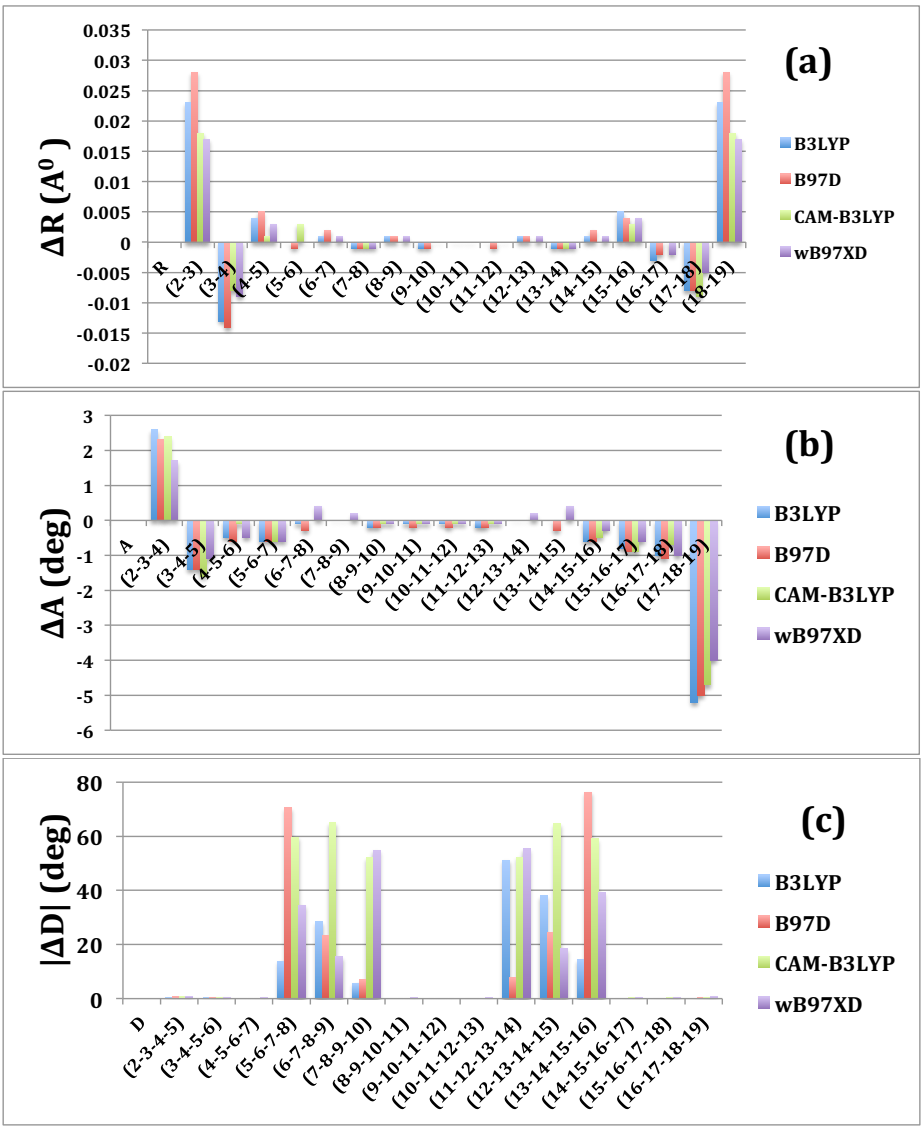

Figure 4.12: Comparison of OPE-ALD with OPE-DTF (without side chains) structures using different DFT approximations as indicated in the figure. In this figure the atoms are labelled according to OPE-ALD numbering (top graph) in Scheme 4.1. This figure shows the difference between (a) bond lengths, (b) bond angles and (c) dihedral angles of oligomers with two different end groups.

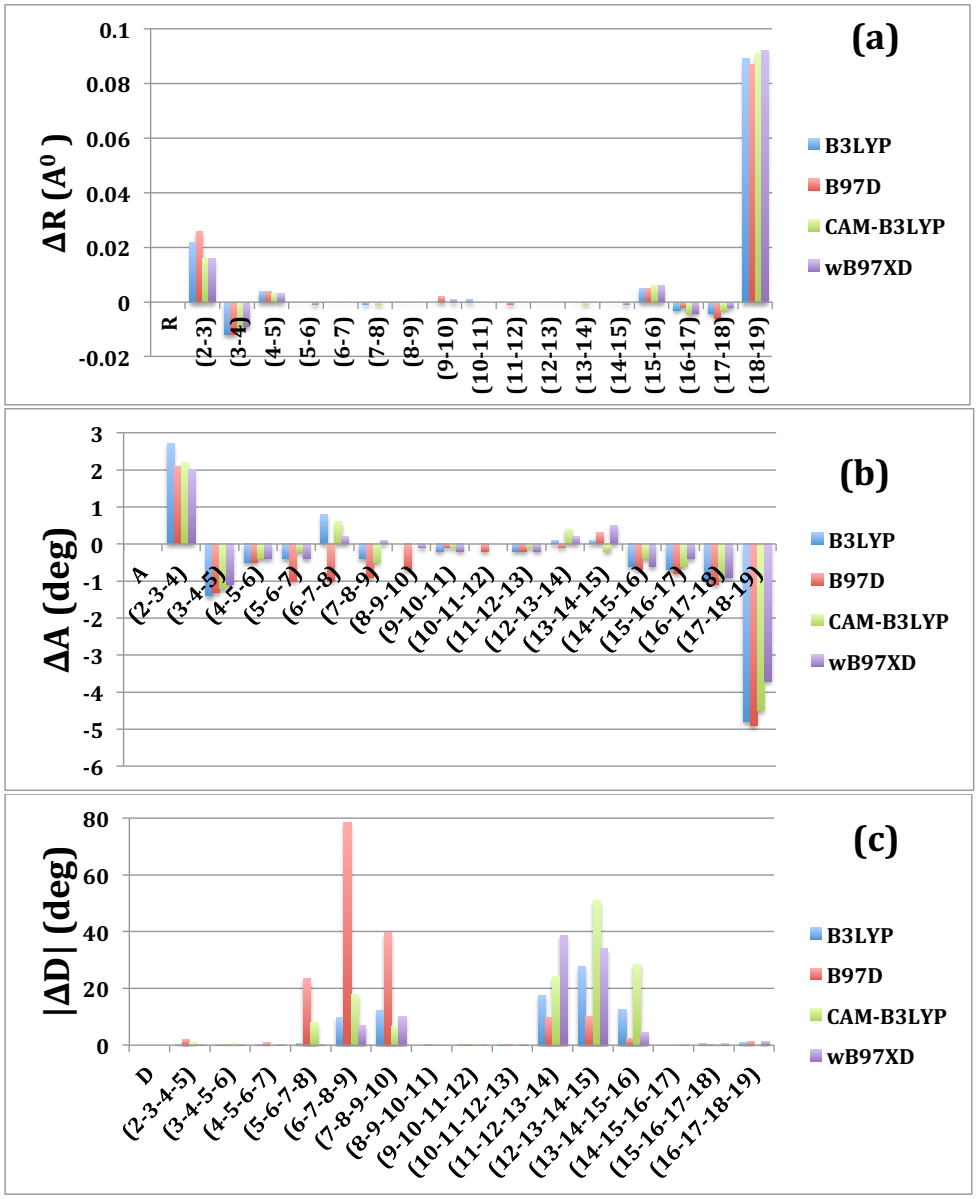

Figure 4.13: Comparison of OPE-ALD with OPE-DTF (with side chains) structures using different DFT approximations as indicated in the figure. In this figure the atoms are labelled according to OPE-ALD numbering (top graph) in Scheme 4.1. This figure shows the difference between (a) bond lengths, (b) bond angles and (c) dihedral angles of oligomers with two different end groups.

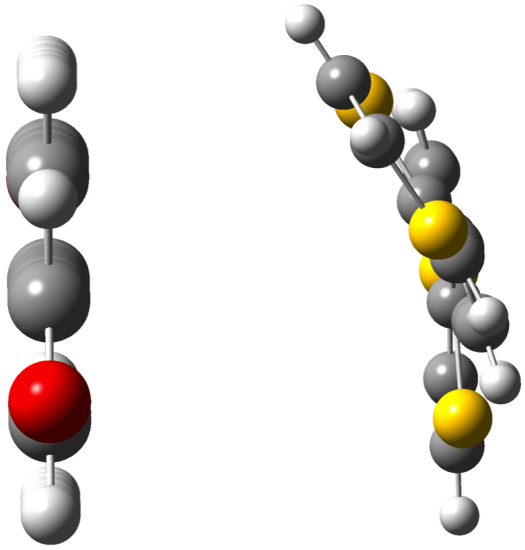

Figure 4.14: Top view of OPE-ALD and OPE-DTF (B97D method) displaying the twist in the backbone of OPE-DTF relative to planar OPE-ALD structure.

4.2.2 Eigenvalues and Dipole Moments

The dipole moments and eigenvalues for OPE-ALD and OPE-DTF are given in Tables 4.1-4.4. These tables show that DTF oligomers are more polarized (have larger dipole moments) and have smaller HOMO-LUMO gaps than ALD oligomers.

4.2.3 Nanotube

The work in this thesis requires that we also optimize the structure of (zigzag) nanotubes using the various DFT approximations (B97D, wB97XD, CAM-B3LYP). In Fig. 4.15 fully geometry optimized structure of (6,5) SWCNT in gas phase is displayed.

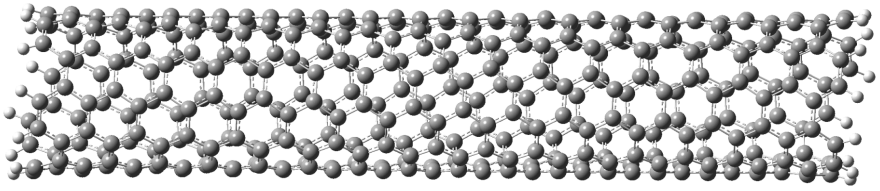

Figure 4.15: Representative optimized structure of SWCNT obtained using DFT/B97D (similar results were obtained with wB97XD and CAM-B3LYP with 6-31G* basis set).

4.3 Conclusions

Different DFT methods give similar structures for OPE-ALD and OPE-DTF backbones. Similarly, for the same oligomer with and without side chains there is a little difference in its backbone structure. Different end groups also do not affect the structure of backbones significantly but DTF end group makes the chain backbone non-planar. OPE-DTF has larger dipole moments than OPE-ALD. The HOMO-LUMO band gaps for OPE-DTF are smaller than those OPE-ALD by less than 0.5 eV for oligomers without side chains but are nearly the same for oligomers with side chains.

Chapter 5

Structure and Electronic Properties of OPE and SWCNT Molecular Combinations

In this chapter, DFT methods are used to explore the interaction between SWCNT and OPE where the OPE can have ALD or DTF as its end group. As described in Chapter 3, the combinations were partially geometry optimized (geometries of oligomers were fully relaxed while the geometry of the nanotube was kept fixed).

5.1 Dispersion Effect on the Geometries and Dipole Moments of OPEs

5.1.1 Geometry of (Interacting) OPEs

In this section, we investigate the effect that the intermolecular interactions between SWCNT and OPE have on the structure of OPEs relative to their gas phase geometry.

This comparison is carried out by looking at differences in bond lengths, bond angles, and dihedral angles between the isolated and the interacting OPEs (see Figs. 5.1-5.4).

Figs. 5.1 and 5.2 show that the differences in bond lengths (in most cases less than 0.002 Å along the backbone) and bond angles (in most cases less than 2°) for oligomers without side chains are very small. The differences in the dihedral angles are more pronounced especially for the central dihedral angles along the ethynylene bonds. The reason for these dihedral angle differences is that in the presence of nanotubes the oligomers tend to wrap themselves around the nanotube (see Figs. 5.6 (b) and 5.7 (b) as examples) to become more planar.

Figs. 5.3 and 5.4 show that the differences in bond lengths and bond angles are larger for oligomer with side chains. The largest differences are observed along the central part of the oligomers and the reason for this is similar to that for oligomer without side chains. That is, oligomers with side chains tend to wrap themselves around nanotubes even more than the oligomers without side chains (see for example, Fig. 5.8 (b) 5.11 (b)). This results in greater distortion of the oligomers' backbones (which is shown in Figs. 5.3 (c) and 5.4 (c)). It should be noted that because of the presence of side chains, the differences in dihedral angle are somewhat smaller than those obtained for oligomers without side chains. This is because side chains contribute to intermolecular interaction with nanotubes and hence lessen the need for the oligomer backbone to distort.

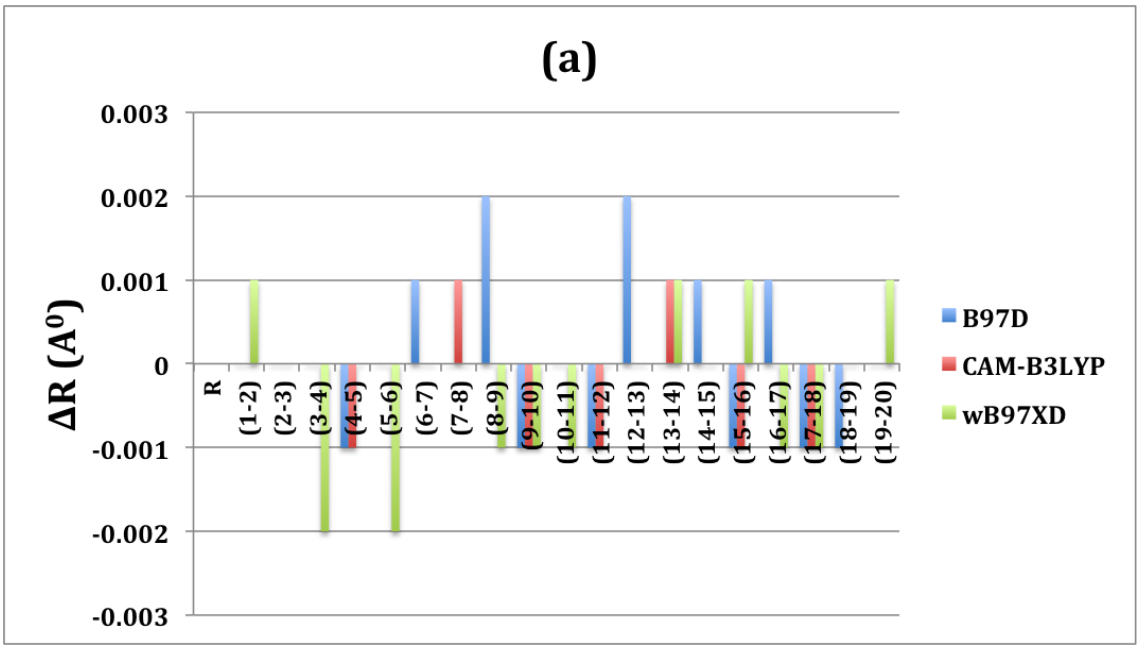
(a)
0.003
0.002
0.001
0
-0.001
-0.002
-0.003
ΔR (A⁰)
R
(1-2)
(2-3)
(3-4)
(4-5)
(5-6)
(6-7)
(7-8)
(8-9)
(9-10)
(10-11)
(11-12)
(12-13)
(13-14)
(14-15)
(15-16)
(16-17)
(17-18)
(18-19)
(19-20)
B97D
CAM-B3LYP
wB97XD

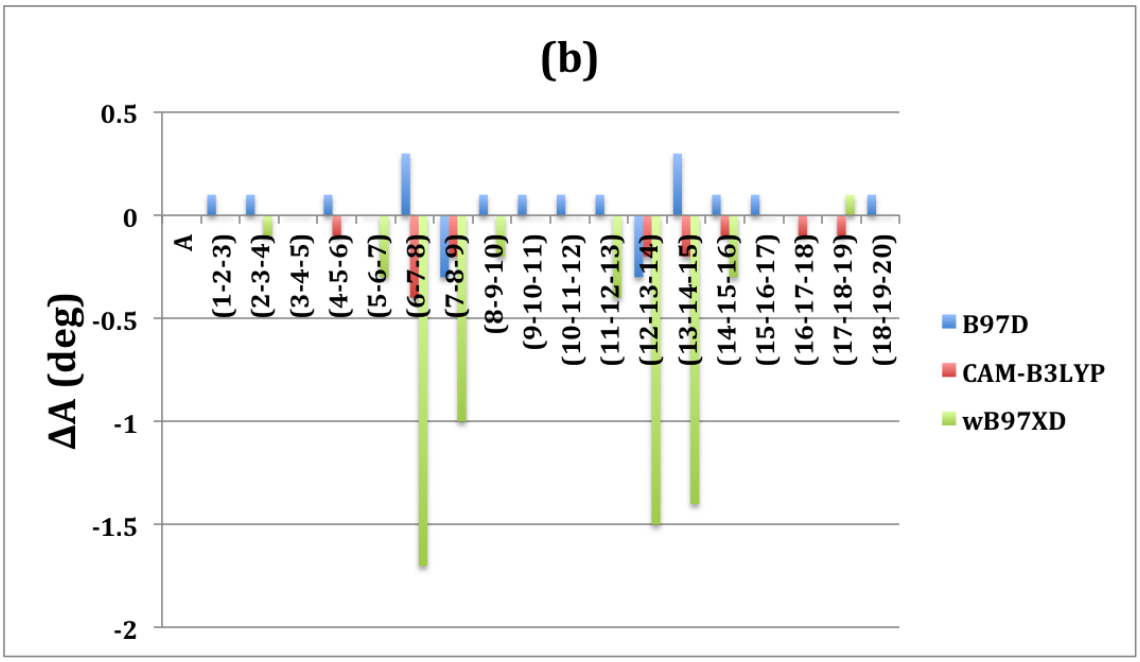
(b)
0.5
0
-0.5
-1
-1.5
-2
ΔA (deg)
A
(1-2-3)
(2-3-4)
(3-4-5)
(4-5-6)
(5-6-7)
(6-7-8)
(7-8-9)
(8-9-10)
(9-10-11)
(10-11-12)
(11-12-13)
(12-13-14)
(13-14-15)
(14-15-16)
(15-16-17)
(16-17-18)
(17-18-19)
(18-19-20)
B97D
CAM-B3LYP
wB97XD

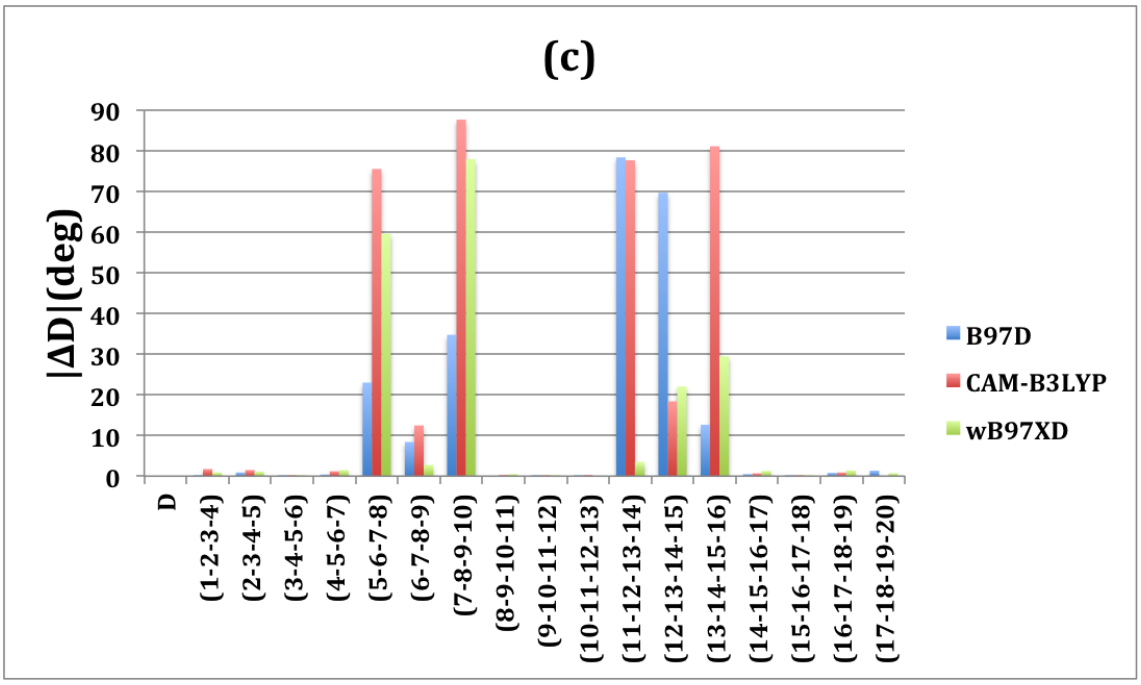

Figure 5.1: Dispersion effect of OPE-ALD (without side chains) obtained using DFT/B97D, /wB97XD, and /CAM-B3LYP with 6-31G* basis set. This figure shows differences between (a) bond lengths, (b) bond angles, and (c) dihedral angles obtained by subtracting the corresponding isolated oligomer values from the interacting oligomer results for a given DFT method as indicated on the figure.

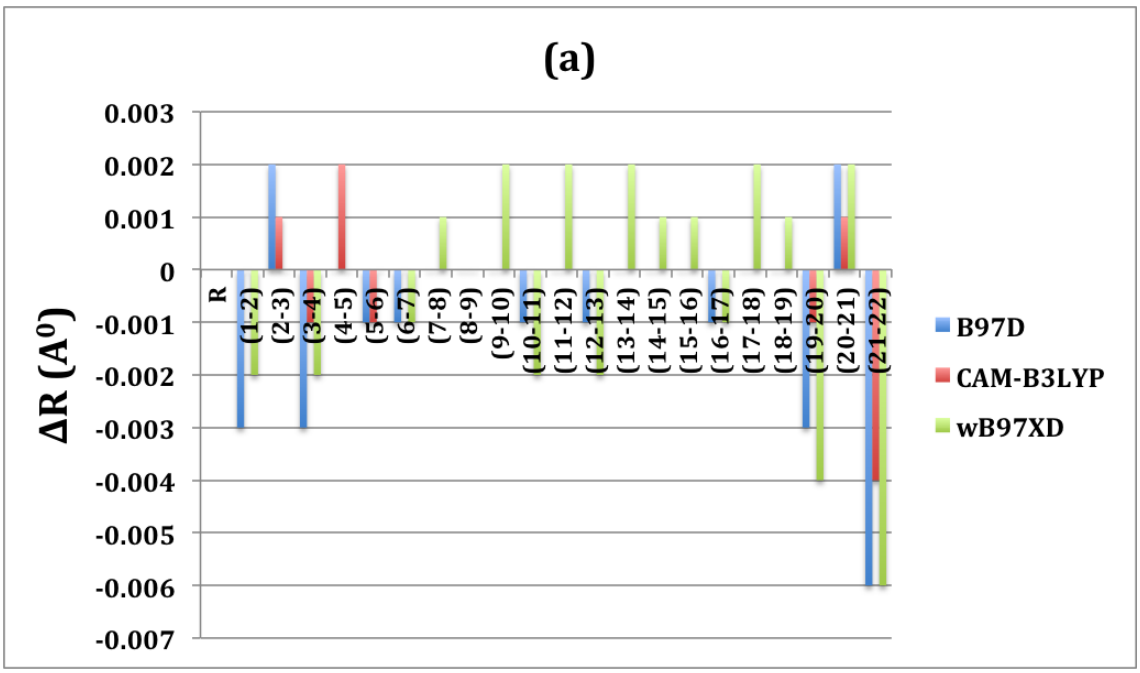

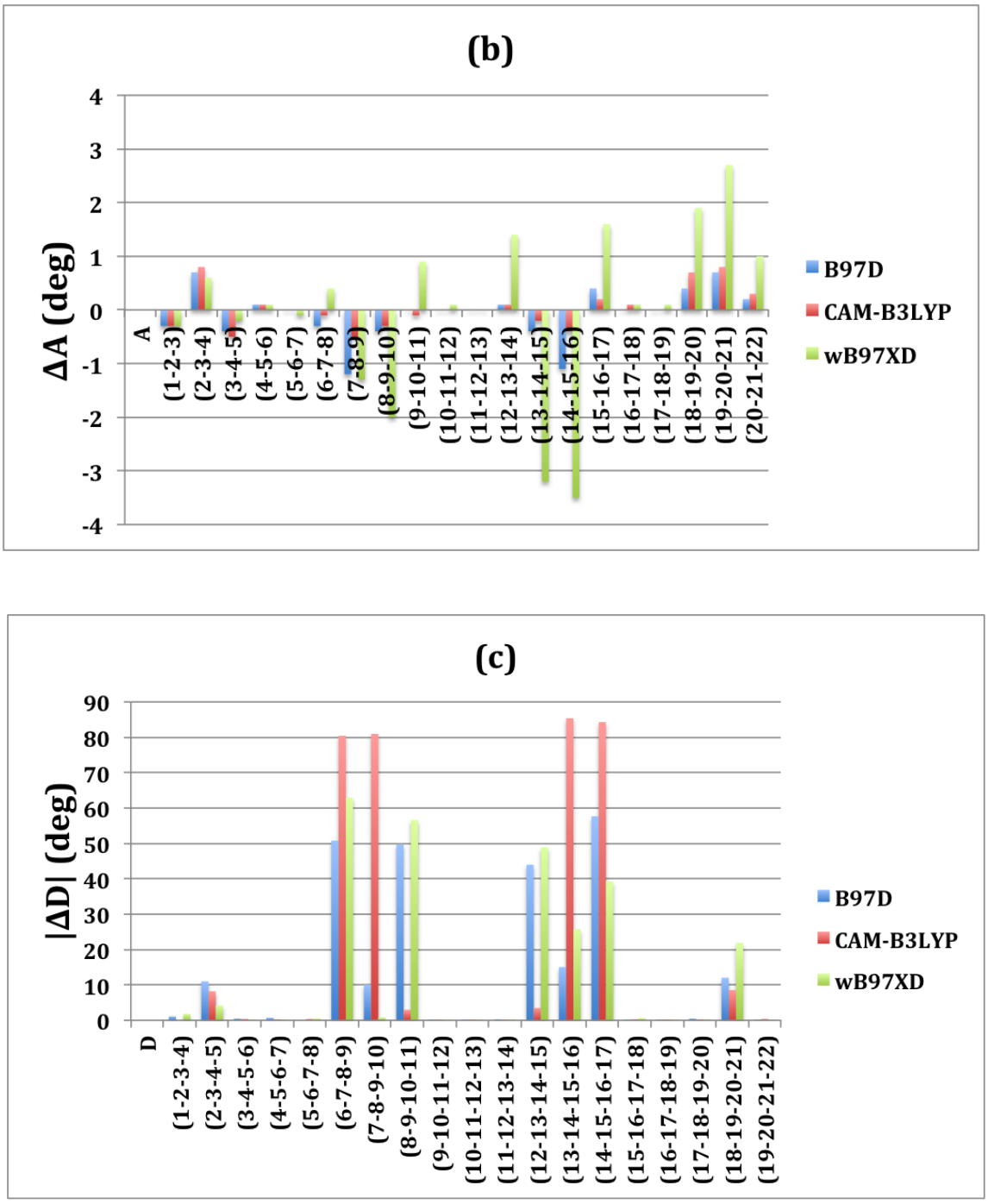

Figure 5.2: Dispersion effect of OPE-DTF (without side chains) obtained using DFT/B97D, /wB97XD, and /CAM-B3LYP with 6-31G* basis set. This figure shows differences between (a) bond lengths, (b) bond angles, and (c) dihedral angles obtained by subtracting the corresponding isolated oligomer values from the interacting oligomer results for a given DFT method as indicated on the figure.

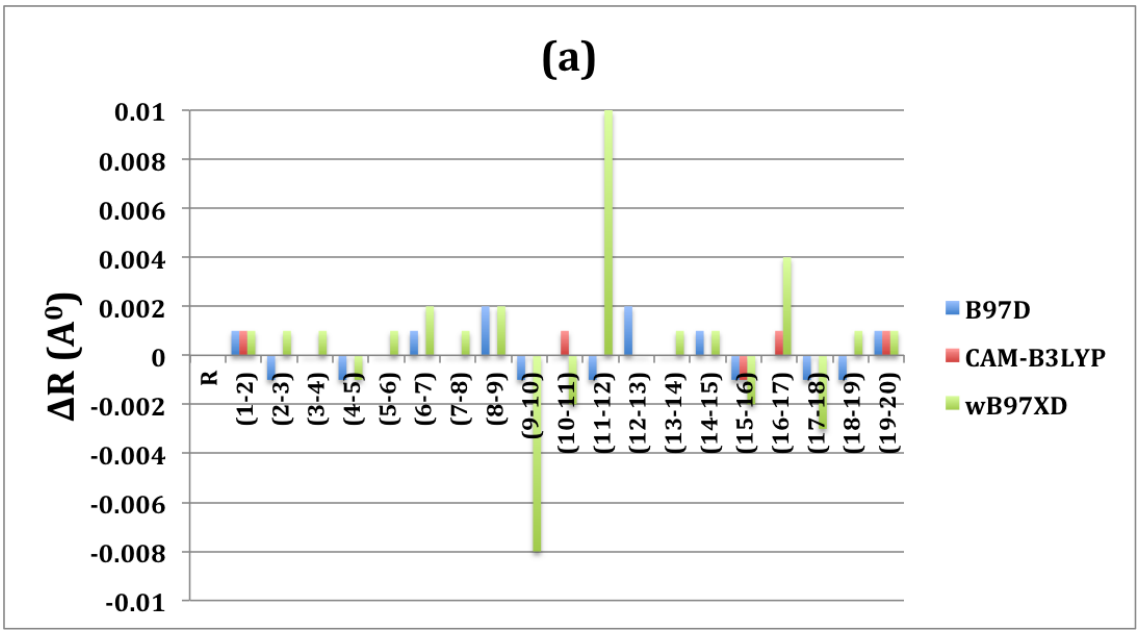
(a)
0.01
0.008
0.006
0.004
0.002
0
-0.002
-0.004
-0.006
-0.008
-0.01
ΔR (A⁰)
R
(1-2)
(2-3)
(3-4)
(4-5)
(5-6)
(6-7)
(7-8)
(8-9)
(9-10)
(10-11)
(11-12)
(12-13)
(13-14)
(14-15)
(15-16)
(16-17)
(17-18)
(18-19)
(19-20)
B97D
CAM-B3LYP
wB97XD

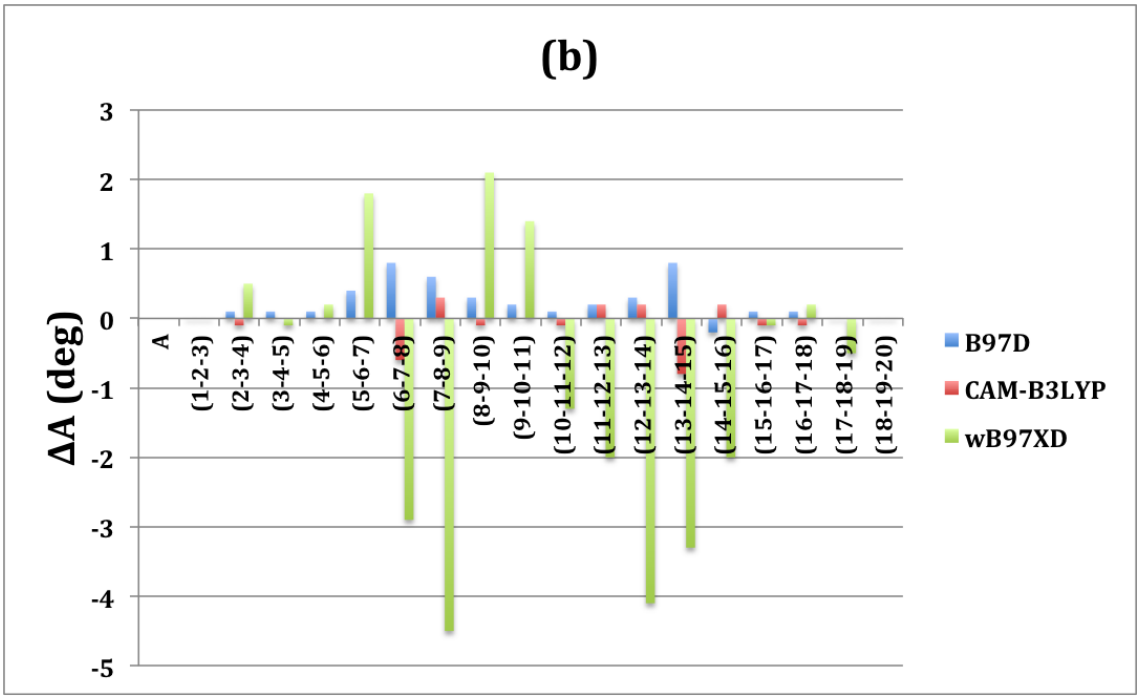
(b)
3
2
1
0
-1
-2
-3
-4
-5
ΔA (deg)
A
(1-2-3)
(2-3-4)
(3-4-5)
(4-5-6)
(5-6-7)
(6-7-8)
(7-8-9)
(8-9-10)
(9-10-11)
(10-11-12)
(11-12-13)
(12-13-14)
(13-14-15)
(14-15-16)
(15-16-17)
(16-17-18)
(17-18-19)
(18-19-20)
B97D
CAM-B3LYP
wB97XD

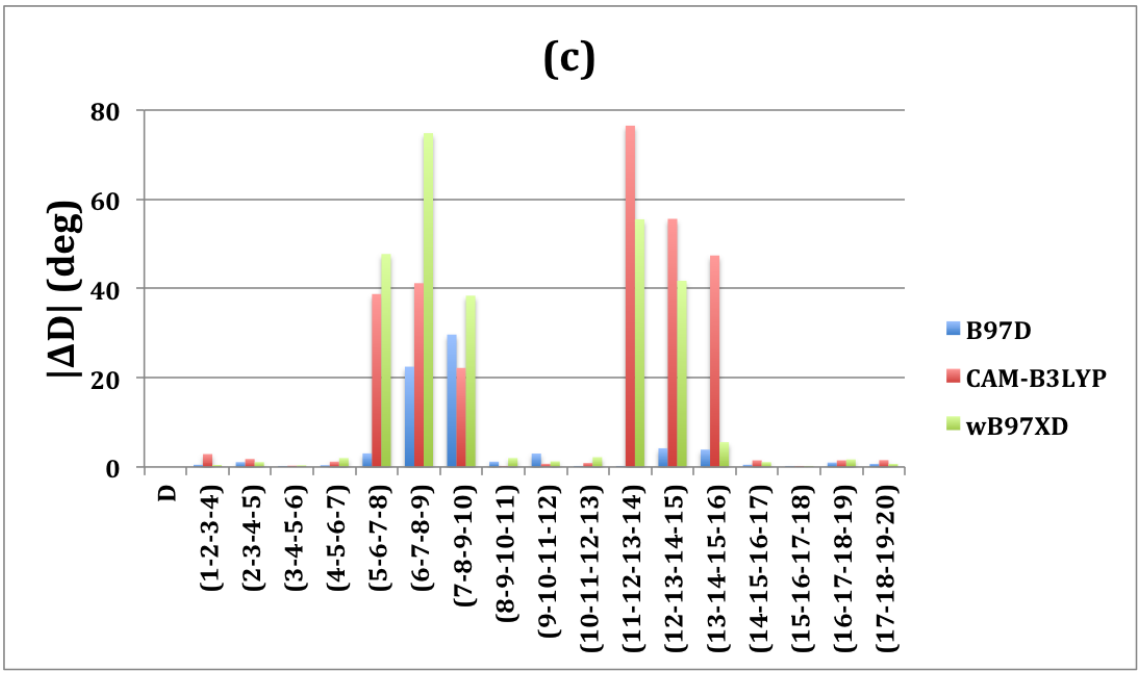

Figure 5.3: Dispersion effect of OPE-ALD (with side chains) obtained using DFT/B97D, /wB97XD, and /CAM-B3LYP with 6-31G* basis set. This figure shows differences between (a) bond lengths, (b) bond angles, and (c) dihedral angles obtained by subtracting the corresponding isolated oligomer values from the interacting oligomer results for a given DFT method as indicated on the figure.

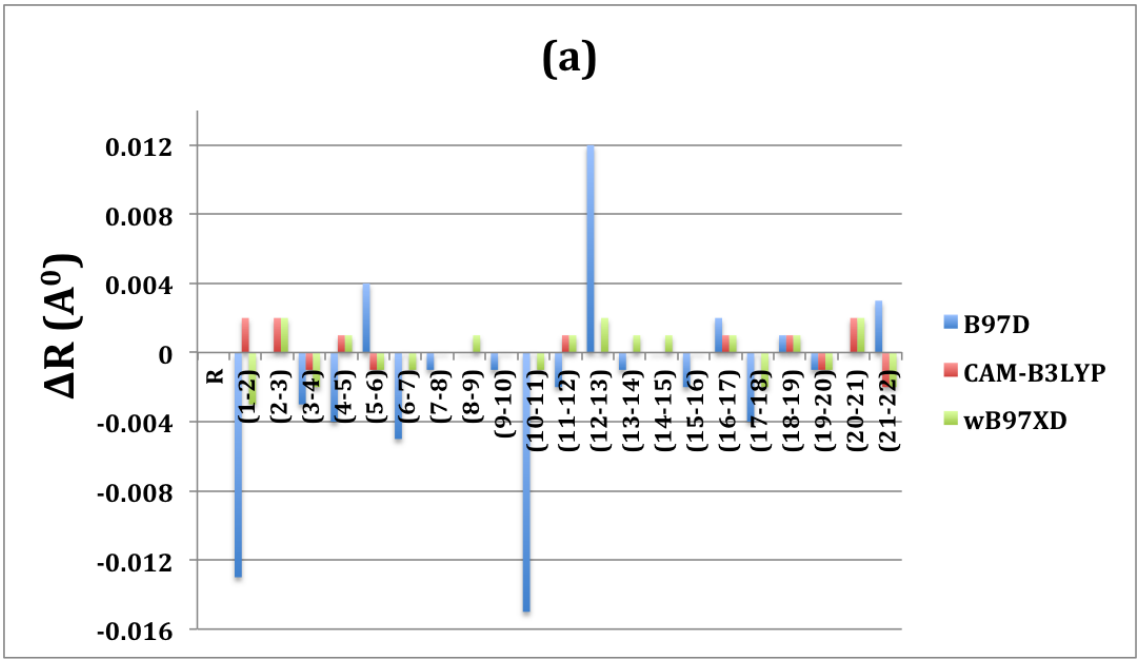

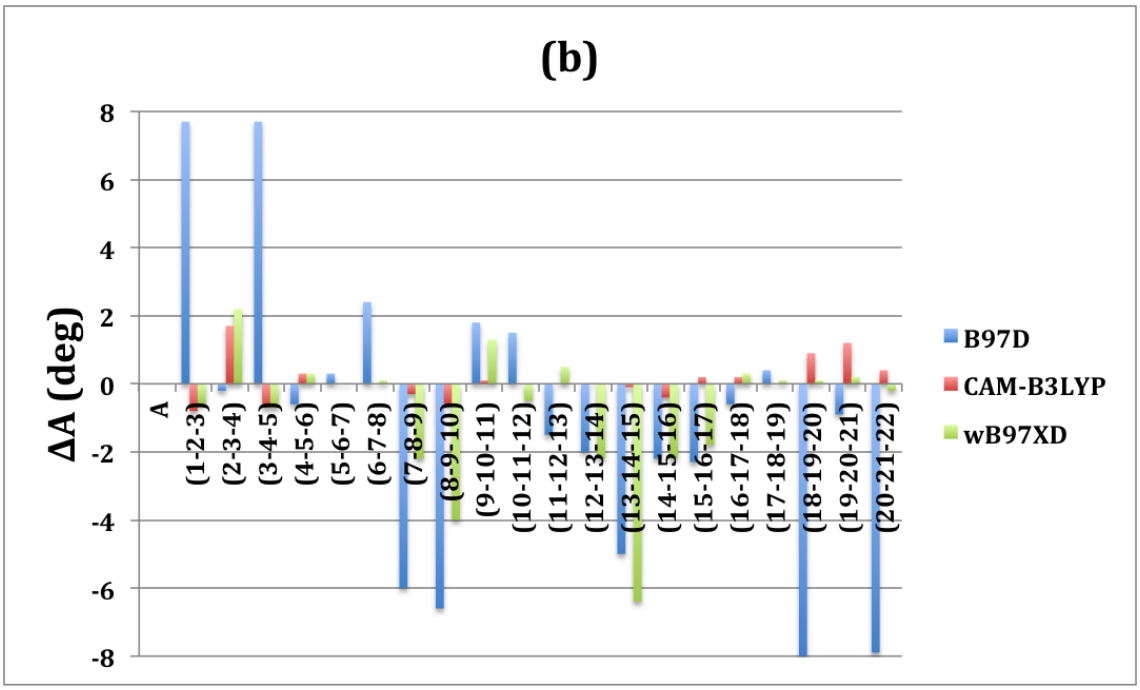

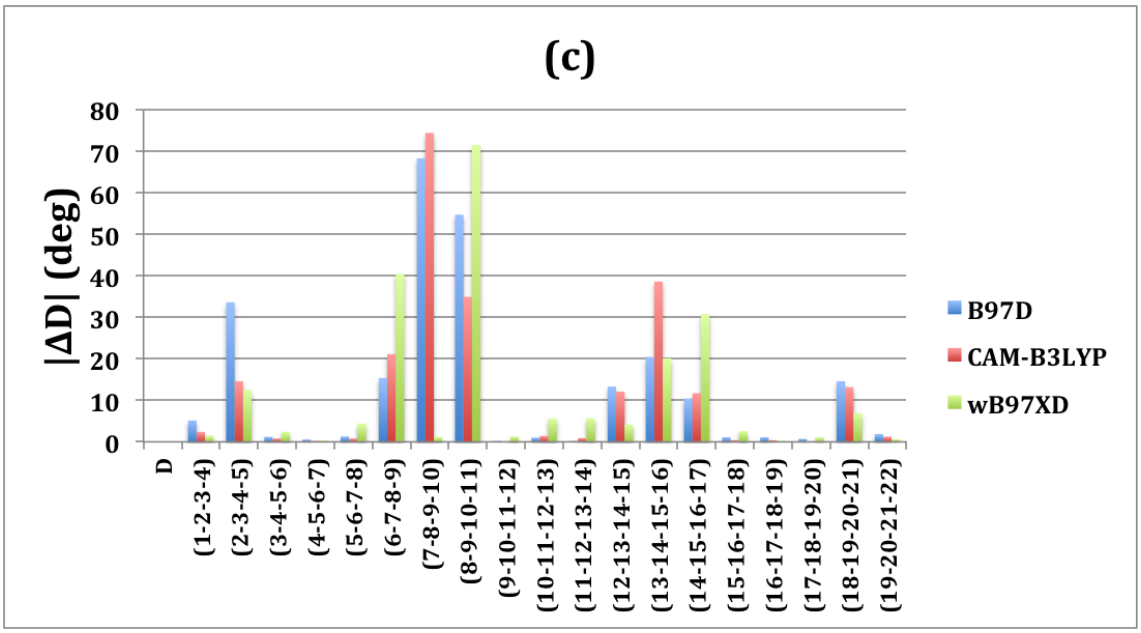

Figure 5.4: Dispersion effect of OPE-DTF (with side chains) obtained using DFT/B97D, /wB97XD, and /CAM-B3LYP with 6-31G* basis set. This figure shows differences between (a) bond lengths, (b) bond angles, and (c) dihedral angles obtained by subtracting the corresponding isolated oligomer values from the interacting oligomer results for a given DFT method as indicated on the figure.

5.1.2 Dipole Moments of the (Interacting) OPEs

For the interacting oligomers we determined the dipole moment components of the oligomers by subtracting the dipole moment components of the nanotube from the dipole moment components of the combination of oligomer and nanotube (see Table in Appendix B). In Fig. 5.5, the dipole moment differences, $\Delta\mu$'s, between dipole moments of isolated and interacting oligomers, (where $\Delta\mu$ is given by Eq. (3.1)) are shown for OPEs without and with side chains. For oligomers without side chains, the interacting OPE-DTF shows somewhat larger changes in dipole moments relative to its gas phase values. This difference in dipole moments is amplified significantly in OPE-DTF with side chains (see Fig. 5.5 (b)). There are no significant changes in dipole moments corresponding to isolated and interacting oligomers for OPE-ALDs without and with side chains. Three DFT methods display similar trends (see Fig. 5.5).

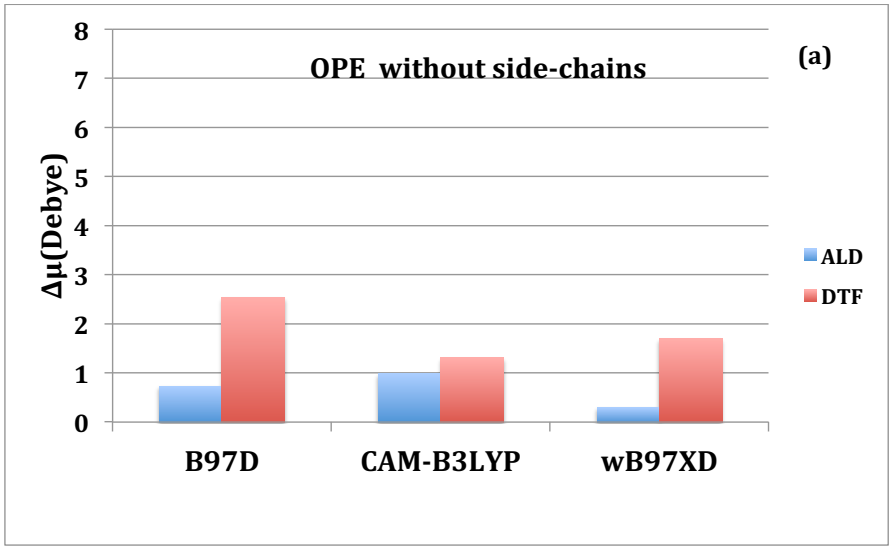

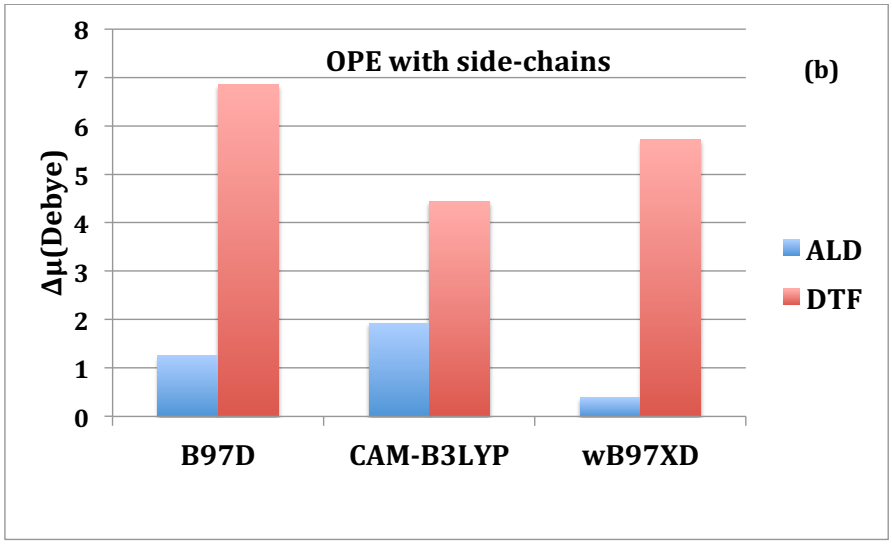

Figure 5.5: Dipole moment differences, $\Delta\mu$'s, between dipole moments of isolated and interacting oligomers, (where $\Delta\mu$ is given by Eq. (3.1)) are shown for OPEs (a) without side chains and (b) with side chains.

5.2 Comparison of DFT Methods

Figs. 5.6 and 5.7 display OPE-ALD and OPE-DTF without side chains interacting with (6,5) SWCNT. Only representative results for DFT/B97D are shown because very similar results were obtained with DFT/wB97XD and /CAM-B3LYP. The main observation from Figs. 5.6 and 5.7 is that the oligomers wrap slightly around and stretch along the nanotube. Therefore, for oligomer without side chains there are small differences between DFT methods.

For oligomers with side chains, DFT methods give somewhat different results which are shown in Figs. 5.8-5.13. The main difference between the methods is that for DFT/B97D and /wB97XD the side chains strongly wrap around the nanotubes for both ALD and DTF ended oligomers. In the case of DFT/wB97XD the oligomer backbone are also positioned at an angle relative to the nanotubes (see Figs. 5.10 (c) and 5.13 (c)) instead of being parallel to them. However, in the case of DFT/CAM-B3LYP, the side chains stretch away from the nanotube (see Figs. 5.9 (b) and 5.12 (b)).

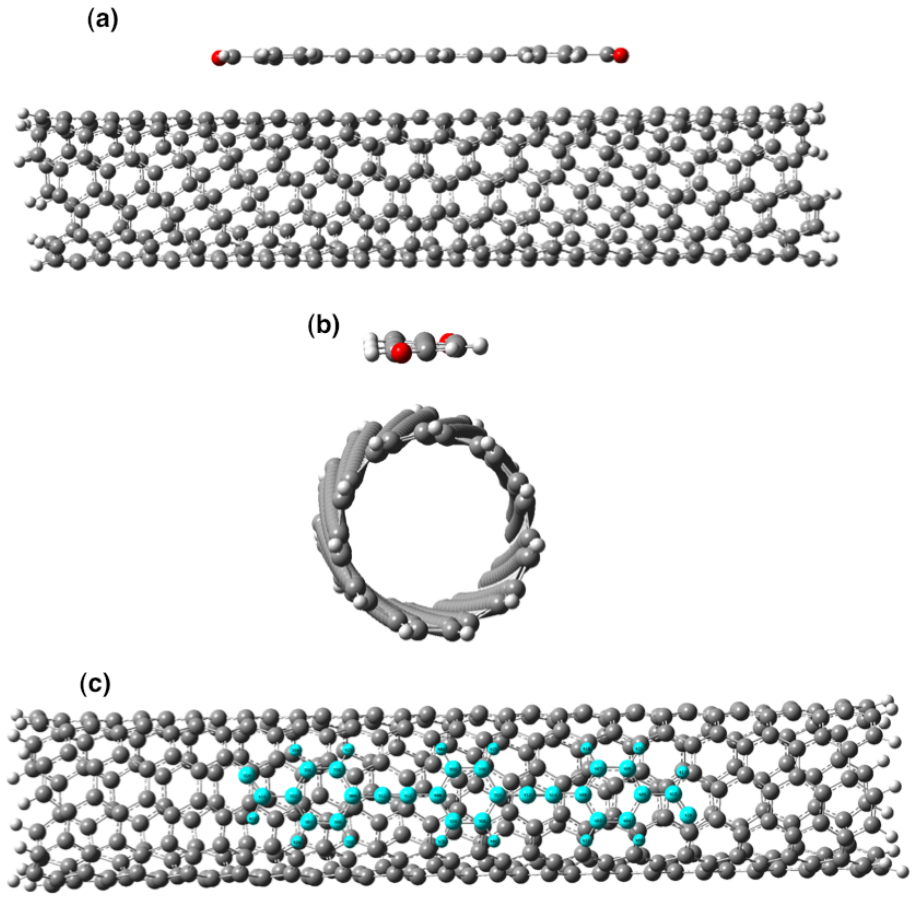

Figure 5.6: Representative optimized structure of OPE-ALD (without side chains) obtained using DFT/B97D (similar results were obtained with wB97XD and CAM-B3LYP with 6-31G* basis set). This figure shows (a) the side view, (b) top view, and (c) top view along chain (with oligomer highlighted) of the oligomer interacting with a single (6,5) nanotube (which is optimized using the same DFT method as the one used for the oligomer).

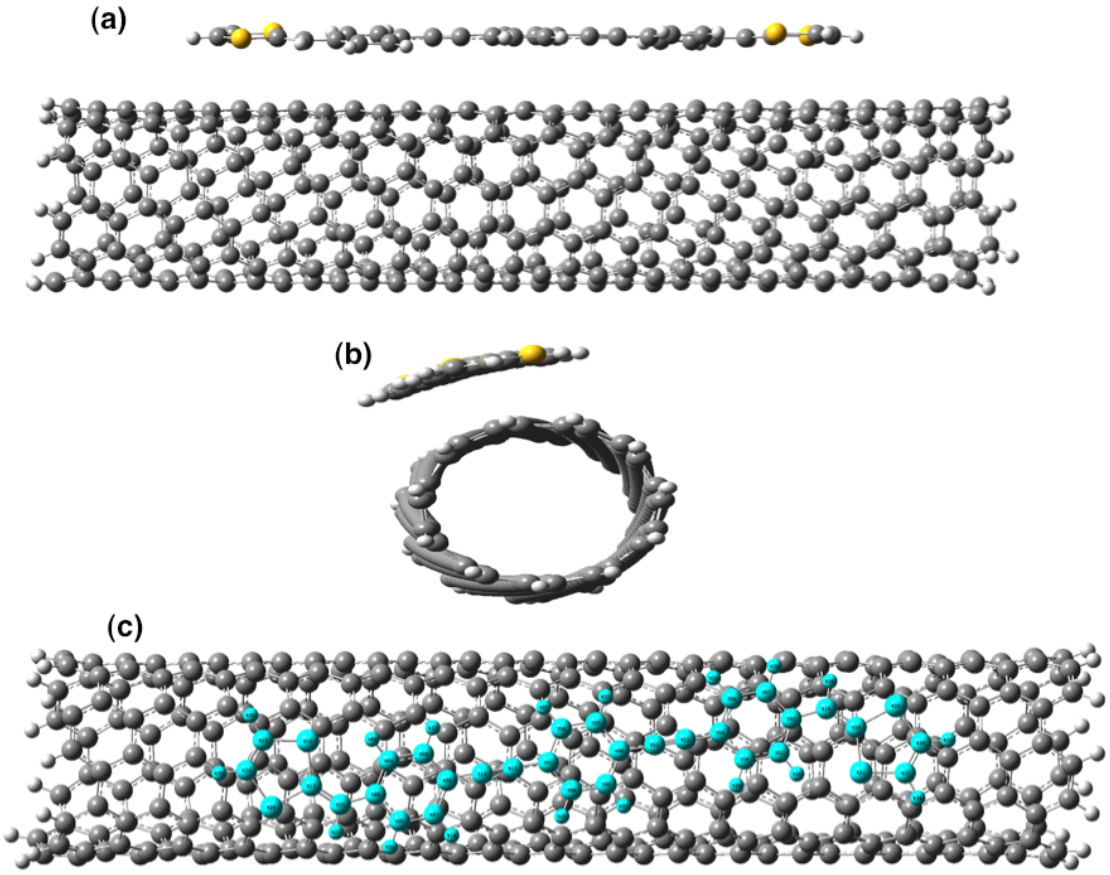

Figure 5.7: Representative optimized structure of OPE-DTF (without side chains) obtained using DFT/B97D (similar results were obtained with wB97XD and CAM-B3LYP with 6-31G* basis set). This figure shows (a) the side view, (b) top view, and (c) top view along chain (with oligomer highlighted) of the oligomer interacting with a single (6,5) nanotube (which is optimized using the same DFT method as the one used for the oligomer).

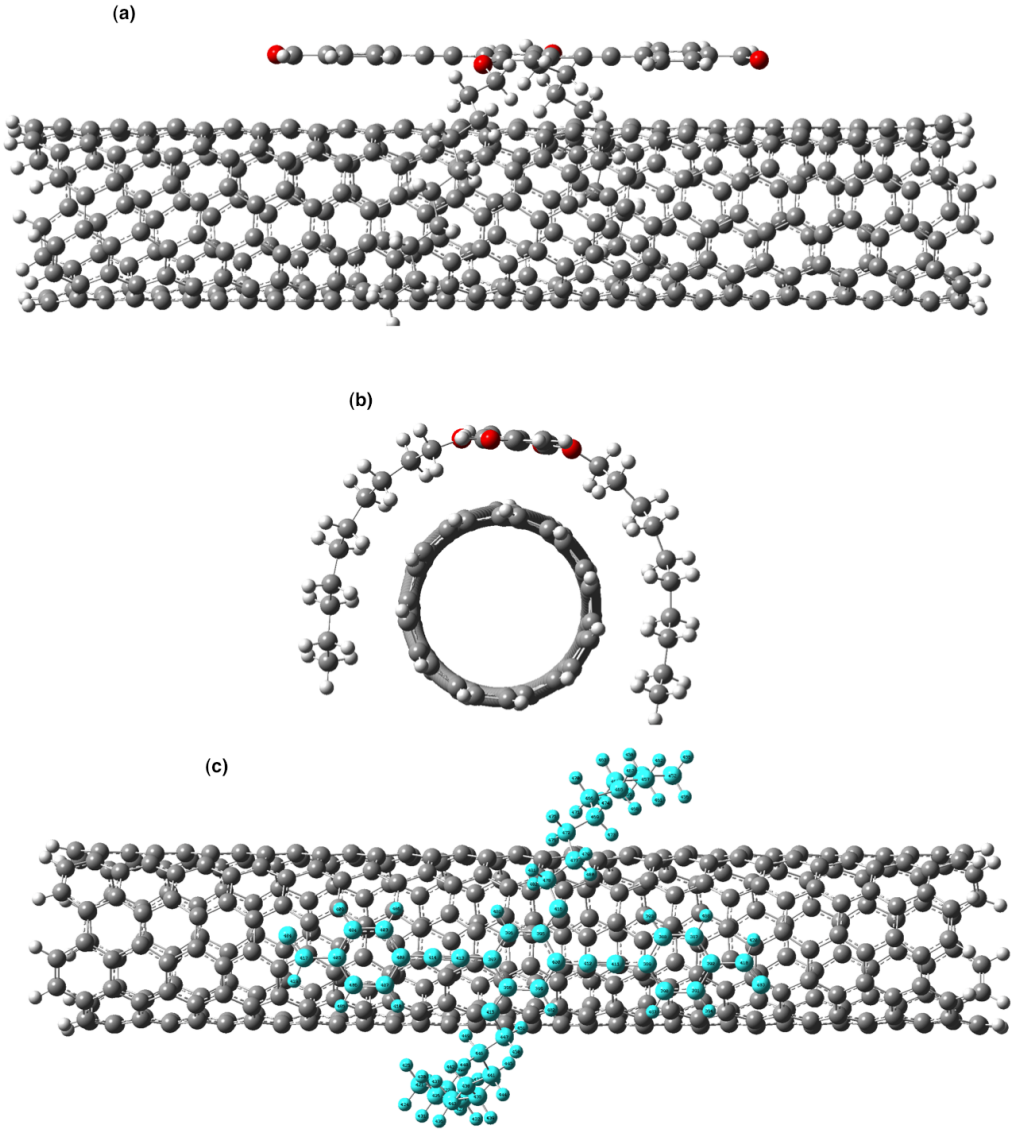

Figure 5.8: Representative optimized structure of OPE-ALD (with side chains) obtained using DFT/B97D (a) the side view, (b) top view, and (c) top view along chain (with oligomer highlighted) of the oligomer wrapped around a single (6,5) nanotube (which is optimized using the same DFT method as the one used for the oligomer).

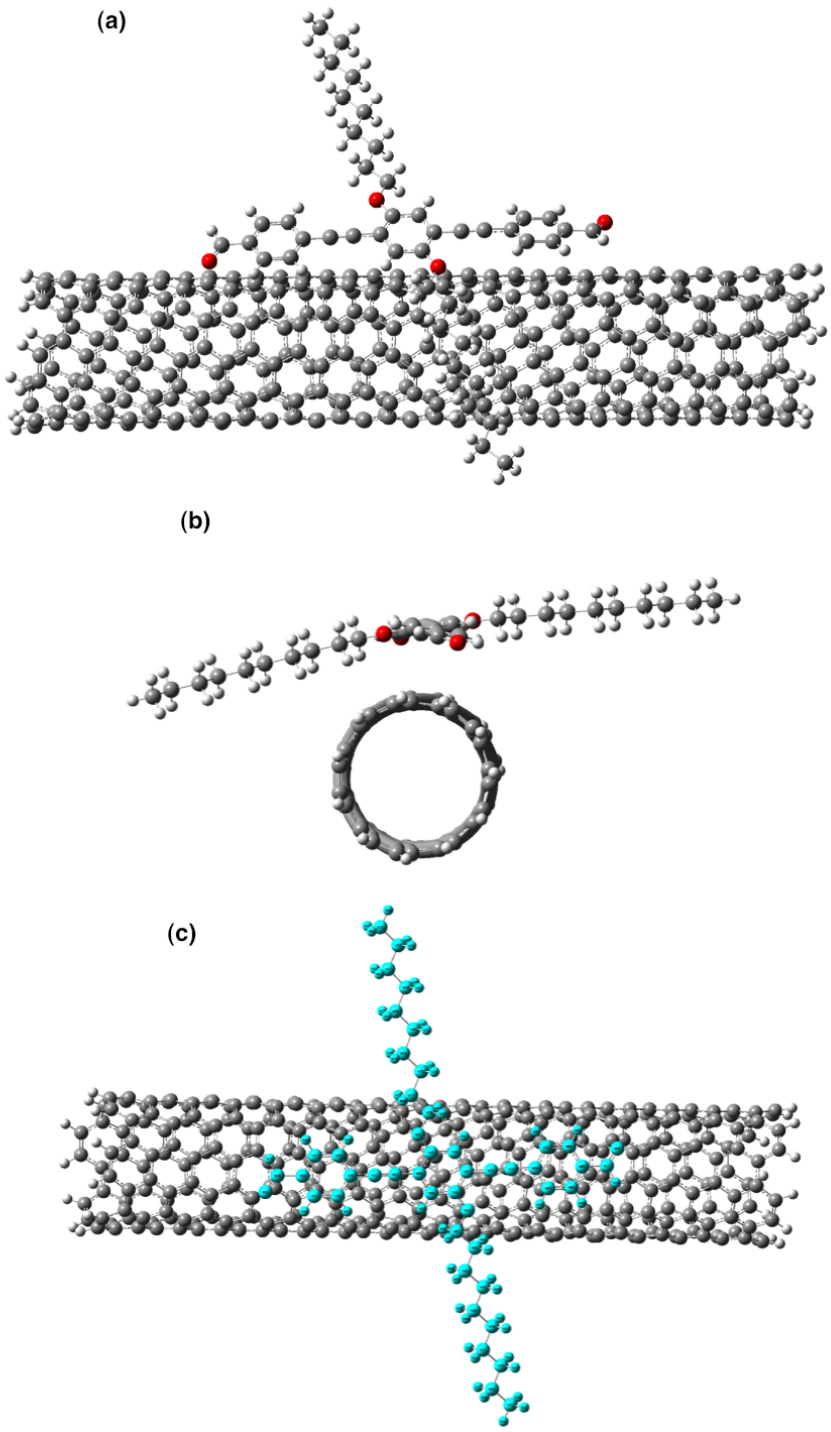

Figure 5.9: Representative optimized structure of OPE-ALD (with side chains) obtained using DFT/CAM-B3LYP (a) the side view, (b) top view, and (c) top view along chain (with oligomer highlighted) of the oligomer interacting with a single (6,5) nanotube (which is optimized using the same DFT method as the one used for the oligomer).

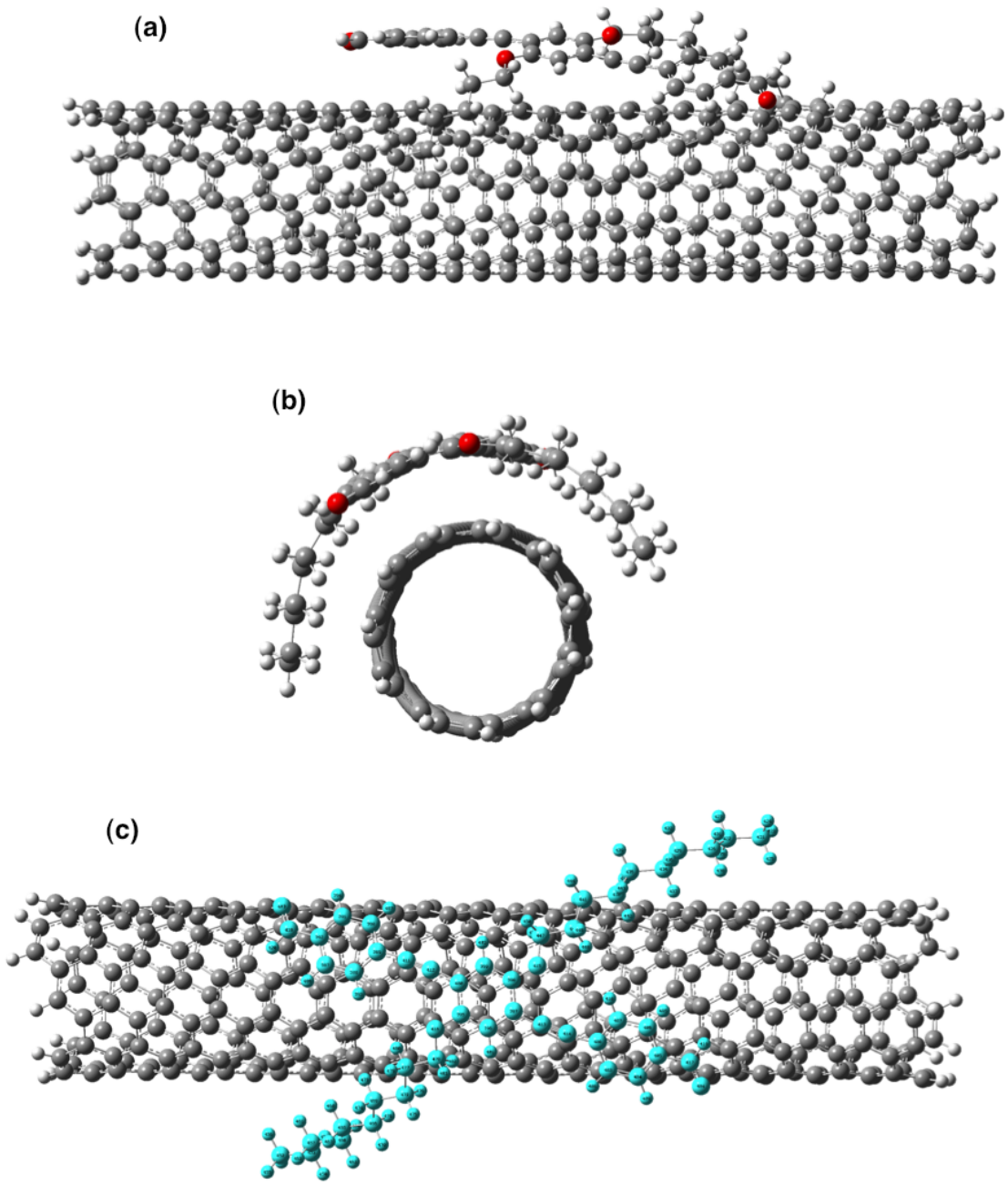

Figure 5.10: Representative optimized structure of OPE-ALD (with side chains) obtained using DFT/wB97XD (a) the side view, (b) top view, and (c) top view along chain (with oligomer highlighted) of the oligomer wrapped around a single (6,5) nanotube (which is optimized using the same DFT method as the one used for the oligomer).

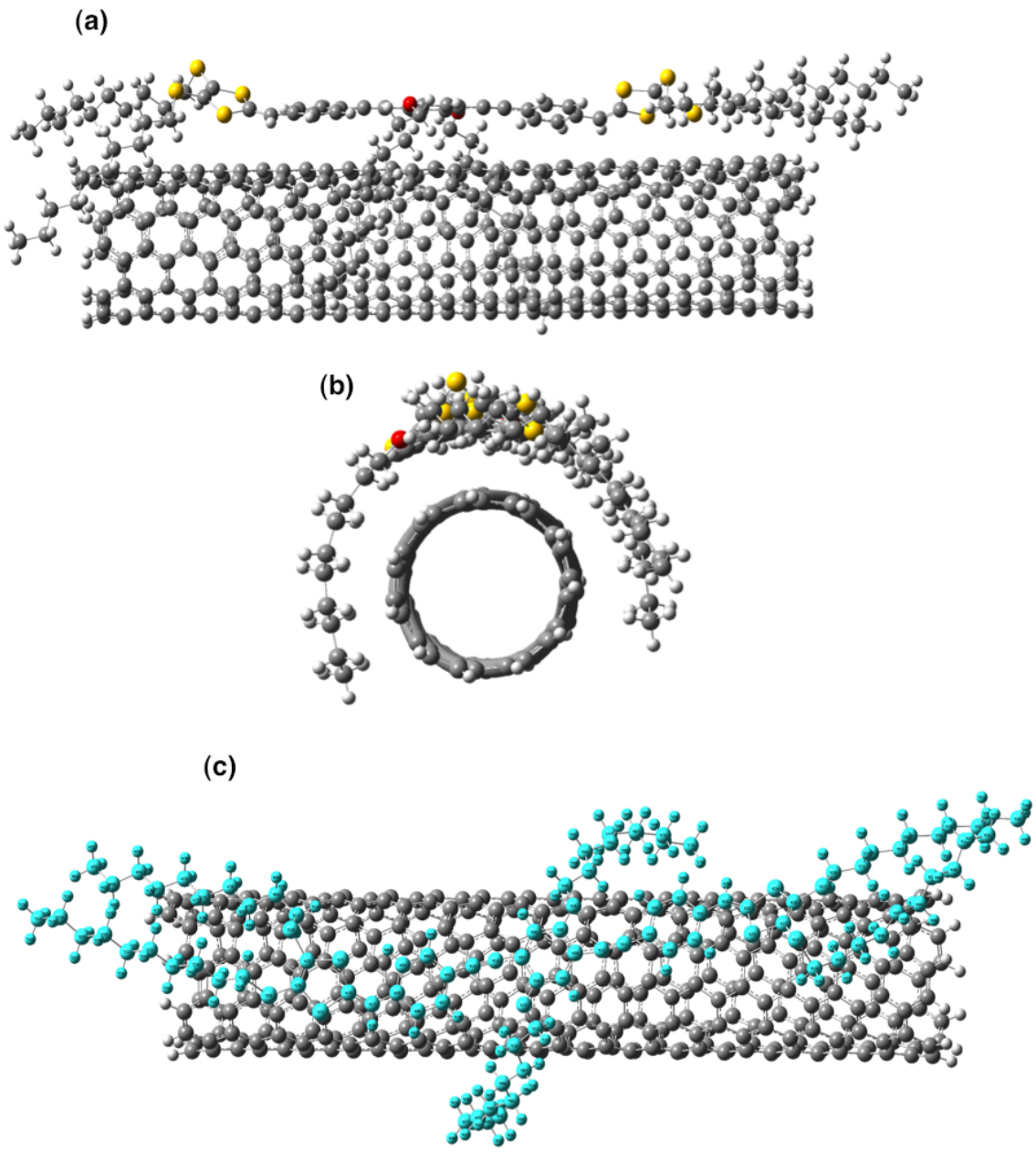

Figure 5.11: Representative optimized structure of OPE-DTF (with side chains) obtained using DFT/B97D (a) the side view, (b) top view, and (c) top view along chain (with oligomer highlighted) of the oligomer wrapped around a single (6,5) nanotube (which is optimized using the same DFT method as the one used for the oligomer).

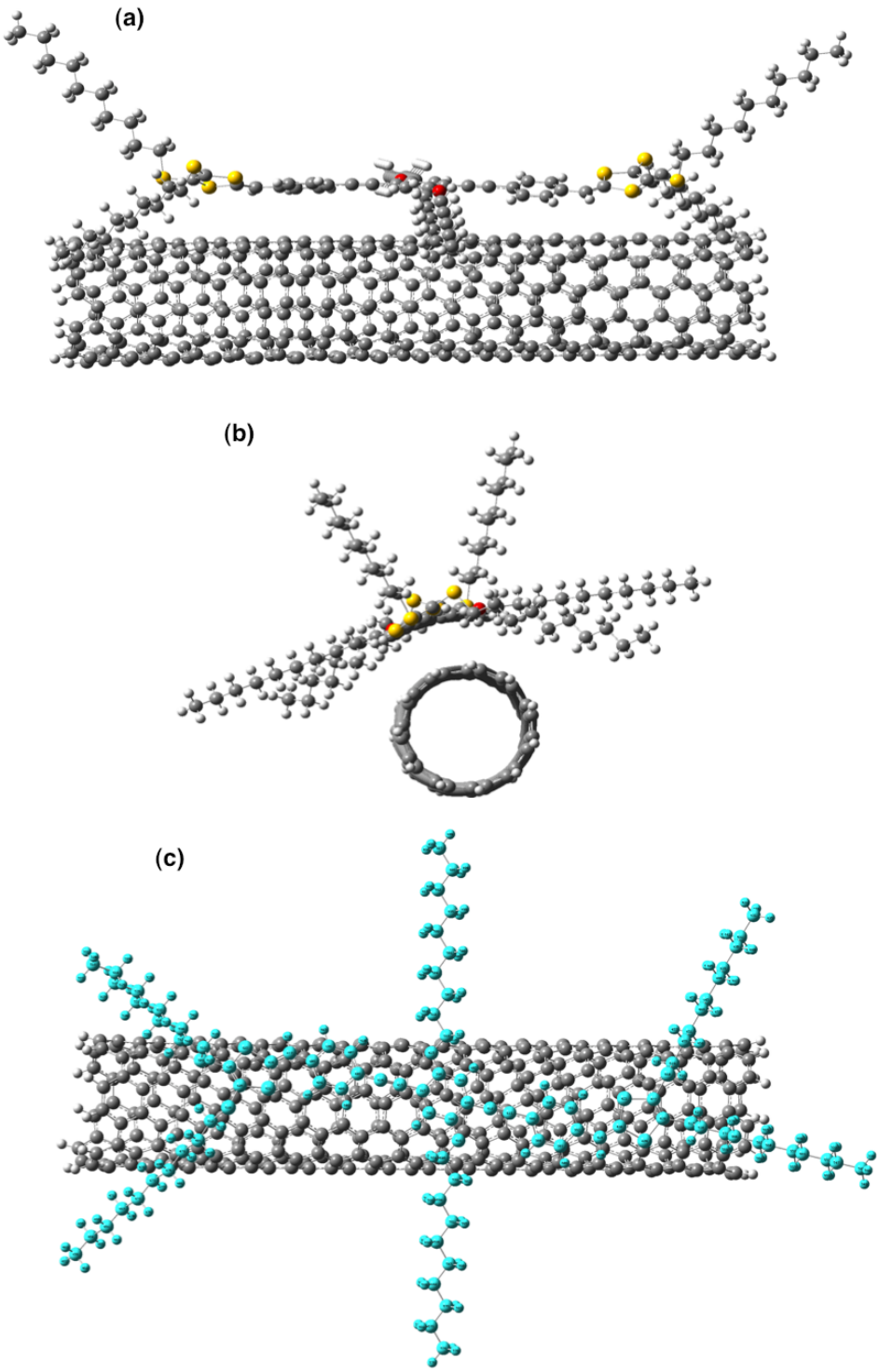

Figure 5.12: Representative optimized structure of OPE-DTF (with side chains) obtained using DFT/CAM-B3LYP (a) the side view, (b) top view, and (c) top view along chain (with oligomer highlighted) of the oligomer wrapped around a single (6,5) nanotube (which is optimized using the same DFT method as the one used for the oligomer).

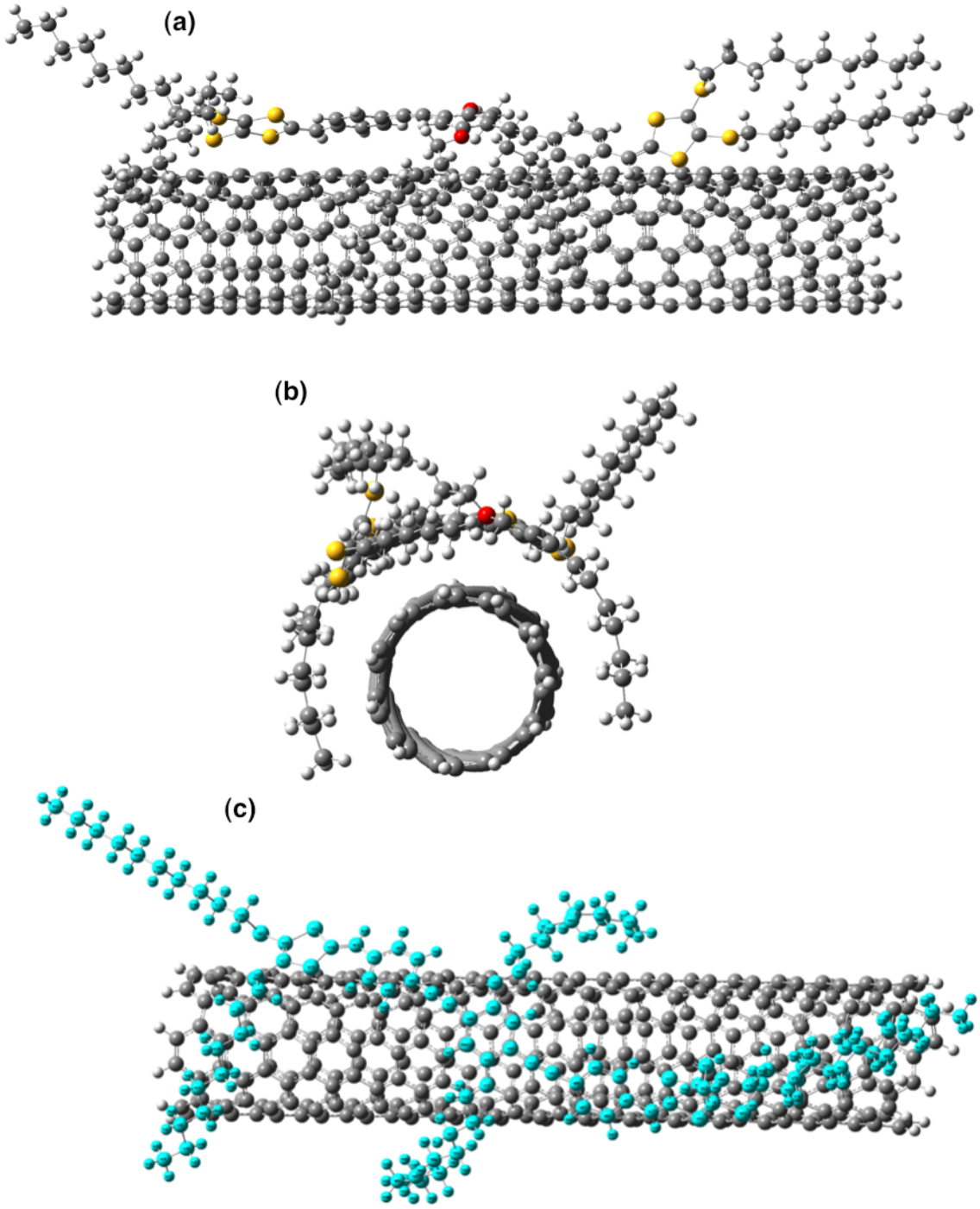

Figure 5.13: Representative optimized structure of OPE-DTF (with side chains) obtained using DFT/wB97XD (a) the side view, (b) top view, and (c) top view along chain (with oligomer highlighted) of the oligomer wrapped around a single (6,5) nanotube (which is optimized using the same DFT method as the one used for the oligomer).

The above discussion regarding the different DFT methods is qualitative (i.e. results are displayed in figures). In order to quantify the differences between methods we compute standard deviations for oligomers with and without side chains for each method. For a set of data (e.g. r_1, r_2, ..., r_N) the standard deviations is defined as

$$\sigma = \sqrt{\frac{1}{(N-1)} \sum_{i=1}^{N} (r_i - \bar{r})^2}. \tag{5.1}$$

where $\bar{r}$ is the mean value of the data. The magnitude of $\sum$ gives indication of the spread of the values in the given data set if two data sets have similar $\sum$'s that is indicative that these two data sets are similar.

Fig. 5.14 shows the standard deviation of bond lengths, bond angles, and dihedral angles for different methods: B97D, wB97XD, and CAM-B3LYP. The standard deviation is a measure of dispersion of a set of data from its mean, which is calculated as the square root of variance (see Eq. 5.1). A low standard deviation indicates that the data points tend to be very close to the mean of the set, the high standard deviation indicates that the data points are spread out over a wider range of values. Fig. 5.14 (a) shows the standard deviation of bond lengths as a function of ALD without side chains, ALD with side chains, DTF without side chains, and DTF with side chains. In all cases B97D shows the smallest dispersion of data for bond lengths. The results for bond lengths also show that the maximum deviation is 0.074 Å for long rang corrected CAM-B3LYP and long range corrected with dispersion corrections wB97XD for OPE-ALD without side chains. Bond angle deviations are shown in Fig. 5.14 (b). The largest bond angle deviation (26.5°) is obtain for CAM-B3LYP for all oligomers with and without side chains. wB97XD give similar results as those obtained for CAM-B3LYP except for OPE-DTF with side chains. In nearly all cases

wB97XD gives the smallest standard deviations for bond angles. Chart (c) in Fig. 5.14 shows that the dihedral angles deviations are very similar for all three methods.

5.3 Dipole Moment Differences due to Side Chains and End Groups

In this section, we investigate the effect of the side chains and end groups on the dipole moments, μ, of the oligomer and nanotube combinations. That is, in these electronic dipole moment studies, we use the results of DFT/B97D, /wB97XD, /CAM-B3LYP calculations of oligomers interacting with SWCNT (see Chapter 3 for details) and compute the corresponding dipole moment differences. The approximate sketch of x, y, and z axes used in the determination of the dipole moment components is shown in Fig. 5.15 for a given oligomer and SWCNT combination. Typically, the three components of dipole moments have the following directions: one (x) is aligned along the length of the SWCNT, the other (y) is perpendicular to the nanotube and points toward the oligomers, and the final one (z) is perpendicular to the other two directions.

5.3.1 Side Chain Effect

First, we look at the effect of side chains on the oligomers and the SWCNT system. Fig. 5.16 shows the difference between dipole moment components of oligomer and SWCNT combinations without side chains and with side chains for OPE-ALD and OPE-DTF. For OPE-ALD for the three DFT methods, there is very little difference (of the order of 1 Debye) between dipole moment components for system with and without side chains. For OPE-DTF, the y component of the dipole moment of the combination is most effected by the presence of side chains. The biggest y component

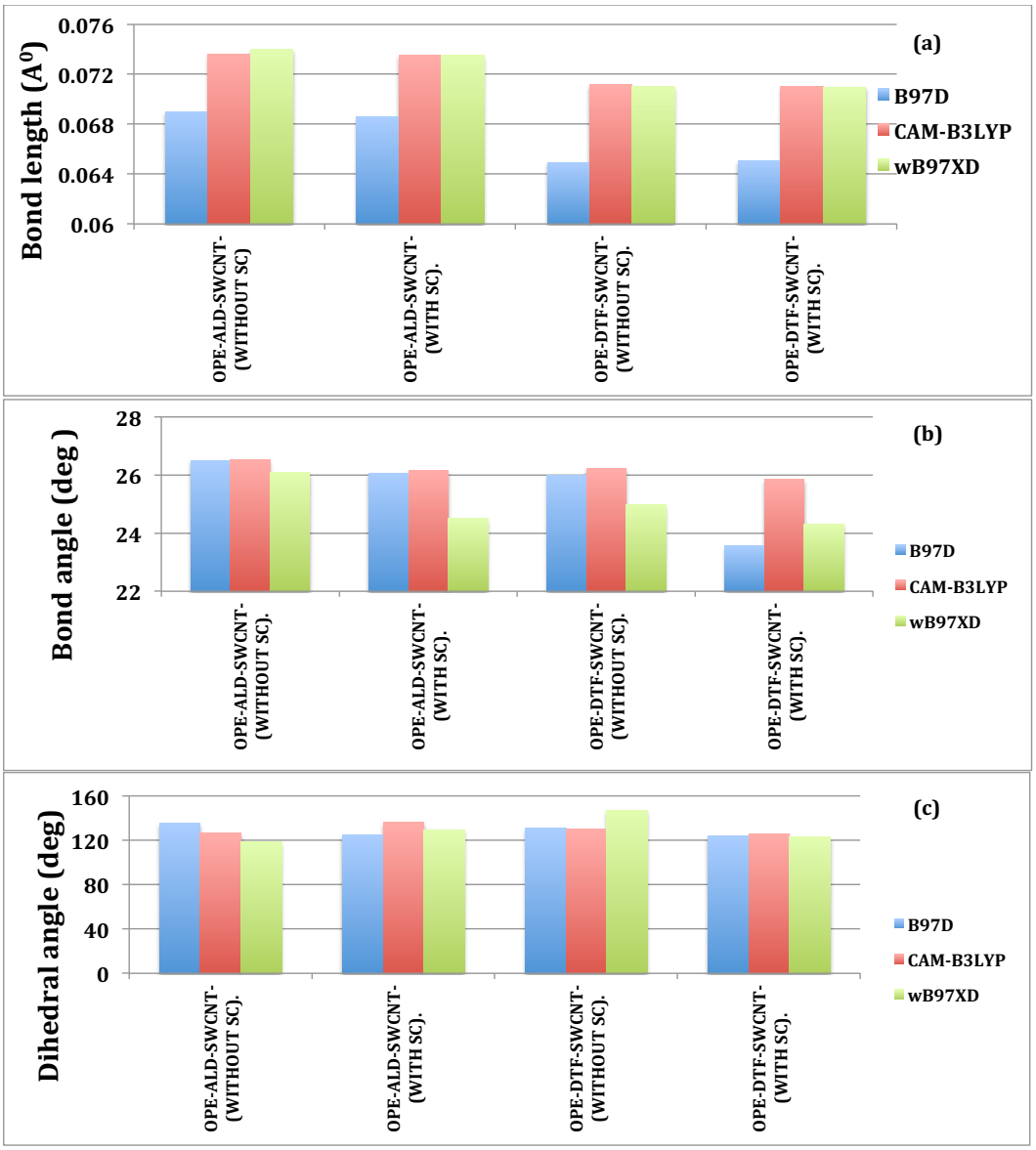

Figure 5.14: Standard deviation (see Eq. 5.1) of OPE-ALD and OPE-DTF with and without side chains interacting with SWCNT obtained using DFT/B97D, /CAM-B3LYP, and /wB97XD. This figure shows standard deviations for (a) bond lengths, (b) bond angles, and (c) dihedral angles.

difference (of the order of 7 Debye) is observed for B97D for OPE-DTF.

In addition to dipole moment components differences we also plotted the total dipole moment differences, $\Delta\mu$ and $\Delta\mu_{Total}$, obtained in two ways (see Chapter 3, Eqs. (3.1) and (3.2)). Once again, $\Delta\mu$ and $\Delta\mu_{Total}$ for combinations containing OPE-ALD are very small, less than 2 Debye, indicating the dipole moment is not affected by the side chains in the OPE-ALD and SWCNT combination. $\Delta\mu$ and $\Delta\mu_{Total}$ are larger for OPE-DTF and SWCNT combination especially for B97D. From the dipole moment component analysis it is clear that the large values for $\Delta\mu$ and $\Delta\mu_{Total}$ are due to the side chains affecting the interaction between the oligomer and nanotube along the y direction in the OPE-DTF and nanotube system.

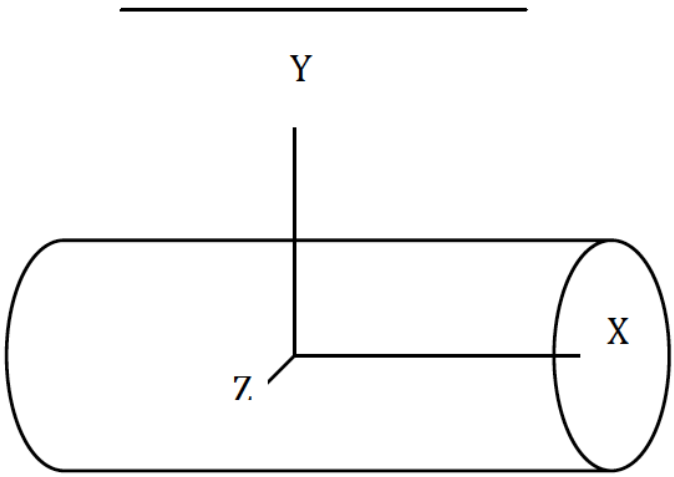

Figure 5.15: The x, y, and z axes used in the determination of the dipole moment direction.

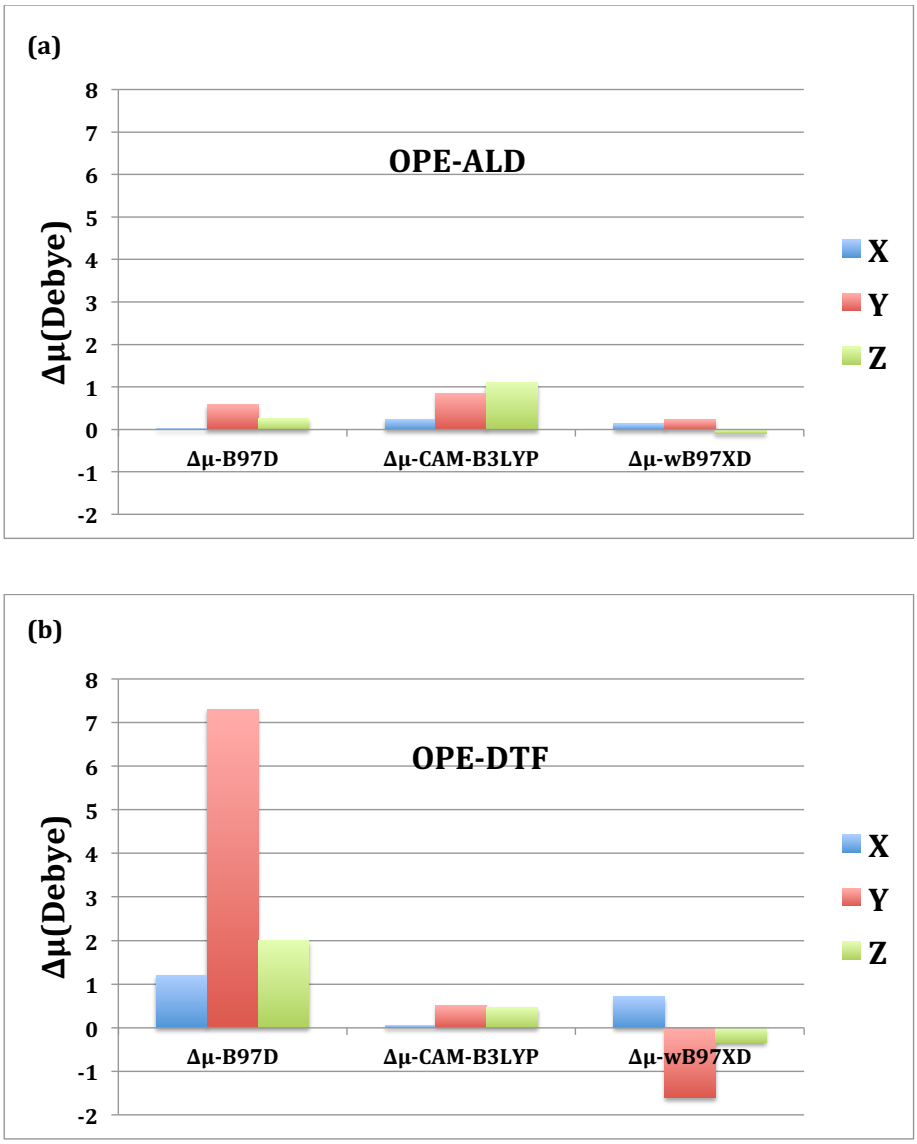

Figure 5.16: The difference between components of the dipole moments of (a) OPE-ALD (without side chains) and (with side chains), (b) OPE-DTF (without side chains) and (with side chains) as obtained using the three approaches: DFT/B97D, /wB97XD, and /CAM-B3LYP.

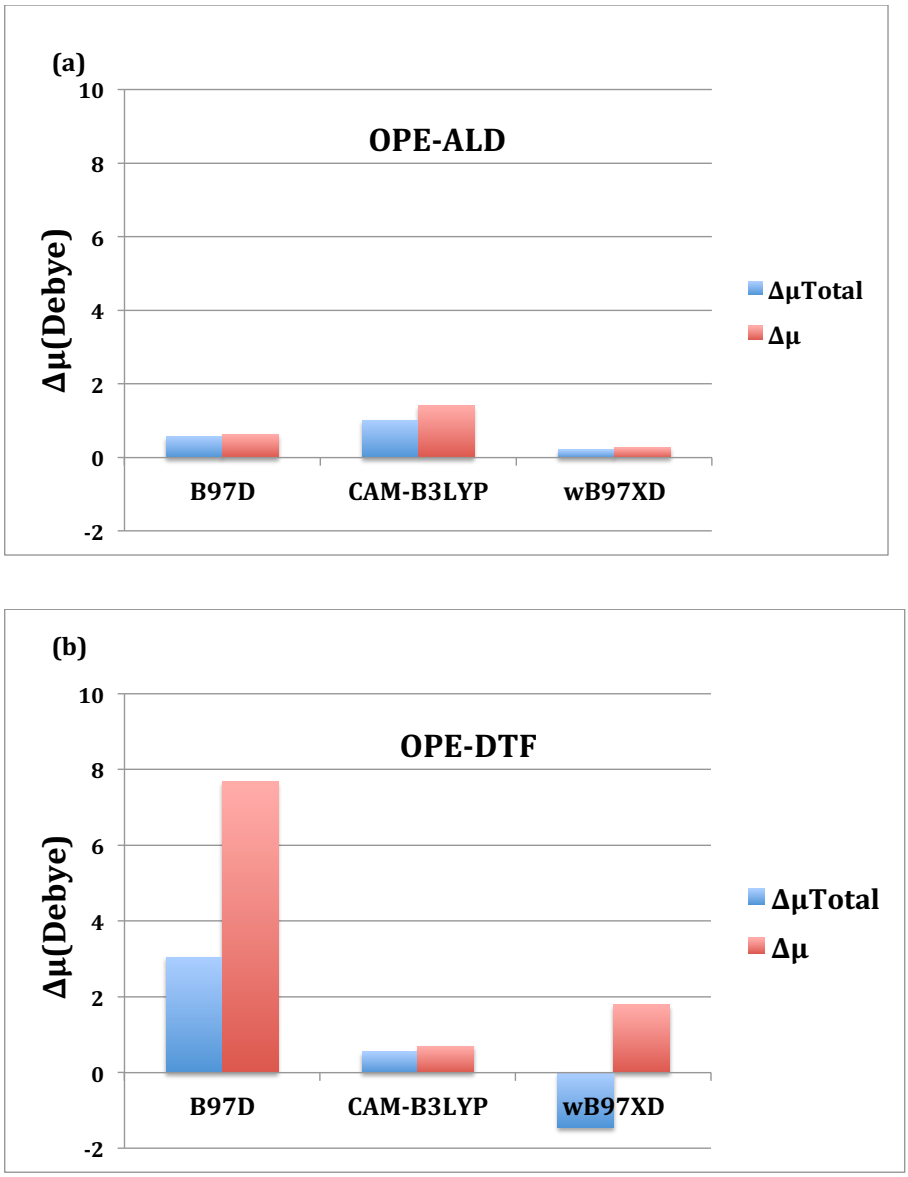

Figure 5.17: The difference between the dipole moments, $\Delta\mu_{Total}$ and $\Delta\mu$, of system containing (a) OPE-ALD (without side chains) and (with side chains), (b) OPE-DTF (without side chains) and (with side chains) obtained using the three approaches: DFT/B97D, /wB97XD, and /CAM-B3LYP.

5.3.2 End Group Effect

We also look at the affect of the end groups on the dipole moments of oligomer and nanotube combinations. In Fig. 5.18 the difference between components of dipole moments of two oligomers with DTF and ALD end groups is shown. In almost all cases, the systems with DTF end group have larger dipole moment components. The biggest differences is in the y component of the combination with side chains for B97D. Fig. 5.19 where, $\Delta\mu$ and $\Delta\mu_{Total}$ are plotted, shows once again that in all cases the combinations with DTF ended oligomers have higher dipole moments.

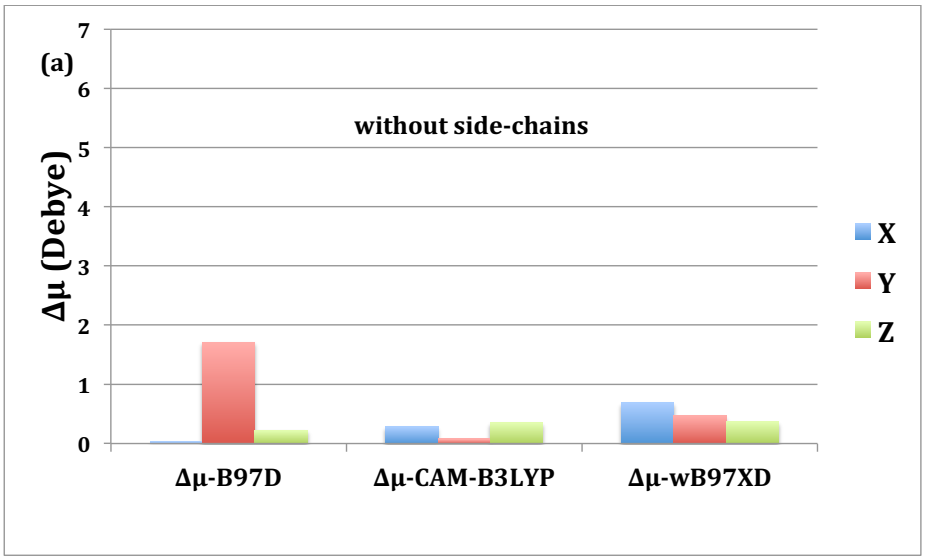

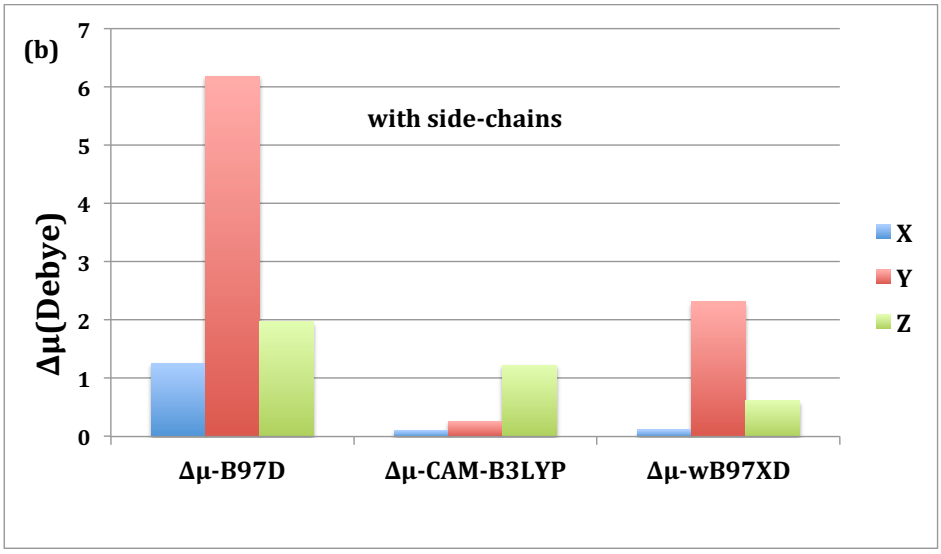

Figure 5.18: The difference between components of dipole moments of two oligomers with DTF and ALD end groups as obtained using the three approaches: DFT/B97D, /wB97XD, and /CAM-B3LYP.

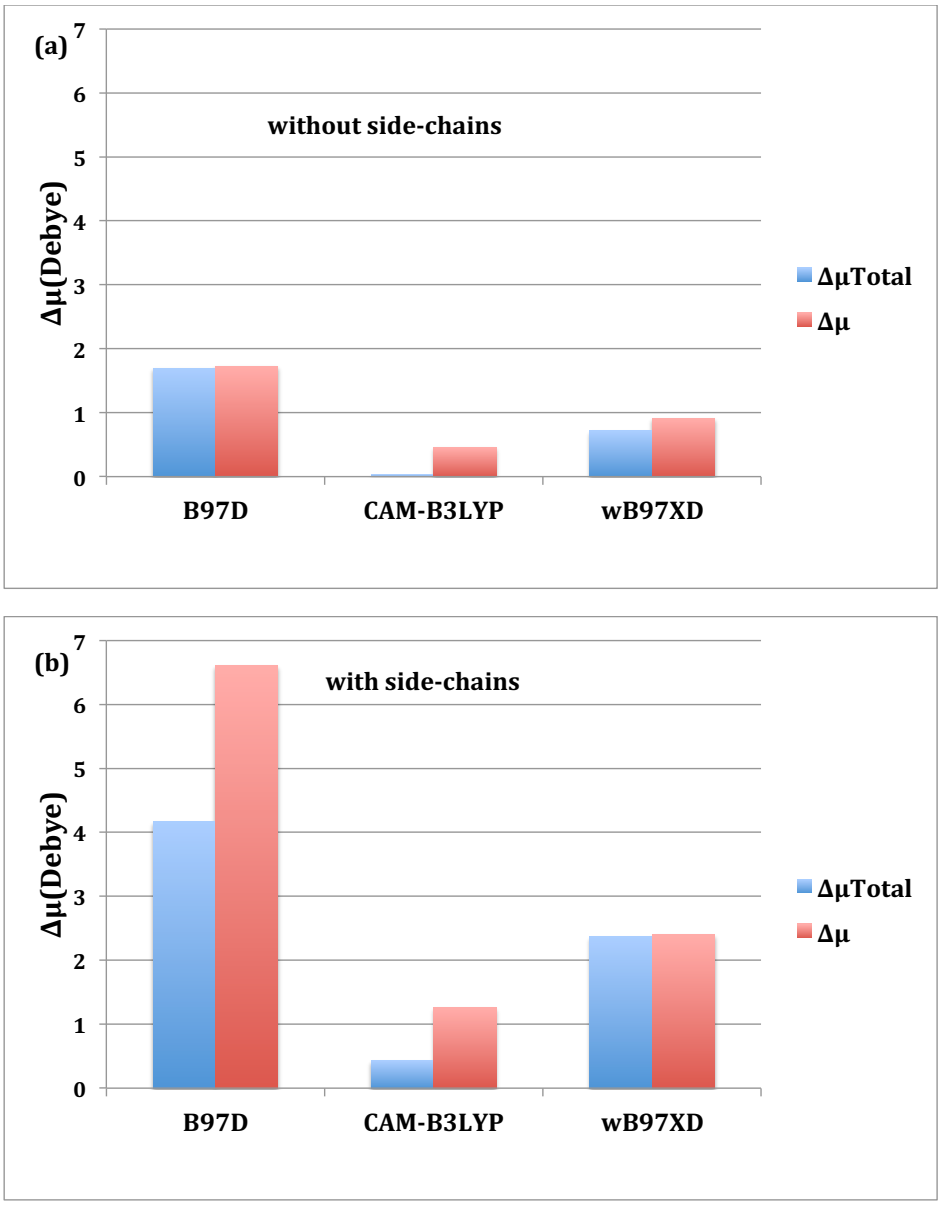

Figure 5.19: The difference between the dipole moments, $\Delta\mu_{Total}$ and $\Delta\mu$, of system containing (a)OPE-DTF and OPE-ALD (without side chains), (b) OPE-DTF and OPE-ALD (with side chains) obtained using the three approaches: DFT/B97D, /wB97XD, and /CAM-B3LYP.

5.4 Binding Energies and Intermolecular Distances

In this section, we carry out further quantitative analysis of the oligomer nanotube interaction. We calculated the binding energy between the SWCNTs and each oligomer, E_b, using the following relation,

$$E_b = E_{total} - (E_{SWCNT} + E_{Oligomer}), \tag{5.2}$$

where E_{total}, E_{SWCNT}, and $E_{Oligomer}$ are the configuration energies of the SWCNTs bound with oligomer, of the isolated SWCNT, and of the isolated oligomer, respectively. Fig. 5.20 and Table 5.1 show that in all cases the binding energy between SWCNT and OPE-DTF is larger than between SWCNT and OPE-ALD. This is true for oligomer with and without side chains. The binding energy for CAM-B3LYP is much smaller (less than 1 eV) than for the two other methods which give binding energies of 2 or more eV. For B97D and wB97XD the side chains increase the binding energies by a factor of two. This can be correlated with the fact that for B97D and wB97XD calculations the side chains wrap around the nanotube and hence increase the binding energies of these system. Table 5.1 also shows that binding energy are inversely proportional to the intermolecular distance between nanotube and the oligomer.

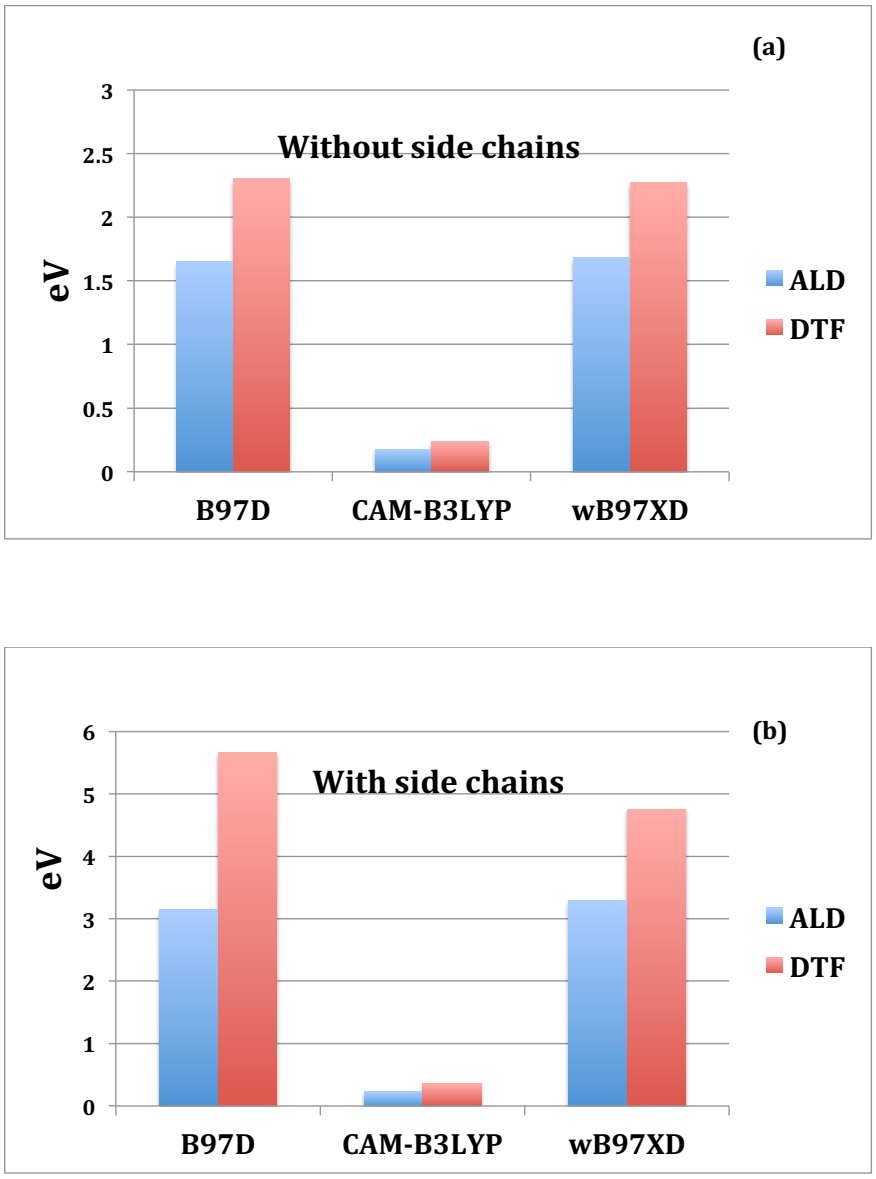

Figure 5.20: Binding energy of SWCNT and OPE (a) without side chains and (b) with side chains obtained using DFT/B97D, /wB97XD, and /CAM-B3LYP.

Table 5.1: Comparison of binding energy (E_b), intermolecular distance (Δd) between SWCNT and oligomers.

(a) (Without side chains)

ALD		
	E_b(eV)	Δd(A°)
B97D	1.65	3.17
CAM-B3LYP	0.177	3.75
wB97XD	1.683	3.28

(b) (Without side chains)

DTF		
	E_b(eV)	Δd(A°)
B97D	2.302	3.12
CAM-B3LYP	0.238	3.68
wB97XD	2.272	3.34

(c) (With side chains)

ALD		
	E_b(eV)	Δd(A°)
B97D	3.145	3.2
CAM-B3LYP	0.231	3.42
wB97XD	3.288	3.02

(d) (With side chains)

DTF		
	E_b(eV)	Δd(A°)
B97D	5.657	3.22
CAM-B3LYP	0.367	3.65
wB97XD	4.755	3.38

5.5 Conclusions

We make the following conclusions for Chapter 5. Comparison of isolated versus interacting geometry of OPEs shows that the largest changes occurs in the dihedral angles involving central bonds due to oligomers wrapping around the nanotubes. For OPE-DTF with and without side chains there are significant changes in dipole moment when OPE-DTF interacts with nanotube. The dipole moment of OPE-ALD with and without side chains is not affected by the presence of the nanotube. In other words, OPE-DTF is more polarizable by the nanotube than OPE-ALD. Comparison of DFT methods give similar results for oligomers without side chains. For oligomer with side chains there are differences between the DFT methods. The results of B97D and wB97XD calculations display side chains wrapping around the nanotube but CAM-B3LYP has side chains pointing away from the nanotube. These result indicate that there is less intermolecular interaction between oligomer and nanotube in the CAM-B3LYP calculations primarily because in the CAM-B3LYP approximation the side chains do not wrap around the nanotube. The analysis of binding energies show that OPE-DTF interacts more strongly with the nanotube in comparison to OPE-ALD (this is true for all DFT methods). CAM-B3LYP method gives the lowest binding energies and the largest intermolecular distance in comparison to B97D and wB97XD methods.

Chapter 6

Summary and Conclusions

In this chapter, we summarize the major results of this work. Our calculations were primarily carried out with the use of the dispersion corrected DFT methods (B97D, wB97XD, and CAM-B3LYP). The geometry parameters and electronic properties of isolated OPEs and OPE/nanotube combinations as obtained from DFT computations are discussed in chapters 4 and 5. The main conclusions are:

- OPE-ALD and OPE-DTF backbones have a similar structures as obtained using different DFT methods;

- The end groups (ALD and DTF) have an effect on the terminal bonds and angles in the oligomers and in OPE-DTF, DTF makes the oligomer somewhat nonplanar;

- For all DFT methods, OPE-DTFs have larger dipole moments than OPE-ALDs;

- The intermolecular interaction between SWCNT and OPE show that the largest changes occur in the dihedral angles involving central bonds along the backbone of the oligomer;

- B97D and wB97XD methods show that OPEs wrap around the SWCNT when side chains are present. CAM-B3LYP does not show this wrapping of side chains around the nanotube;

- The dipole moments of SWCNT and OPE-DTF combinations have higher dipole moments than combinations with OPE-ALD with and without side chains;

- The binding energies of OPE-DTF/nanotube are larger than the binding energies of OPE-ALD/nanotube. This correlates with intermolecular distances (OPE-DTF are closer to the nanotube than OPE-ALD).

The overall conclusion of this thesis is that OPE-DTFs interact more strongly with the nanotubes than OPE-ALDs especially when side chains are present. Finally, we comment on which DFT approximation is the most appropriate for these types of non-covalently bonded molecular system calculations. Our results suggest that B97D overestimates the intermolecular interactions (the side chains wrap too much around SWCNT) while CAM-B3LYP tends to underestimate the intermolecular interactions (the side chains interact weakly with SWCNT). It seams that wB97XD gives the most accurate results since it does not appear to overestimate or to underestimate intermolecular interactions. The future work could test other dispersion corrected DFT methods (see reference [93]) to study the interaction between oligomers and nanotubes. We could also investigate other oligomers interacting with SWCNTs (see for example [37]) and compare these (future) calculations with our results.

Bibliography

[1] A. Hirsch. *The era of carbon allotropes*. Nature Materials **9**, 868-871 (2010).

[2] R. Chang and K. Goldsby. *Chemistry*. McGraw-Hill Higher Education. (2012).

[3] D. T. Colbert and R. E. Smalleley *Past, Present, and Future of Fullerene Nanotubes: Buckytubes. Perspectives on Fullerene Nanotechnology*. Kluwer Academic Publishers. **3**, 3-10 (2002).

[4] H. Kroto, J. R. Heath, S. C. O' Brien , R. F. Curl, and R. E. Smalley *C_60: Buckminsterfullerene*. Nature **318** (6042), 162-163 (1985).

[5] F. Diederich and Y. Rubin. *Synthetic Approaches toward Molecular and Polymeric Carbon Allotropes*. Angew. Chem. Int. Ed. Engl. **31**, 1101-1123 (1992).

[6] M. Monthioux and V. L. Kuznetsov, *Who Should be Given the Credit for the Discovery of Carbon Nanotubes?* Carbon. **44** (9), 1621-1623 (2006).

[7] S. Iijima. *Helical Microtubules of Graphitic Carbon*. Nature. **354**, 56-58 (1991).

[8] C. D, K. Zhang, C. Zhong, F. Huang and Y. Cao. *Recent Advances in Water/Alcohol-soluble π-Conjugated Materials: New Materials and Growing Applications in Solar Cells*. Chem. Soc. Rev. **42**, 9071-9104 (2013).

[9] L. N. Cella, W. Chen, N. V. Myung, and A. Mulchandani. *Single-Wall Carbon Nanotubes-Based Chemiresistive Affinity Biosensors for Small Molecules: Ultrasensitive Glucose Detection*. J. Am. Chem. Sco. **132** (14), 5024-5026 (2010).

[10] B. Sup Shim, W. Chen , C. Doty, C. Xu, and N. A. Kotov. *Smart Electronic Yarns and Wearable Fabrics for Human Biomonitoring made by Carbon Nanotube Coating with Polyelectrolytes*. Nano Lett. **8** (12), 4151-4157 (2008).

[11] D. E. Luzzi, B. W. Smith. *Carbon Cage Structures in Single Wall Carbon Nanotubes Materials*. Carbon **38** (11), 1751-1756 (2000).

[12] G. D. M. S. Dresselhaus and R. Saito. *Physics of Carbon Nanotubes*. Carbon. **33**, 883-891 (1995).

[13] D. S. Bethune, C. H. Kiang, M. S. Devries, G. Gorman, R. Savoy, J. Vazquez, and R. Beyers. *Cobalt-catalyzed Growth of Carbon Nanotubes With Single-Atomic Layerwalls*. Nature Lett. **363**, 605-607 (1993).

[14] K. D. Ausman, R. Piner, O. Lourie, R. S. Ruoff, and M. Korobov. *Organic Solvent Dispersions of Single-walled Carbon Nanotubes: Toward Solutions of Pristine Nanotubes*. Phys. Chem. B **104** (38), 8911-8915 (2000).

[15] H. Omachi, T. Nakayama, E. Takahashi, Y. Segawa, and K. Itami. *Initiation of Carbon Nanotube Growth by Well-defined Carbon Nanorings*. Nature Chem. **5**, 572-576 (2013).

[16] R. Andrews, D. Jacques, M. Minot, and T. Rantell. *Fabrication of Carbon Multiwall Nanotube/Polymer composites by Shear Mixing*. Macromol. Mater. Eng. **287** (6), 395-403 (2002).

[17] N. Karousis, N. Tagmatarchis and D. Tasis. *Current Progress on the Chemical Modification of Carbon Nanotubes*. Chem. Rev. **110** (9), 5366-5397 (2010).

[18] R. S. Ruoff, D. Qian, and W. K. Liu. *Mechanical Properties of Carbon Nanotubes: Theoretical Predictions and Experimental Measurements*. C. R. Physique. **4**, 993-1008 (2003).

[19] T. J. Skotheim, *Handbook of Conducting Polymers*. **1** and **2**, M. Dekker Inc. New York (1986).

[20] A. Kraft, A. C. Grimsdale, and A. B. Holmes. *Electroluminescent Conjugated Polymers-Seeing Polymers in a New Light*. Angew. Chem. Int. Ed. **37**, 402-428 (1998).

[21] T. C. Clarke, R. H. Geiss, J. F. Kwak, and G. B. Street. *Highly Conducting Transition Metal Derivatives of Polyacetylene*. J. Chem. Soc., Chem. Comm. **338**, 489-490 (1978).

[22] J. H. Burroughes, D. D. C. Bradley, A. R. Brown, R. N. Marks, K. Mackay, R. H. Friend, P. L. Burns, A. B. Holmes. *Light-Emitting Diodes Based on Conjugated Polymers*. Nature **347**, 539-541 (1990).

[23] A. J. Heeger. *Semiconducting and Metallic Polymers: The Fourth Generation of Polymeric Materials*. Phys. Chem. B **105** (36), 8475-8491 (2001).

[24] M. Ates, T. Karazehir, and A. S. Sarac. *Conducting Polymers and Their Applications*. Phys. Chem. **2** (3), 224-240 (2012).

[25] A. Dodabalapur. *Organic and Polymer Transistors for Electronics*. Materials Today. **9** (4), 24-30 (2006).

[26] M. Ates, T. Karazehir, and A. S. Sarac. *Conducting Polymers and their Applications*. Phys. Chem. **2** (3), 224-240 (2012).

[27] Z. Bao, A. B. Chwang, L. Loo, and R. A. Segalman, editor. *In Conjugated Organic Materials-Synthesis, Structure, Device, and Applications*. Mater. Res. Soc. Symp. Proc. 937E, Warrendale, PA, **0937** (2006).

[28] R. E. Martin and F. Diederich. *Linear Monodisperse π-Conjugated Oligomers: Model Compounds for Polymers and More*. Angew. Chem. Int. Ed. **38**, 1350-1377 (1999).

[29] G. O. Shonaike, S. G. Advani, *Advanced Polymeric Materials: Structure Property Relationships*. CRC Press. Boca Raton. FL. USA. (2003).

[30] N. Zhou, L. Wang, D. W. Thompson, Y. Zhao *OPE/OPV H-mers: Synthesis, Electronic properties, and Spectroscopic Responses to Binding with Transition Metal Ions*. Tetrahedron **67**, 125-143 (2011).

[31] N. Zhou, L. Wang, D. W. Thompson, Y. Zhao *H-Shaped OPE/OPV Oligomers: A New Member of 2D Conjugated Fluorophore Cores*. Org. Lett. **10**, 3001-3004 (2008).

[32] P. Umari, O. Petrenko, S. Taioli, and M. M. De Souza. *Communication: Electronic Band Gaps of Semiconducting Zig-Zag Carbon Nanotubes from Many-Body Perturbation Theory Calculations*. Chem. Phys. **136**, (181101), 1-4 (2012).

[33] D. T. Colbert. *Single-Wall Nanotubes: a New Option for Conductive Plastics and Engineering Polymers*. Plastics Additives. Compd. **3**, 18-25 (2003).

[34] P. Kim, L. Shi, A. Majumar, P. L. McEuen. *Thermal Transport Measurements of Individual Multi Walled Composites for Thermal Management.* Appl. Phys. Lett. **87** (21),2155021-4 (2001).

[35] M. J. Biercuk, M. C. Llaguno, M. Radosvljevic, J. K. Hyun, and A. T. Johnson. *Carbon Nanotube Composites for Thermal Management.* Appl. Phys. Lett. **80** (15), 2767-2769 (2002).

[36] T. Kim, S. J. Yang and C. R. Park. *Carbon Nanomaterials in Organic Photovoltaic Cells.* Carbon Lett. **12** (4), 194-206 (2011); M.S. Dresselhaus, G. Dresslhous and P. Avouris, *Carbon Nanotubes: Synthesis, Structure, Properties and Application.* Springer. Berlin. Germany. (2001).

[37] I. Pochorovsk, H. Wang, J. I. Feldblyum, X. Zhang, A. L. Antaris, and Z. Bao. *H-Bonded Superamolecular Polymer for the Selective Dispersion and Subsequent Release of Larg-Diameter Semiconducting Single-Wall Carbon Nanotubes.* J. Am. Chem. Soc. **137**, 4328-4331 (2015).

[38] W. D. Zhang, L. Shen, I. Y. Phang and T. X. Liu. Macromolecules. **37**, 256-259 (2004).

[39] Shieh, Y.-T.; Chen, J.-Y.; Twuc, Y.-K.; Chen, W.-J. Polym. Int. **61**, 554 (2011).

[40] K. Mulla and Y. Zhao. *When Dithiafulvenyl Functionalized π-Conjugated Oligomers Meet Fullerenes and Single-Walled Carbon Nanotubes.* J. Mater. Chem. C. **1** 5116-5127 (2013).

[41] K. Mulla, S. Liang, H. Shaik, E. A. Younes, A. Adronov, and Y. Zhao. *Dithiafulvenyl-grafted Phenylene Ethynylene Polymers as Selective and Reversible Dispersants for Single-Walled Carbon Nanotubes.* Chem. Commun. **51**, 149-152 (2015).

[42] J. Wiley and S. Ltd. *Encyclopedia of Computational Chemistry*. **5**,(1998).

[43] C. J. Cramer. *Essentials of Computational Chemistry: Theories and Models*. Wiley, 2nd edition. (2004).

[44] W. J. Hehre. *Practical Strategies for Electronic Structure Calculations Wavefunction*. (1995).

[45] W.J. Hehre, L. Radom, P.V.R. Schleyer and J.A. Pople. *Ab Initio Molecular Orbital Theory*. John Wiley and Sons. New York. (1985).

[46] M.J.S. Dewar. *The Molecular Orbital Theory of Organic Chemistry*. McGraw-Hill. New York. (1969).

[47] E. Lewars. *Computational Chemistry: Introduction to the Theory and Applications of Molecular and Quantum Mechanics*. Kluwer Academic Publishers. London. (2003).

[48] J. Leszczynski and M. K. Shukla. *Practical Aspects of Computational Chemistry I*. Springer Heidelberg Dordrecht London New York. (2009).

[49] J. A. Pople and D. L. Beveridge. *Approximation Molecular Orbital Theory*. McGraw-Hill. New York. Chap. **1** and **2**, (1970).

[50] R. F. W. Bader. *Atoms in Molecules*. Oxford University Press. New York. (1990).

[51] A. Szabo and N. S. Ostlund. *Modern Quantum Chemistry. Macmillan*. New York. (1982).

[52] D. R. Hartree. *The Wave Mechanics of an Atom with a non-Coulomb Central Field. Part III. Term Values and Intensities in Series in Optical Spectra*. Proc. Camb. Phil Soc. **24** (3), 426-437 (1928).

[53] J. B. Foresman and A. Frisch. *Exploring Chemistry with Orbital*. Oxford University Press, New York. (1993).

[54] C. C. J. Roothaan. *New Developments in Molecular Orbital Theory*. Rev. Mod. Phys. **23** 69-89 (1951).

[55] G. G. Hall. *The Molecular Orbital Theory of Chemical Valency. VIII. A Method of Calculating Ionization Potentials*. Proc. Roy. Soc. A **205**, 541-552 (1951).

[56] Y. Jean. and F. Volatron. *An Introduction to Molecular Orbitals*. New York. Oxford University Press. (1993).

[57] R. G. Parr and W. Yang. *Density Functional Theory of Atoms and Molecules*. Oxford University Press. New York. (1989).

[58] E. H. Lieb and B. Simon. *The Thomas-Fermi Theory of Atoms, Molecules and Solids*. Adv. Math. **23**, 22-116 (1977).

[59] R. O. Mueller, A. R. P. Rau and L. Spruch. *Statistical Model of Atoms in Intense Magnetic Fields*. Phys. Rev. Lett. **26**, 1136-1139 (1971).

[60] P. Hohenberg, W. Kohn. *Inhomogeneous Electron Gas*. Phys. Rev. **136**, 864-871 (1964).

[61] R. Lesar. *Introduction to Computational Materials Science*. Materials Research Society. (2013).

[62] C. Fiolhais, F. Nogueira, and M. Marques. *A Primer in Density Functional Theory*. Springer.Physics and Astronomy. (2003).

[63] I. N. Levine. *Quantum Chemistry*. Prentice Hall. New Jersey, Saddle River. (2000).

[64] A. D. Becke. *Perspective: Fifty years of Density-Functional Theory in Chemical Physics*. Chem. Phys. **140** (18), 18A301-18 (2014).

[65] W. Kohn, LJ. Sham. *Perspective on " Self-Consistent Equations Including Exchange and Correlation Effects"*. Phys. Rev. A **140**, 133-1138 (1965).

[66] F. Jensen. *Introduction to Computational Chemistry*. New York. **101**, 208 (1997).

[67] J. W. Mintmire and C. T. White. *Local-Density-Functional Results for The Dimerization of Trans-Polyacetylene: Relationship to the Band-Gap Problem*. Phys. Rev. B **35** (8), 4180 (1987).

[68] V. J. Stenger. *The Unconsious Quantum,* Prometheus. Amherst. New York. (1995).

[69] E. Runge and E. K. U. Gross. *Density-Functional Theory for Time-Dependent Systems*. Phys. Rev. Lett. **52** (997),12-19 (1984).

[70] E. K. U. Gross, M. Petersilka and T. Grabo *Conventional Quantum Chemical Correlation Energy versus Density-Functional Correlation Energy*. J. Am. Chem. Soc. **629**, (1996).

[71] D. Joulbert, editor *Density Functional: Theory and Applications*. Springer, Berlin, 19-29 (1998).

[72] H. Eschrig. *The Fundamentals of Density Functional Theory*. Teubner. Stuttgart. (1995).

[73] S. H. Vosko, L. Wilk, and M. Nusair. *Accurate Spin-Dependent Electron Liquid Correlation Energies for Local Spin Density Calculations: a Critical Analysis*. Can. J. Phys. **58** (8), 1200-1211 (1980).

[74] C. Lee, W. Yang, and R. G. Parr. *Development of the Colle-Salvetti Correlation-Energy Formula into a Functional of The Electron Density*. Phys. Rev. B **37**, 785-789 (1988).

[75] S. Grimme. *Accurate description of van der Waals complexes by density functional theory including empirical corrections*. Comput. Chem. **25**, 1463-1476 (2004).

[76] S. Grimme. J. Comput. *Semiempirical GGA-Type Density Functional Constructed with a Long-Rang Dispersion Correction*. Comput. Chem. **27** (15), 1787-99 (2006).

[77] R. Kobayashi, and R. D. Amos. *The Application of CAM-B3LYP to the Charge-Transfer Band Problem of the Zincbacteriochlorin-Bacteriochlorin Complex*. Chem. Phys. Lett. **420**, 106-109 (2006).

[78] T. Yanai, D. P. Tew, and N. C. Handy. *A New Hybrid Exchange-Correlation Functional Using the Coulomb-Attenuating Method (CAM-B3LYP)*. Chem. Phys. Lett. **393**, 51-57 (2004).

[79] Y. Tawada, T. Tsuneda, S. Yanagisawa, T. Yanai, and K. Hirao. *A Long-Range-Corrected Time-Dependent Density Functional Theory*. Chem. Phys. **120**, 8425-8433 (2004).

[80] R. G. Parr and W. Yang. *Density-Functional Theory of Atoms and Molecules*. Oxford University Press, Oxford. (1989).

[81] J. D. Chai and M. H. Gordon. *Systematic Optimization of Long-Range Corrected Hybrid Density Functionals*. Chem. Phys. **128**, 084106 (2008).

[82] W. J. Hehre, R. Ditchfield, and J. A. Pople. *Self-Consistent Molecular-Orbital Methods. IX. An Extended Gaussian-Type Basis for Molecular-Orbital Studies of Organic Molecules*. Chem. Phys. **54**, 724-728 (1971).

[83] A. D. Becke. *Perspective: Fifty years of Density-Functional Theory in Chemical Physics*. Chem. Phys. **140** (18), 18A301-18 (2014).

[84] K. Burke. *Perspective on Density Functional Theory*. Chem. Phys. **136** (15), 150901-9 (2012).

[85] Gaussian 09, Revision A.02, M.J. Frisch, G. W. Trucks, H. B. Schlegel, G. E. Scuseria, M. A. Robb, J. R. Cheeseman, G. Scalmani, V. Barone, B. Mennucci, G. A. Petersson, H. Nakatsuji, M. Caricato, X. Li, H. P. Hratchian, A. F. Izmaylov, J. Bloino, G. Zheng, J. L. Sonnenberg, M. Hada, M. Ehara, K. Toyota, R. Fukuda, J. Hasegawa, M. Ishida, T. Nakajima, Y. Honda, O. Kitao, H. Nakai, T. Vreven, J. A. Montgomery, Jr., J. E. Peralta, F. Ogliaro, M. Bearpark, J. J. Heyd, E. Brothers, K. N. Kudin, V. N. Staroverov, R. Kobayashi, J. Normand, K. Raghavachari, A. Rendell, J. C. Burant, S. S. Iyengar, J. Tomasi, M. Cossi, N. Rega, J. M. Millam, M. Klene, J. E. Knox, J. B. Cross, V. Bakken, C. Adamo, J.Jaramillo, R. Gomperts, R.E. Stratmann, O. Yazyev, A. J. Austin, R. Cammi, C. Pomelli, J. W. Ochterski, R. L. Martin, K. Morokuma, V. G. Zakrzewski, G. A. Voth, P. Salvador, J. J. Dannenberg, S. Dapprich, A.D. Daniels. Farkas, J. B. Foresman, J. V. Ortiz, J. Cioslowski, and D. J. Fox, Gaussian, Inc., Wallingford CT, AC. (2009).

[86] W. J. Hehre, L. Radom, P. V. R. Schleyer, and J. A. Pople. *AB Initio Molecular Orbital Theory*. Wiley Interscience. New York. (1985).

[87] VMD 1.9.1 *Visial Molecular Dynamics* www.ks.uiuc.edu/Research/vmd/

[88] ACD/ChemSketch www.acdlabs.com/resources/freeware/chemsketch/

[89] Gauss View 5.0.8 *User Reference* www.gaussview.com.

[90] *Wolfram Mathematica* version 9.0 www.wolfram.com/mathematica/

[91] J. Chen, M. A. Reed, A. M. Rawlett, and J. M. Tour. *Large On-Off Ratios and Negative Differential Resistance in a Molecular Electronic Device*. Science **286**, 1550-1552 (1999).

[92] T. V. Voorhis and G. E. Scuseria. *A Novel Form for the Exchange-Correlation Energy Functional*. Chem. Phys. **109** (2), 400-410 (1998).

[93] A. J. Cohen, P. Mori-Sanchez, and W. Yang *Challenges for Density Functional Theory*. Chem. Rev. **112**, 289-320 (2012).

Appendix A

Geometry of Gas Phase OPEs

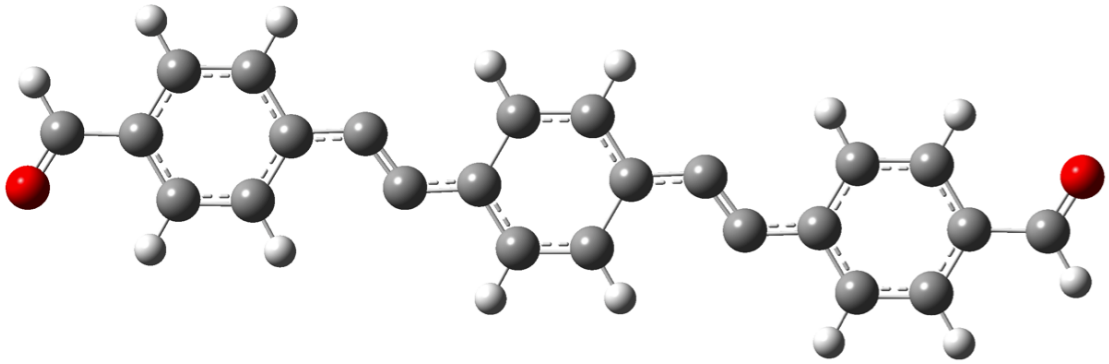

Figure A.1: Representative optimized structure of OPE-ALD (without side chains) in gas phase obtained using MM (UFF).

Table A.1: Selected bond lengths (R) (in A°), bond angles (A) (in degrees), and dihedral angles (D) (in degrees) of OPE-ALD (without side chains) the labelling of atoms is shown in Scheme 4.1.

	B97D	wB97XD	CAM-B3LYP	B3LYP	UFF
R					
(1-2)	**1.225**	**1.210**	**1.210**	**1.216**	**1.221**
(2-3)	**1.482**	**1.481**	**1.477**	**1.478**	**1.478**
(3-4)	**1.410**	**1.396**	**1.396**	**1.402**	**1.402**
(4-5)	**1.395**	**1.387**	**1.382**	**1.388**	**1.398**
(5-6)	**1.421**	**1.403**	**1.405**	**1.411**	**1.403**
(6-7)	**1.419**	**1.428**	**1.426**	**1.421**	**1.399**
(7-8)	**1.228**	**1.210**	**1.208**	**1.217**	**1.254**
(8-9)	**1.418**	**1.428**	**1.426**	**1.421**	**1.396**
(9-10)	**1.421**	**1.403**	**1.402**	**1.411**	**1.488**
(10-11)	**1.392**	**1.385**	**1.383**	**1.386**	**1.394**
(11-12)	**1.421**	**1.403**	**1.402**	**1.411**	**1.398**
(12-13)	**1.418**	**1.428**	**1.426**	**1.421**	**1.396**
(13-14)	**1.228**	**1.210**	**1.208**	**1.217**	**1.254**
(14-15)	**1.419**	**1.428**	**1.426**	**1.421**	**1.399**
(15-16)	**1.424**	**1.405**	**1.402**	**1.414**	**1.411**
(16-17)	**1.391**	**1.384**	**1.385**	**1.385**	**1.398**
(17-18)	**1.413**	**1.398**	**1.394**	**1.404**	**1.404**
(18-19)	**1.482**	**1.481**	**1.477**	**1.478**	**1.477**
(19-20)	**1.225**	**1.210**	**1.210**	**1.216**	**1.221**
A					
(1-2-3)	**124.9**	**124.4**	**124.3**	**124.6**	**121.1**
(2-3-4)	**119.7**	**119.9**	**120.1**	**120.1**	**119.6**
(3-4-5)	**120.6**	**120.4**	**120.1**	**120.5**	**120.5**
(4-5-6)	**120.0**	**119.9**	**120.3**	**120.1**	**120.6**
(5-6-7)	**120.5**	**120.2**	**120.2**	**120.4**	**118.2**
(6-7-8)	**179.6**	**179.9**	**179.8**	**179.8**	**124.1**
(7-8-9)	**179.9**	**179.8**	**179.9**	**179.9**	**123.5**
(8-9-10)	**120.6**	**120.4**	**120.5**	**120.6**	**122.5**
(9-10-11)	**120.6**	**120.4**	**120.5**	**120.7**	**120.4**
(10-11-12)	**120.6**	**120.4**	**120.5**	**120.7**	**120.8**
(11-12-13)	**120.6**	**120.3**	**120.5**	**120.6**	**118.5**
(12-13-14)	**179.9**	**179.8**	**179.9**	**179.9**	**123.5**
(13-14-15)	**179.6**	**179.9**	**179.8**	**179.8**	**124.1**

Table A.2: Contiune.

(14-15-16)	**120.3**	**120.2**	**120.3**	**120.4**	**122.8**
(15-16-17)	**120.3**	**120.2**	**120.0**	**120.4**	**120.4**
(16-17-18)	**120.3**	**120.1**	**120.4**	**120.3**	**120.4**
(17-18-19)	**120.7**	**120.1**	**120.1**	**120.4**	**121.2**
(18-19-20)	**124.9**	**124.4**	**124.3**	**124.6**	**121.1**
D					
(1-2-3-4)	**-179.9**	**-179.9**	**-180.0**	**-179.9**	**-179.8**
(2-3-4-5)	**-179.9**	**-179.9**	**-180.0**	**-179.9**	**179.9**
(3-4-5-6)	**-0.001**	**0.0017**	**0.000**	**0.0009**	**0.025**
(4-5-6-7)	**-179.9**	**179.9**	**180.0**	**-179.9**	**-179.8**
(5-6-7-8)	**-179.0**	**-173.2**	**-179.0**	**-178.9**	**-179.9**
(6-7-8-9)	**151.7**	**-5.040**	**0.000**	**16.75**	**-179.8**
(7-8-9-10)	**27.31**	**178.4**	**179.9**	**162.2**	**0.245**
(8-9-10-11)	**179.9**	**-179.9**	**-180.0**	**179.9**	**179.8**
(9-10-11-12)	**0.003**	**0.000**	**0.000**	**0.000**	**0.087**
(10-11-12-13)	**179.9**	**179.9**	**-180.0**	**179.9**	**179.8**
(11-12-13-14)	**150.4**	**0.405**	**-0.121**	**17.95**	**-179.8**
(12-13-14-15)	**-149.4**	**1.948**	**0.125**	**-16.94**	**179.9**
(13-14-15-16)	**-0.958**	**-2.401**	**-0.004**	**-1.054**	**0.044**
(14-15-16-17)	**-179.9**	**-179.9**	**-180.0**	**-179.9**	**-179.9**
(15-16-17-18)	**-0.001**	**0.000**	**0.00**	**0.0007**	**0.020**
(16-17-18-19)	**-179.9**	**-179.9**	**-180.0**	**-179.9**	**179.9**
(17-18-19-20)	**-0.0006**	**-0.006**	**0.000**	**0.000**	**0.084**

Table A.3: Selected bond lengths (R) (in A°), bond angles (A) (in degrees), and dihedral angles (D) (in degrees) of OPE-ALD (with side chains) the labelling of atoms is shown in Scheme 4.1.

	B97D	wB97XD	CAM-B3LYP	B3LYP	UFF
R					
(1-2)	**1.225**	**1.210**	**1.210**	**1.227**	**1.221**
(2-3)	**1.480**	**1.479**	**1.476**	**1.477**	**1.477**
(3-4)	**1.411**	**1.396**	**1.394**	**1.402**	**1.402**
(4-5)	**1.394**	**1.386**	**1.384**	**1.388**	**1.397**
(5-6)	**1.422**	**1.403**	**1.402**	**1.411**	**1.411**
(6-7)	**1.416**	**1.426**	**1.425**	**1.419**	**1.399**
(7-8)	**1.228**	**1.210**	**1.208**	**1.217**	**1.255**
(8-9)	**1.414**	**1.424**	**1.423**	**1.417**	**1.405**
(9-10)	**1.431**	**1.409**	**1.407**	**1.418**	**1.407**
(10-11)	**1.398**	**1.390**	**1.387**	**1.392**	**1.414**
(11-12)	**1.417**	**1.400**	**1.400**	**1.409**	**1.403**
(12-13)	**1.414**	**1.424**	**1.423**	**1.417**	**1.406**
(13-14)	**1.228**	**1.210**	**1.208**	**1.217**	**1.254**
(14-15)	**1.416**	**1.426**	**1.425**	**1.419**	**1.398**
(15-16)	**1.424**	**1.406**	**1.405**	**1.414**	**1.411**
(16-17)	**1.391**	**1.383**	**1.381**	**1.385**	**1.398**
(17-18)	**1.413**	**1.398**	**1.396**	**1.405**	**1.404**
(18-19)	**1.480**	**1.479**	**1.476**	**1.477**	**1.478**
(19-20)	**1.225**	**1.210**	**1.210**	**1.217**	**1.221**
A					
(1-2-3)	**125.1**	**124.5**	**124.4**	**124.7**	**121.1**
(2-3-4)	**119.7**	**119.9**	**120.1**	**120.1**	**119.5**
(3-4-5)	**120.6**	**120.4**	**120.4**	**120.6**	**120.5**
(4-5-6)	**120.0**	**119.9**	**120.0**	**120.1**	**120.4**
(5-6-7)	**119.7**	**119.7**	**120.1**	**120.3**	**122.8**
(6-7-8)	**177.7**	**178.0**	**178.9**	**179.3**	**123.9**
(7-8-9)	**178.5**	**179.2**	**178.9**	**178.7**	**124.9**
(8-9-10)	**120.1**	**119.7**	**120.3**	**120.6**	**118.3**
(9-10-11)	**119.4**	**119.1**	**119.2**	**119.2**	**118.8**
(10-11-12)	**121.3**	**120.9**	**121.2**	**121.4**	**121.6**
(11-12-13)	**120.5**	**120.3**	**119.9**	**119.9**	**116.1**
(12-13-14)	**178.5**	**179.2**	**178.9**	**178.7**	**125.5**
(13-14-15)	**177.7**	**178.0**	**178.9**	**179.3**	**124.3**
(14-15-16)	**121.1**	**120.7**	**120.5**	**120.5**	**122.9**
(15-16-17)	**120.3**	**120.2**	**120.3**	**120.4**	**120.3**
(16-17-18)	**120.3**	**120.1**	**120.2**	**120.3**	**120.4**
(17-18-19)	**120.7**	**120.3**	**120.1**	**120.4**	**121.2**

Table A.4: Contiune.

(18-19-20)	**125.1**	**124.5**	**124.4**	**124.8**	**121.1**
D					
(1-2-3-4)	**-179.9**	**179.8**	**179.9**	**179.9**	**-179.9**
(2-3-4-5)	**179.9**	**-179.8**	**-179.9**	**-179.9**	**179.8**
(3-4-5-6)	**0.001**	**-0.047**	**0.004**	**0.007**	**0.023**
(4-5-6-7)	**-179.8**	**179.6**	**179.8**	**179.8**	**-179.8**
(5-6-7-8)	**6.016**	**-16.34**	**-8.445**	**-15.73**	**0.146**
(6-7-8-9)	**9.865**	**-56.59**	**-159.4**	**-152.0**	**179.9**
(7-8-9-10)	**-15.3**	**66.7**	**167.5**	**167.6**	**-179.6**
(8-9-10-11)	**179.3**	**-179.0**	**-179.6**	**-179.5**	**179.8**
(9-10-11-12)	**0.198**	**-0.258**	**-0.101**	**-0.145**	**-0.065**
(10-11-12-13)	**179.3**	**-179.0**	**-179.6**	**-179.5**	**-179.9**
(11-12-13-14)	**-164.0**	**112.8**	**12.27**	**12.17**	**-179.5**
(12-13-14-15)	**-9.954**	**56.57**	**159.2**	**151.8**	**-179.8**
(13-14-15-16)	**173.7**	**-163.5**	**-171.3**	**-163.9**	**0.384**
(14-15-16-17)	**-179.7**	**179.5**	**179.8**	**179.8**	**179.7**
(15-16-17-18)	**-0.027**	**0.064**	**0.005**	**0.008**	**0.065**
(16-17-18-19)	**179.9**	**-179.9**	**-179.9**	**-179.9**	**-179.9**
(17-18-19-20)	**-0.030**	**0.099**	**-0.028**	**-0.014**	**0.115**

Table A.5: Selected bond lengths (R) (in A°), bond angles (A) (in degrees), and dihedral angles (D) (in degrees) of OPE-DTF (without side chains) the labelling of atoms is shown in Scheme 4.1.

	B97D	wB97XD	CAM-B3LYP	B3LYP	UFF
R					
(1-2)	1.795	1.779	1.779	1.789	1.794
(2-3)	1.368	1.347	1.346	1.357	1.345
(3-4)	1.454	1.464	1.459	1.455	1.480
(4-5)	1.424	1.405	1.404	1.415	1.401
(5-6)	1.390	1.384	1.381	1.384	1.398
(6-7)	1.422	1.403	1.402	1.411	1.411
(7-8)	1.417	1.427	1.426	1.420	1.399
(8-9)	1.229	1.211	1.209	1.218	1.255
(9-10)	1.417	1.427	1.426	1.420	1.399
(10-11)	1.422	1.403	1.402	1.412	1.402
(11-12)	1.392	1.385	1.383	1.386	1.398
(12-13)	1.422	1.403	1.402	1.411	1.411
(13-14)	1.417	1.427	1.426	1.420	1.399
(14-15)	1.229	1.211	1.209	1.218	1.255
(15-16)	1.417	1.427	1.426	1.420	1.399
(16-17)	1.420	1.401	1.399	1.409	1.403
(17-18)	1.393	1.386	1.385	1.388	1.398
(18-19)	1.421	1.403	1.403	1.412	1.404
(19-20)	1.454	1.464	1.459	1.455	1.477
(20-21)	1.368	1.347	1.346	1.357	1.395
(21-22)	1.788	1.775	1.775	1.782	1.798
A					
(1-2-3)	120.1	120.6	120.2	120.1	119.1
(2-3-4)	131.3	128.9	130.3	131.3	124.5
(3-4-5)	117.4	118.2	117.7	117.5	119.1
(4-5-6)	122.0	121.5	121.7	121.9	120.5
(5-6-7)	120.6	120.4	120.4	120.6	120.4
(6-7-8)	121.1	120.8	120.8	121.0	122.8
(7-8-9)	179.9	179.5	179.8	179.9	124.0
(8-9-10)	179.9	179.6	179.9	179.9	124.1
(9-10-11)	120.8	120.5	120.6	120.8	118.1
(10-11-12)	120.8	120.5	120.6	120.8	120.6
(11-12-13)	120.8	120.5	120.6	120.8	120.4
(12-13-14)	120.8	120.4	120.6	120.8	122.8
(13-14-15)	179.9	179.6	179.9	179.9	124.1
(14-15-16)	179.9	179.5	179.8	179.8	124.1
(15-16-17)	120.9	120.5	120.8	121.0	118.2
(16-17-18)	121.2	120.8	120.9	121.2	120.6
(17-18-19)	121.4	121.1	121.1	121.3	120.4

Table A.6: Continue.

(18-19-20)	**125.7**	**124.1**	**124.8**	**125.6**	**121.5**
(19-20-21)	**131.3**	**128.9**	**130.3**	**131.5**	**124.5**
(20-21-22)	**127.5**	**126.5**	**127.0**	**127.4**	**123.0**
D					
(1-2-3-4)	**-179.2**	**-179.5**	**-179.6**	**-179.6**	**-179.9**
(2-3-4-5)	**-168.4**	**-154.8**	**-162.9**	**-171.3**	**-133.0**
(3-4-5-6)	**179.3**	**179.1**	**179.4**	**179.5**	**-178.4**
(4-5-6-7)	**0.46**	**0.539**	**0.467**	**0.339**	**1.049**
(5-6-7-8)	**-179.8**	**-179.5**	**-179.8**	**-179.9**	**179.9**
(6-7-8-9)	**108.3**	**138.7**	**59.69**	**12.76**	**0.662**
(7-8-9-10)	**51.67**	**-20.55**	**65.03**	**-168.3**	**-179.7**
(8-9-10-11)	**-159.7**	**123.5**	**-127.8**	**156.5**	**-179.9**
(9-10-11-12)	**179.9**	**179.6**	**179,9**	**-179.9**	**-179.4**
(10-11-12-13)	**-0.002**	**-0.044**	**-0.032**	**0.014**	**0.002**
(11-12-13-14)	**-179.9**	**-179.6**	**-179.9**	**179.9**	**179.4**
(12-13-14-15)	**21.83**	**55.89**	**52.17**	**-110.9**	**-0.011**
(13-14-15-16)	**55.14**	**-20.38**	**64.97**	**-55.07**	**-179.8**
(14-15-16-17)	**-77.26**	**-41.53**	**-120.7**	**166.7**	**179.6**
(15-16-17-18)	**179.7**	**179.5**	**179.7**	**179.9**	**-179.7**
(16-17-18-19)	**-0.191**	**-0.529**	**-0.308**	**-0.076**	**-1.009**
(17-18-19-20)	**-179.5**	**-179.2**	**-179.5**	**-179.8**	**178.1**
(18-19-20-21)	**12.24**	**26.16**	**17.88**	**6.90**	**47.28**
(19-20-21-22)	**2.302**	**2.271**	**1.701**	**1.05**	**5.668**

Table A.7: Selected bond lengths (R) (in A°), bond angles (A) (in degrees), and dihedral angles (D) (in degrees) of OPE-DTF (with side chains) the labelling of atoms is shown in Scheme 4.1.

	B97D	wB97XD	CAM-B3LYP	B3LYP	UFF
R					
(1-2)	**1.787**	**1.775**	**1.774**	**1.788**	**1.774**
(2-3)	**1.367**	**1.346**	**1.344**	**1.356**	**1.345**
(3-4)	**1.454**	**1.463**	**1.460**	**1.455**	**1.481**
(4-5)	**1.423**	**1.405**	**1.404**	**1.414**	**1.401**
(5-6)	**1.390**	**1.383**	**1.381**	**1.384**	**1.397**
(6-7)	**1.422**	**1.404**	**1.402**	**1.411**	**1.411**
(7-8)	**1.416**	**1.426**	**1.425**	**1.419**	**1.399**
(8-9)	**1.228**	**1.210**	**1.209**	**1.218**	**1.254**
(9-10)	**1.414**	**1.424**	**1.423**	**1.417**	**1.400**
(10-11)	**1.429**	**1.408**	**1.407**	**1.418**	**1.407**
(11-12)	**1.398**	**1.390**	**1.387**	**1.391**	**1.401**
(12-13)	**1.418**	**1.400**	**1.400**	**1.409**	**1.410**
(13-14)	**1.414**	**1.424**	**1.423**	**1.417**	**1.401**
(14-15)	**1.228**	**1.210**	**1.209**	**1.217**	**1.255**
(15-16)	**1.416**	**1.427**	**1.425**	**1.419**	**1.398**
(16-17)	**1.419**	**1.400**	**1.399**	**1.409**	**1.401**
(17-18)	**1.393**	**1.387**	**1.385**	**1.388**	**1.396**
(18-19)	**1.421**	**1.402**	**1.402**	**1.411**	**1.404**
(19-20)	**1.454**	**1.463**	**1.460**	**1.456**	**1.479**
(20-21)	**1.367**	**1.345**	**1.344**	**1.355**	**1.396**
(21-22)	**1.783**	**1.771**	**1.772**	**1.778**	**1.796**
A					
(1-2-3)	**120.7**	**120.7**	**120.8**	**120.1**	**119.3**
(2-3-4)	**130.7**	**129.5**	**129.6**	**131.6**	**124.9**
(3-4-5)	**117.6**	**117.9**	**117.9**	**117.4**	**118.9**
(4-5-6)	**121.9**	**121.5**	**121.6**	**122.0**	**120.5**
(5-6-7)	**120.5**	**120.3**	**120.4**	**120.6**	**120.3**
(6-7-8)	**120.7**	**120.1**	**120.3**	**120.7**	**122.7**
(7-8-9)	**178.7**	**177.8**	**178.3**	**178.5**	**123.6**
(8-9-10)	**179.4**	**179.1**	**179.4**	**179.1**	**124.7**
(9-10-11)	**120.8**	**119.8**	**120.3**	**120.6**	**118.4**
(10-11-12)	**119.5**	**119.3**	**119.3**	**119.4**	**120.1**
(11-12-13)	**121.5**	**120.9**	**121.2**	**121.4**	**120.8**
(12-13-14)	**120.7**	**120.5**	**120.0**	**120.1**	**122.2**
(13-14-15)	**178.6**	**179.0**	**178.5**	**178.6**	**124.0**
(14-15-16)	**177.4**	**177.5**	**179.1**	**179.2**	**124.3**
(15-16-17)	**121.8**	**121.3**	**120.9**	**121.1**	**118.0**
(16-17-18)	**121.1**	**120.6**	**120.9**	**121.1**	**120.5**

Table A.8: Continue.

(17-18-19)	**121.4**	**121.0**	**121.1**	**121.3**	**120.5**
(18-19-20)	**125.6**	**124.0**	**124.6**	**125.2**	**121.5**
(19-20-21)	**131.2**	**128.6**	**130.0**	**130.9**	**124.8**
(20-21-22)	**128.1**	**126.9**	**127.3**	**127.8**	**122.6**
D					
(1-2-3-4)	**-177.3**	**-178.4**	**-176.9**	**-179.8**	**-178.5**
(2-3-4-5)	**-164.8**	**-158.6**	**-158.8**	**-177.5**	**-137.4**
(3-4-5-6)	**177.8**	**179.7**	**179.1**	**-179.5**	**-176.3**
(4-5-6-7)	**0.325**	**0.359**	**0.504**	**0.062**	**0.865**
(5-6-7-8)	**-179.0**	**179.4**	**179.9**	**179.4**	**178.0**
(6-7-8-9)	**29.37**	**-16.67**	**-0.485**	**-15.02**	**0.150**
(7-8-9-10)	**88.37**	**-49.69**	**-177.4**	**-142.4**	**-178.9**
(8-9-10-11)	**-125.1**	**56.72**	**174.1**	**155.2**	**177.9**
(9-10-11-12)	**179.4**	**-179.0**	**-179.8**	**-179.5**	**-178.5**
(10-11-12-13)	**-0.035**	**-0.228**	**-0.0004**	**-0.174**	**1.112**
(11-12-13-14)	**-179.6**	**-179.3**	**179.6**	**179.8**	**177.6**
(12-13-14-15)	**173.9**	**151.6**	**-11.93**	**-5.320**	**-2.862**
(13-14-15-16)	**0.153**	**22.55**	**-149.9**	**179.4**	**179.8**
(14-15-16-17)	**-176.1**	**-168.1**	**160.2**	**176.5**	**176.6**
(15-16-17-18)	**179.7**	**179.3**	**-179.7**	**-179.8**	**-178.6**
(16-17-18-19)	**-0.416**	**-0.485**	**-0.388**	**-0.615**	**-1.978**
(17-18-19-20)	**-178.7**	**-178.5**	**-179.7**	**-178.9**	**177.4**
(18-19-20-21)	**12.15**	**27.45**	**19.019**	**12.56**	**41.67**
(19-20-21-22)	**1.329**	**1.542**	**1.912**	**1.675**	**11.12**

Appendix B

Geometry of (Interacting) OPEs

Table B.1: Selected bond lengths (R) (in A°), bond angles (A) (in degrees), and dihedral angles (D) (in degrees) of OPE-ALD (without side chains) interacting with SWCNT the labelling of atoms is shown in Scheme 4.1.

	B97D	**wB97XD**	**CAM-B3LYP**
R			
(1-2)	**1.225**	**1.211**	**1.210**
(2-3)	**1.482**	**1.481**	**1.477**
(3-4)	**1.410**	**1.394**	**1.396**
(4-5)	**1.394**	**1.387**	**1.381**
(5-6)	**1.421**	**1.401**	**1.405**
(6-7)	**1.420**	**1.428**	**1.426**
(7-8)	**1.228**	**1.210**	**1.209**
(8-9)	**1.420**	**1.427**	**1.426**
(9-10)	**1.420**	**1.402**	**1.401**
(10-11)	**1.392**	**1.384**	**1.383**
(11-12)	**1.420**	**1.403**	**1.401**
(12-13)	**1.420**	**1.428**	**1.426**
(13-14)	**1.228**	**1.211**	**1.209**
(14-15)	**1.420**	**1.428**	**1.426**
(15-16)	**1.423**	**1.406**	**1.401**
(16-17)	**1.392**	**1.383**	**1.385**
(17-18)	**1.412**	**1.397**	**1.393**
(18-19)	**1.481**	**1.481**	**1.477**
(19-20)	**1.225**	**1.211**	**1.210**
A			
(1-2-3)	**125.0**	**124.4**	**124.3**
(2-3-4)	**119.8**	**119.8**	**120.1**
(3-4-5)	**120.6**	**120.4**	**120.1**
(4-5-6)	**120.1**	**119.9**	**120.2**
(5-6-7)	**120.5**	**119.9**	**120.2**
(6-7-8)	**179.9**	**178.2**	**179.4**
(7-8-9)	**179.6**	**178.8**	**179.7**
(8-9-10)	**120.7**	**120.2**	**120.5**
(9-10-11)	**120.7**	**120.4**	**120.5**
(10-11-12)	**120.7**	**120.4**	**120.5**
(11-12-13)	**120.7**	**119.9**	**120.5**
(12-13-14)	**179.6**	**178.3**	**179.7**
(13-14-15)	**179.9**	**178.5**	**179.6**
(14-15-16)	**120.4**	**119.9**	**120.2**
(15-16-17)	**120.4**	**120.2**	**120.0**
(16-17-18)	**120.3**	**120.1**	**120.3**
(17-18-19)	**120.7**	**120.2**	**120.0**
(18-19-20)	**125.0**	**124.4**	**124.3**

Table B.2: Contiune.

D			
(1-2-3-4)	**179.8**	**-179.0**	**-1.746**
(2-3-4-5)	**179.0**	**178.8**	**178.5**
(3-4-5-6)	**0.047**	**-0.094**	**-0.110**
(4-5-6-7)	**-179.5**	**-178.4**	**-178.8**
(5-6-7-8)	**158.0**	**66.42**	**76.55**
(6-7-8-9)	**143.3**	**-2.304**	**12.46**
(7-8-9-10)	**62.06**	**-79.55**	**-87.78**
(8-9-10-11)	**-179.9**	**179.4**	**179.7**
(9-10-11-12)	**0.161**	**-0.182**	**0.048**
(10-11-12-13)	**179.7**	**179.9**	**-179.7**
(11-12-13-14)	**-108.0**	**3.918**	**102.2**
(12-13-14-15)	**100.3**	**23.97**	**-18.26**
(13-14-15-16)	**11.69**	**-31.85**	**-81.13**
(14-15-16-17)	**179.4**	**178.6**	**179.3**
(15-16-17-18)	**0.063**	**0.148**	**0.012**
(16-17-18-19)	**-179.1**	**-178.5**	**-179.1**
(17-18-19-20)	**-1.335**	**-0.709**	**179.6**

Table B.3: Selected bond lengths (R) (in A°), bond angles (A) (in degrees), and dihedral angles (D) (in degrees) of OPE-ALD (with side chains) interacting with SWCNT the labelling of atoms is shown in Scheme 4.1.

	B97D	**wB97XD**	**CAM-B3LYP**
R			
(1-2)	**1.226**	**1.211**	**1.211**
(2-3)	**1.479**	**1.480**	**1.476**
(3-4)	**1.411**	**1.397**	**1.394**
(4-5)	**1.393**	**1.385**	**1.384**
(5-6)	**1.422**	**1.404**	**1.402**
(6-7)	**1.417**	**1.428**	**1.425**
(7-8)	**1.228**	**1.211**	**1.208**
(8-9)	**1.416**	**1.426**	**1.423**
(9-10)	**1.430**	**1.401**	**1.407**
(10-11)	**1.398**	**1.388**	**1.388**
(11-12)	**1.416**	**1.410**	**1.400**
(12-13)	**1.416**	**1.424**	**1.423**
(13-14)	**1.228**	**1.211**	**1.208**
(14-15)	**1.417**	**1.427**	**1.425**
(15-16)	**1.423**	**1.404**	**1.404**
(16-17)	**1.391**	**1.387**	**1.382**
(17-18)	**1.412**	**1.395**	**1.396**
(18-19)	**1.479**	**1.480**	**1.476**
(19-20)	**1.226**	**1.211**	**1.211**
A			
(1-2-3)	**125.1**	**124.5**	**124.4**
(2-3-4)	**119.8**	**120.4**	**120.0**
(3-4-5)	**120.7**	**120.3**	**120.4**
(4-5-6)	**120.1**	**120.1**	**120.0**
(5-6-7)	**120.1**	**121.5**	**120.1**
(6-7-8)	**178.5**	**175.1**	**178.3**
(7-8-9)	**179.1**	**174.7**	**179.2**
(8-9-10)	**120.4**	**121.8**	**120.2**
(9-10-11)	**119.6**	**120.5**	**119.2**
(10-11-12)	**121.4**	**119.6**	**121.1**
(11-12-13)	**120.7**	**118.3**	**120.1**
(12-13-14)	**178.8**	**175.1**	**179.1**
(13-14-15)	**178.5**	**174.7**	**178.1**
(14-15-16)	**120.9**	**118.7**	**120.7**
(15-16-17)	**120.4**	**120.1**	**120.2**
(16-17-18)	**120.4**	**120.3**	**120.1**
(17-18-19)	**120.7**	**119.8**	**120.1**
(18-19-20)	**125.1**	**124.5**	**124.4**

Table B.4: Contiune.

D			
(1-2-3-4)	**-179.4**	**-0.651**	**177.0**
(2-3-4-5)	**178.8**	**-178.7**	**-178.1**
(3-4-5-6)	**0.173**	**0.332**	**-0.289**
(4-5-6-7)	**-179.4**	**177.6**	**178.6**
(5-6-7-8)	**2.968**	**-148.6**	**-47.21**
(6-7-8-9)	**-12.62**	**18.24**	**-118.2**
(7-8-9-10)	**14.38**	**151.7**	**145.3**
(8-9-10-11)	**-178.1**	**-177.0**	**-179.7**
(9-10-11-12)	**-2.814**	**1.008**	**0.618**
(10-11-12-13)	**-179.1**	**176.8**	**178.7**
(11-12-13-14)	**-164.1**	**-11.68**	**-64.24**
(12-13-14-15)	**-14.15**	**14.83**	**-76.42**
(13-14-15-16)	**-177.6**	**10.94**	**141.29**
(14-15-16-17)	**179.2**	**-178.4**	**-178.3**
(15-16-17-18)	**0.092**	**0.106**	**-0.203**
(16-17-18-19)	**-178.9**	**178.2**	**178.4**
(17-18-19-20)	**-0.730**	**-179.4**	**-1.572**

Table B.5: Selected bond lengths (R) (in A°), bond angles (A) (in degrees), and dihedral angles (D) (in degrees) of OPE-DTF (without side chains) interacting with SWCNT the labelling of atoms is shown in Scheme 4.1.

	B97D	**wB97XD**	**CAM-B3LYP**
R			
(1-2)	**1.792**	**1.777**	**1.779**
(2-3)	**1.370**	**1.347**	**1.347**
(3-4)	**1.451**	**1.462**	**1.458**
(4-5)	**1.424**	**1.405**	**1.406**
(5-6)	**1.389**	**1.384**	**1.380**
(6-7)	**1.421**	**1.402**	**1.402**
(7-8)	**1.417**	**1.428**	**1.426**
(8-9)	**1.229**	**1.211**	**1.209**
(9-10)	**1.417**	**1.429**	**1.426**
(10-11)	**1.421**	**1.401**	**1.402**
(11-12)	**1.392**	**1.387**	**1.383**
(12-13)	**1.421**	**1.401**	**1.402**
(13-14)	**1.417**	**1.429**	**1.426**
(14-15)	**1.229**	**1.212**	**1.209**
(15-16)	**1.417**	**1.428**	**1.426**
(16-17)	**1.419**	**1.400**	**1.399**
(17-18)	**1.393**	**1.388**	**1.385**
(18-19)	**1.421**	**1.404**	**1.403**
(19-20)	**1.451**	**1.460**	**1.458**
(20-21)	**1.370**	**1.349**	**1.347**
(21-22)	**1.782**	**1.769**	**1.771**
A			
(1-2-3)	**119.8**	**120.3**	**119.9**
(2-3-4)	**132.0**	**129.5**	**131.1**
(3-4-5)	**117.0**	**118.0**	**117.2**
(4-5-6)	**122.1**	**121.6**	**121.8**
(5-6-7)	**120.6**	**120.3**	**120.4**
(6-7-8)	**120.8**	**121.2**	**120.7**
(7-8-9)	**178.7**	**178.2**	**179.3**
(8-9-10)	**179.5**	**177.6**	**179.6**
(9-10-11)	**120.8**	**121.4**	**120.5**
(10-11-12)	**120.8**	**120.6**	**120.6**
(11-12-13)	**120.8**	**120.5**	**120.6**
(12-13-14)	**120.9**	**121.8**	**120.7**
(13-14-15)	**179.5**	**176.4**	**179.7**
(14-15-16)	**178.8**	**176.0**	**179.4**
(15-16-17)	**121.3**	**122.1**	**121.0**
(16-17-18)	**121.2**	**120.9**	**121.0**

Table B.6: Continue.

(17-18-19)	**121.4**	**121.2**	**121.1**
(18-19-20)	**126.1**	**126.0**	**125.5**
(19-20-21)	**132.0**	**131.6**	**131.1**
(20-21-22)	**127.7**	**127.5**	**127.3**
D			
(1-2-3-4)	**-178.1**	**-177.7**	**-179.6**
(2-3-4-5)	**-179.4**	**-159.0**	**-171.1**
(3-4-5-6)	**-178.8**	**-179.6**	**-179.8**
(4-5-6-7)	**-0.264**	**0.628**	**0.178**
(5-6-7-8)	**179.8**	**178.8**	**179.4**
(6-7-8-9)	**20.91**	**-158.4**	**-39.87**
(7-8-9-10)	**41.61**	**-19.70**	**-15.93**
(8-9-10-11)	**-70.03**	**-179.9**	**49.24**
(9-10-11-12)	**179.7**	**-179.8**	**-179.7**
(10-11-12-13)	**-0.153**	**0.050**	**-0.015**
(11-12-13-14)	**-179.6**	**-179.9**	**179.8**
(12-13-14-15)	**113.2**	**173.0**	**-131.3**
(13-14-15-16)	**40.09**	**5.350**	**-20.41**
(14-15-16-17)	**-160.4**	**177.7**	**143.6**
(15-16-17-18)	**-179.5**	**-178.9**	**-179.4**
(16-17-18-19)	**-0.205**	**-0.276**	**-0.287**
(17-18-19-20)	**179.0**	**178.9**	**179.8**
(18-19-20-21)	**0.225**	**4.278**	**9.322**
(19-20-21-22)	**2.417**	**2.285**	**1.296**

Table B.7: Selected bond lengths (R) (in A°), bond angles (A) (in degrees), and dihedral angles (D) (in degrees) of OPE-DTF (with side chains) interacting with SWCNT the labelling of atoms is shown in Scheme 4.1.

	B97D	wB97XD	CAM-B3LYP
R			
(1-2)	1.774	1.772	1.776
(2-3)	1.367	1.348	1.346
(3-4)	1.451	1.461	1.459
(4-5)	1.419	1.406	1.405
(5-6)	1.394	1.382	1.380
(6-7)	1.417	1.403	1.402
(7-8)	1.415	1.426	1.425
(8-9)	1.228	1.211	1.209
(9-10)	1.413	1.424	1.423
(10-11)	1.414	1.407	1.407
(11-12)	1.396	1.391	1.388
(12-13)	1.430	1.402	1.400
(13-14)	1.413	1.425	1.423
(14-15)	1.228	1.211	1.209
(15-16)	1.414	1.427	1.425
(16-17)	1.421	1.401	1.400
(17-18)	1.389	1.385	1.385
(18-19)	1.422	1.403	1.403
(19-20)	1.453	1.462	1.459
(20-21)	1.367	1.347	1.346
(21-22)	1.786	1.769	1.770
A			
(1-2-3)	128.4	120.1	120.0
(2-3-4)	130.5	131.7	131.3
(3-4-5)	125.3	117.2	117.2
(4-5-6)	121.3	121.8	121.9
(5-6-7)	120.8	120.3	120.4
(6-7-8)	123.1	120.2	120.3
(7-8-9)	172.7	175.6	178.0
(8-9-10)	172.8	175.1	178.8
(9-10-11)	122.6	121.1	120.4
(10-11-12)	121.0	118.8	119.3
(11-12-13)	120.0	121.4	121.2
(12-13-14)	118.7	118.3	120.0
(13-14-15)	173.6	172.6	178.4
(14-15-16)	175.2	175.3	178.7
(15-16-17)	119.5	119.5	121.1
(16-17-18)	120.5	120.9	121.1

Table B.8: Continue.

(17-18-19)	**121.8**	**121.1**	**121.1**
(18-19-20)	**117.6**	**124.1**	**125.5**
(19-20-21)	**130.3**	**128.8**	**131.2**
(20-21-22)	**120.2**	**126.7**	**127.7**
D			
(1-2-3-4)	**-2.447**	**-179.9**	**-179.3**
(2-3-4-5)	**-18.41**	**-171.1**	**-173.4**
(3-4-5-6)	**-179.0**	**-177.3**	**179.9**
(4-5-6-7)	**-0.253**	**0.684**	**0.265**
(5-6-7-8)	**177.7**	**175.0**	**179.1**
(6-7-8-9)	**-166.6**	**-57.12**	**-21.6**
(7-8-9-10)	**-23.37**	**-48.49**	**-103.0**
(8-9-10-11)	**-179.8**	**128.2**	**139.2**
(9-10-11-12)	**-179.2**	**-177.7**	**179.8**
(10-11-12-13)	**-1.048**	**5.360**	**1.431**
(11-12-13-14)	**179.7**	**173.6**	**178.7**
(12-13-14-15)	**-7.193**	**-24.27**	**-24.02**
(13-14-15-16)	**-20.29**	**2.432**	**-111.3**
(14-15-16-17)	**14.33**	**42.62**	**148.5**
(15-16-17-18)	**-178.6**	**-176.7**	**-179.3**
(16-17-18-19)	**-1.522**	**-0.426**	**0.009**
(17-18-19-20)	**-179.4**	**179.6**	**179.7**
(18-19-20-21)	**165.4**	**20.59**	**5.844**
(19-20-21-22)	**-176.8**	**2.171**	**0.671**

Table B.9: Dipole moments of ALD.

Dipole moment of ALD- WITHOUT SIDE CHAIN - B97D

	μc	μn	μ'		μo	Δμ
X	-0.0166	-0.0037	-0.0129		0	0.731980642
Y	0.7	0.0283	0.6717		0	
Z	-0.148	0.1426	-0.2906		0	
Total	0.7158	0.1454	0.5704		0.0001	

Dipole moment of ALD-WITHOUT SIDE CHAIN - CAM-B3LYP

	μc	μn	μ'		μo	Δμ
X	-0.2484	0.0001	-0.2485		0	0.991509365
Y	0.9044	0.0003	0.9041		0	
Z	-0.2115	0.1109	-0.3224		0	
Total	0.9615	0.1109	0.8506		0	

Dipole moment for ALD-WITHOUT SIDE CHAIN - wB97XD

	μc	μn	μ'		μo	Δμ
X	0.0161	0.0003	0.0158		0.0001	0.300512246
Y	0.5997	0.0027	0.597		-0.0001	
Z	-0.0767	0.0926	-0.1693		-0.0009	
Total	0.6048	0.0926	0.5122		0.0009	

Dipole moment of ALD-WITH SIDE CHAIN -B97D

	μc	μn	μ'		μo	Δμ
X	-0.0374	-0.0037	-0.0337		0.0004	1.259299817
Y	1.2864	0.0283	1.2581		0	
Z	0.1	0.1426	-0.0426		0.0005	
Total	1.2908	0.1454	1.1454		0.0006	

Dipole moment for ALD-WITH SIDE CHAIN- CAM-B3LYP

	μc	μn	μ'		μo	Δμ
X	-0.0071	0.0001	-0.0072		0	1.927305269
Y	1.7627	0.0003	1.7624		0	
Z	0.8919	0.1109	0.781		0.001	
Total	1.9755	0.1109	1.8646		0.001	

Dipole moment for ALD-WITH SIDE CHAIN-wB97XD

	μc	μn	μ'		μo	Δμ
X	-0.1196	0.0003	-0.1199		-0.0001	0.39416319
Y	0.3682	0.0027	0.3655		-0.0002	
Z	0.009	0.0926	-0.0836		0.0017	
Total	0.3872	0.0926	0.2946		0.0018	

Table B.10: Dipole moments of DTF.

Dipole moment of DTF- WITHOUT SIDE CHAIN - B97D

	μc	μn	μ'		μo	Δμ
X	0.0143	-0.0037	0.018		-0.0003	2.526820029
Y	2.4107	0.0283	2.3824		-0.0005	
Z	0.0748	0.1426	-0.0678		0.7726	
Total	2.4119	0.1454	2.2665		0.7726	

Dipole moment of DTF - WITHOUT SIDE CHAIN - CAM-B3LYP.

	μc	μn	μ'		μo	Δμ
X	0.0376	0.0001	0.0375		0.0001	1.314843656
Y	0.9836	0.0003	0.9833		0.0001	
Z	0.1371	0.1109	0.0262		0.8984	
Total	0.9938	0.1109	0.8829		0.8984	

Dipole moment of DTF - WITHOUT SIDE CHAIN - wB97XD.

	μc	μn	μ'		μo	Δμ
X	0.7059	0.0003	0.7056		0.0001	1.699118198
Y	1.0754	0.0027	1.0727		0.0005	
Z	0.2924	0.0926	0.1998		1.3132	
Total	1.3192	0.0926	1.2266		1.3132	

Dipole moment of DTF-WITH SIDE CHAIN-B97D

	μc	μn	μ'		μo	Δμ
X	1.223	-0.0037	1.2267		3.0085	6.850948656
Y	-4.8999	0.0283	-4.9282		1.0983	
Z	2.0708	0.1426	1.9282		4.6562	
Total	5.4583	0.1454	5.3129		5.6514	

Dipole moment of DTF-WITH SIDE CHAIN-CAM-B3LYP

	μc	μn	μ'		μo	Δμ
X	0.1018	0.0001	0.1017		1.8694	4.439269126
Y	1.499	0.0003	1.4987		2.3545	
Z	-0.3332	0.1109	-0.4441		3.5371	
Total	1.539	0.1109	1.4281		4.6421	

Dipole moment of DTF-WITH SIDE CHAIN-wB97XD

	μc	μn	μ'		μo	Δμ
X	-0.0031	0.0003	-0.0034		1.772	5.721104649
Y	2.6821	0.0027	2.6794		-0.1716	
Z	0.6288	0.0926	0.5362		5.1677	
Total	2.7548	0.0926	2.6622		5.4658	